The Dissertation Committee for Gunja Rajesh Pandav
certifies that this is the approved version of the following dissertation:

Computational Modeling of Fluctuations and Phase Behavior in Polymeric Systems

Committee:

Venkat Ganesan, Supervisor

Christopher Ellison

Isaac Sanchez

Thomas Truskett

Graeme Henkelman

Keith Johnston

Computational Modeling of Fluctuations and Phase Behavior in Polymeric Systems

by

Gunja Rajesh Pandav, B.Tech.; M.Tech.

DISSERTATION

Presented to the Faculty of the Graduate School of

The University of Texas at Austin

in Partial Fulfillment

of the Requirements

for the Degree of

DOCTOR OF PHILOSOPHY

THE UNIVERSITY OF TEXAS AT AUSTIN

August 2015

Dedicated to my parents, Rama and Rajesh Pandav, and brother, Kapil Pandav.

Acknowledgments

I express my sincere gratitude to my research supervisor Prof. Venkat Ganesan for his guidance and support throughout the course of my PhD. His insights and guidance has greatly helped me develop as a researcher. This dissertation would not have been complete without his ideas, knowledge, and constant encouragement.

I am very appreciative of the insight and support that has been provided to me by my thesis committee members: Prof. Christopher Ellison, Prof. Graeme Henkelman, Prof. Isaac Sanchez, Prof. Thomas Truskett, and Prof. Keith Johnston.

Additionally, I would like to extend my thanks to Dr. Victor Pryamitsyn for sharing his insights on many aspects of polymer physics and patiently responding innumerable questions. I would like to specially thank him for his insights and help for Chapter 6. I thank my colleagues Dr. David Trombly, Dr. Thomas Lewis, Dr. Santosh Mogurampelly, Dylan Kipp, Vaidya Sethuraman and Kriti Mishra for the help and feedback along the way.

I had the fortune of spending time with some wonderful friends. I would like to thank Amey, Shravya, Aarti, Akshay, Shilpi, Garima, Pallavi, Siddharth and Ani for the fun times and amazing company. I would like to thank Sam and Lynn for helpful discussions and encouraging advice.

Most importantly, I would like to thank my parents and family for their exceptional support and understanding throughout these years. Finally, I would like to thank my dear fiancé, Akhilesh. Thank you for always being there for me. You have made this time spent at UT and Austin the most memorable days of my life and I look forward to many more years we are going to spend together.

Computational Modeling of Fluctuations and Phase Behavior in Polymeric Systems

Publication No. _____

Gunja Rajesh Pandav, Ph.D.
The University of Texas at Austin, 2015

Supervisor: Venkat Ganesan

This research focuses on the computational modeling of fluctuations, interactions, phase behavior and structural characteristics of multicomponent polymeric systems. The role of fluctuations is studied in the context of block copolymer melts and polymer blends stabilized using copolymers exhibiting different sequence architectures. The relationship between interparticle interactions and structural characteristics of the aggregates formed in particle-polymer solutions is examined for charged nanoparticle-polymer and charged dendrimer-polyelectrolyte system. A hybrid Monte Carlo and self consistent field theory approach employed in single chain in mean field simulations (SCMF) is utilized in order to achieve the equilibrium morphologies/aggregates in such polymeric systems.

We examine the effect of composition fluctuations on the phase behavior of polydisperse block copolymer melts quantified in terms of fluctuation-

induced shift in the order-disorder transition temperature from the corresponding mean-field predictions. Fluctuation effects can also play an important role in stabilizing bicontinuous microemulsions phases. To study this effect, we examine polymer blend systems compatibilized by a copolymer having different sequence architectures such as monodisperse and polydisperse block copolymer, and gradient copolymer. We systematically assess the efficiency of such system in forming bicontinuous microemulsions phases. We also study the effect of sequence architecture on the phase behavior of gradient copolymer solutions.

We extend above framework to account for electrostatic effects arising from charged polymers and dendrimers. Using such a framework, we characterize the clusters formed due to electrostatic binding between oppositely charged dendrimers and polyelectrolytes. Our results indicate that, the binding is maximum when the charge on dendrimers is balanced by the charge on the polyelectrolytes. We extend the above study to probe the phase behavior of charged nanoparticles suspended in polymer solutions. We examine the influence of polymer concentration, particle volume fraction, and particle charge on the structure and size of clusters. We also examine the influence of multibody effects on the resulting structure of nanoparticle clusters. The charged nanoparticle-polymer solution is seen to exhibit significant multibody effects and the effective two-body interparticle potentials are seen to be a function of nanoparticle density.

Table of Contents

List of Tables

List of Figures

Chapter 1

Introduction

The research work described in this dissertation focuses on studying fluctuations, structure/morphology of polymer solution/melt and nanoparticle-polymer mixtures. Polymers can be synthesized with a wide range of architecture, compositions and chain lengths, thereby imparting flexibility in tuning the structural, thermodynamic and mechanical properties. Moreover, when polymers are added to nanoparticle suspensions, their properties can have a significant influence on interparticle interactions, phase behavior and structure of aggregates. The objectives of this research are to study these multicomponent systems in order to (i) develop an understanding of fluctuation effects and its implications on the phase behaviour of polymer melts and (ii) to examine the interactions and phase behavior of nanoparticle-polymer systems.

One of the theoretical methods to study the equilibrium properties of polymeric systems is the self consistent field theory (SCFT).[1–4] SCFT models the characteristics of polymer mixtures through a mean-field approximation. In a nutshell, the idea behind the SCFT is to model the conformational characteristics of the interacting polymer chains by an equivalent system of ideal polymer chains interacting with fluctuating position dependent potential

field which depends self consistently on the overall distribution of the polymers themselves. Much of the success of the SCFT can be attributed to the extended size of polymer molecules as they can be described by a small number of coarse-grained parameters such as radius of gyration of polymer (R_g) and incompatibility between polymer segments characterized by Flory-Huggins parameter χ ($\chi \propto 1/T$ where T denotes the temperature).[5, 6] On the other hand, SCFT fails to capture some effects which are dependent on the number of chains per unit volume. Such effects lead to a deviation from mean-field behavior which becomes significant and is believed to increase with decreasing number of chains per unit volume. Such effects arise from fluctuations in polymeric systems.

One of the objectives of this work is to quantify the fluctuation effects mentioned above and study their influence on the phase behavior and morphology of the polymeric systems. Previous studies have extensively examined such effects in flexible AB diblock copolymers[6] and have demonstrated substantial influence of composition fluctuations on the order-disorder transition (ODT) defined as the temperature at which the disordered diblock copolymer melt transitions to an ordered state. As a result of such composition fluctuations, the phase boundaries between ordered and disordered states were seen to shift to lower temperatures.[5, 7–10] In the context of polymer blends compatibilized using copolymers, a new phase termed as bicontinuous microemulsion (BμE) has also been predicted to appear as a result of similar fluctuation effects in the vicinity of phase transition from microscopically ordered to a phase

separated regime.[11–21] In this work, we present results which strengthen our understanding of such effects in polymer blend systems and also examine the influence of different sequence architectures of copolymers on the formation of BμE phase.

Polymers are commonly used as additives to nanoparticle suspensions as a versatile approach to control the interactions, phase behavior and structure of the system. Not surprisingly, a lot of research is focused on understanding the ability of polymer to induce and control the interactions in nanoparticle suspensions.[22–31] Some of the industrial applications where nanoparticle-polymer systems and their phase behavior play an important role include protein separation,[32–34] colloidal stabilization, food preservation,[23] protein recovery from industrial by-products,[35–37] and polymer nanocomposites.[38, 39] Such systems exhibit a complex interplay of interactions depending upon the size and structure of the polymer, the particle size relative to the polymer, and the solvent quality. If either or both the components of nanoparticle-polymer mixture are charged, one more level of complexity is added due to the electrostatic interactions. Proteins (modeled as nanoaprticles) and polysaccharides (modeled as polyelectrolytes) are the biopolymers which are abundantly found in living organisms and also in numerous engineered products that exploit biomaterials. Numerous biological processes such as protein transcription, antigen-antibody reactions or enzymatic channeling etc., involve formation of aggregates of such biopolymers governed by electrostatic interactions. The natural association of these biopolymers plays a

pivotal role in maintenance of cell membranes and organelles, aggregation between of histones and DNA, and enzyme catalysis. However, under certain physical conditions, the incompatibility between proteins and polysaccharides contribute to cell partition.

A different, albeit related system, wherein hyper-branched polymer molecules known as dendrimers electrostatically bind to charged genetic material are being explored in the context of gene therapy.[40–46] Such a system is similar to nanoparticle-charged polymer system discussed above wherein the dendrimer molecules represent a soft nanoparticle which is penetrable by polymers. Second objective of this work is to examine the relationship between the interactions and the structure of the particles/dendrimers suspended in polymer solution. Specifically, we explore the vast parameter space available for these systems to target the sought-after morphologies required for specific applications. These interesting problems and the goals of this dissertation are discussed in more detail in the forthcoming subsections.

1.1 Fluctuation Effects in Polymeric Systems

Numerous soft matter systems display intriguing behavior in the vicinity of phase transitions as a consequence of fluctuation effects pertaining to local variation in temperature/composition. Polymeric melts having a high molecular weight (MW) are regarded as systems wherein the fluctuation effects are largely suppressed and SCFT can be readily used to predict the phase behavior. However, for systems having low MW, the fluctuation effects have

been shown to lead to important quantitative corrections to mean-field theories of polymer melts. These issues have motivated the extension of mean-field theories to capture effects of fluctuations in systems exhibiting complex sequence architectures.

Towards above objective, we utilize single chain in mean field (SCMF) simulation methodology. The SCMF methodology proposed by Muller and coworkers[47–53] is a Monte Carlo (MC) simulation approach wherein the intramolecular bonded interactions of the polymers are accounted in an exact manner, whereas, the nonbonded pairwise interactions are replaced by inhomogeneous potential fields acting on the polymer monomers. Such potential fields are usually taken to correspond to the mean-field limit of the model and is expressed as a function of the spatially varying polymer densities and segmental volume fractions. In the implementation of SCMF, such potential fields are determined on-the-fly using the instantaneous values for the inhomogeneous polymer densities and volume fractions. Due to the absence of direct pairwise intermolecular interactions, such methods are computationally efficient and enable significant parallelization. Most importantly, the SCMF methodology accounts for fluctuation effects and allows us to study large scale systems. For instance, the BμE phases are formed as a result of thermal fluctuations and possess a characteristic lengthscale of 100 nm. The SCMF methodology is particularly useful to study such large scale systems. In this section of the dissertation, using SCMF methodology, we examine the importance of fluctuations and their effect on the phase behavior of various multicomponent

polymeric systems.

1.2 Phase Behavior of Gradient Copolymer Solutions

With the development of advanced polymerization techniques, a precise control over polymer properties by controlling their physicochemical characteristics such as molecular weight, chain architecture, sequence chemistry, etc. can be achieved.[54–57] As a consequence, synthesis of new classes of copolymers, such as gradient copolymers, comb copolymers, star copolymers etc., is now becoming common.[58–61] In this research work, we study a class of such polymers termed *gradient copolymers.*[62–67] Gradient copolymers are random copolymers which exhibit a gradual change in monomer composition along the length of the polymer.[68, 69] A number of uses have been proposed for such a class of polymers, which include applications such as reinforcement agents,[70] damping materials[71] and thermoplastic elastomers.[72][73] In this work, we examine the effect of their sequence architecture on the phase behavior in solution conditions. Gradient copolymers have also gained significant attention in the context of interfacial modifiers. Hence, we also examine gradient copolymers as compatibilizing agents for polymer blend systems.

1.3 Interactions and Clustering in Nanoparticle - Polymer Solutions

Polymers added to a suspension of charged nanopaticles is a complex system wherein the interactions are governed by two competing effects, viz.,

short range depletion attraction induced by addition of polymers and long range electrostatic repulsion between charged particles. The depletion interaction is a purely entropic effect in which the nanoparticles experience a polymer-mediated attractive interaction.[74–76] Such short range depletion attraction is expected to drive the aggregation of particles and thus the growth of large clusters. However, the long-range electrostatic interactions are expected to dominate for larger clusters and lead to equilibrium clusters possessing a preferred size. Thus, there is a significant interest in relating the cluster structure and sizes to the effective interparticle interactions.

Such particle-polymer systems represent a generic model for even more complex systems such as protein-DNA interactions where the protein can be viewed as a nanoparticle in its globular state and the DNA can be represented as a stiff polymer. Hence, the underlying physics behind binding/aggregation in such system can be readily extracted from the much simpler nanoparticle-polymer system. In the context of gene therapy, a similar system of dendrimer-polyeletrolyte is being explored due to the increasing need for effective gene delivery vectors to enhance the efficiency of drug delivery and gene therapy systems.[40–46] In support of the utility of dendrimers for gene delivery applications, a number of experimental studies have reported the formation of nanoscale complexes/aggregates in the dilute solution of charged dendrimers and DNA molecules.[77–89] Thus, there is a significant interest in understanding the effect of conformational properties of dendrimer and polymer, solvent quality on the aggregates/clusters formed in the solution.

Despite the importance of the above problems, the theoretical advances have been limited to studying single or a few particles/dendrimers dispersed in polymer solution.[90–104] Full scale particle based simulations such as molecular dynamics and MC simulations become computationally expensive if the charged particles/dendrimers, polymers and ions are treated on an equal footing whereas in field based approaches such as SCFT, the characterization of aggregates becomes difficult. The SCMF methodology, on the other hand, is able to overcome these shortcomings making this methodology ideal to study the particle/dendrimer-polymer systems. Thus, in this work, we extend the SCMF framework to enable multiparticle simulations of nanoparticle-polymer, dendrimer-polymer mixtures in order to study the structure of clusters formed in such systems.

1.4 Outline of Dissertation

1.4.1 Fluctuation Effects on the Order-Disorder Transition in Polydisperse Copolymer Melts

We examine the influence of fluctuation effects on the order-disorder transition (ODT) of polydisperse copolymer systems. We consider two model systems: (i) Molecular weight polydisperse systems represented by AB diblock copolymer melts having monodisperse A blocks and polydisperse B blocks; and (ii) Compositionally polydisperse symmetric diblock copolymer systems. In each case, we present results for the fluctuation-induced shift in the ODT from the corresponding mean-field predictions. In both models, an increase in

polydispersity enhances the influence of fluctuations. Moreover, for compositionally polydisperse systems, we observe that the effect of fluctuations show similar trends in systems containing quenched and annealed representation of sequences.

1.4.2 Efficacy of Different Block Copolymers in Facilitating Microemulsion Phases in Polymer Blend Systems

In this chapter, we consider the ternary blend system of A and B homopolymers mixed with block copolymers containing A and B segments, and probe the efficacy of different copolymer configurations in promoting the formation of microemulsion phases. Specifically, we consider: (a) Monodisperse diblock copolymers; (b) Diblock copolymers with bidisperse molecular weights (MW); (c) Block copolymers having MW polydispersity in one of the blocks; (d) Diblock copolymers having monodisperse MW but bidispersity in average composition; and (e) Gradient copolymers exhibiting a linear variation in the average composition. Using single chain in mean field simulations effected in two dimensions, we probe the onset of formation and the width of the bicontinuous microemulsion channel in the ternary phase diagram of homopolymer blended with compatibilizer. We observed that diblock copolymers having bidisperse composition are most efficient (i. e. microemulsion phases occupy the largest area of phase diagram) in forming microemulsions. On the other hand, monodisperse diblock copolymers and diblock copolymers having bidisperse MW distribution form microemulsions with the least amount of compatibilizers. We rationalize our results by explicitly quantifying the interfacial

activity and the influence of fluctuation effects in the respective copolymer systems.

1.4.3 Phase Behavior of Gradient Copolymer Solutions

We use computer simulations to study the phase separation behavior of amphiphilic linear gradient copolymer solution under poor solvent conditions. Using Bond Fluctuation model and parallel tempering algorithm, we explore the influence of the gradient strength (the largest difference in the instantaneous composition along the copolymer) upon the phase separation characteristics. Under poor solvent conditions, the chains collapse to form micelle-like aggregates. We find that the critical temperature for this transition exhibits a linear dependence on the gradient strength of the copolymers. A systematic quantification of the cluster characteristics formed during the phase separation also reveals a strong dependence of aggregation numbers and the bridging statistics upon the gradient strength of the copolymers. Analysis of our results reveals that the critical parameter determining the thermodynamic behavior of gradient copolymers is in fact the average length of the hydrophobic sequences in the gradient copolymers. We demonstrate that the latter provides a useful measure to quantitatively predict the critical transition temperature of the gradient copolymer solution. We also present a few results from the framework of an annealed representation of the sequences of the gradient copolymer to demonstrate the limitations arising from such a model representation.

1.4.4 Computer Simulations of Dendrimer and Polyelectrolyte Complexes

We carry out a systematic analysis of static properties of the clusters formed by complexation between charged dendrimers and linear polyelectrolyte (LPE) chains in a dilute solution under good solvent conditions. We analyze the structure of the clusters through radial distribution functions of the dendrimer, cluster size and charge distributions. The effects of LPE length, charge ratio between LPE and dendrimer, the influence of salt concentration and the dendrimer generation number are examined. Systems with short LPEs showed reduced propensity for aggregation with dendrimers leading to formation of smaller clusters. In contrast, larger dendrimers and longer LPEs lead to larger clusters with significant bridging. Increasing salt concentration was seen to reduce aggregation between dendrimers as a result of screening of electrostatic interactions. Generally, maximum complexation was observed in systems with equal amount of net dendrimer and LPE charges, whereas either excess LPE or dendrimer concentrations resulted in reduced clustering between dendrimers.

1.4.5 Interactions, Clustering and Multibody Effects of Charged Nanoparticles in Uncharged Polymer Solutions

We study the polymer-mediated interactions between charged particles suspended in polymer solution and examine their effect on the structure of aggregates. We present an extension of the single chain in mean field simulation method to study the charged particle-uncharged polymer system. We

examine the effect of particle charge, polymer concentration and particle volume fraction on aggregation between particles. The structure of aggregates are characterized using particle-particle radial distribution functions, cluster size distribution, and fractal analysis. We observe that the aggregation between particles increase with particle volume fraction and/or polymer concentration, decreasing particle charge. We also examined the influence of multibody effects on the structure of charged particle-polymer system. Specifically, we examined whether the effective two-body potentials are able to reproduce the structure observed in multiparticle simulation. Our results indicate that the effective two body approximation overpredicts the aggregation between particles even at dilute particle concentrations.

Chapter 2

Fluctuation Effects on the Order-Disorder Transition in Polydisperse Copolymer Melts

2.1 Introduction

Numerous soft matter systems display intriguing behavior in the vicinity of phase transitions as a consequence of thermal fluctuation effects. However, large molecular weight (MW) polymeric melts have often been regarded as a system in which fluctuation effects are by and large suppressed (except for conditions very close to phase transitions) such that their thermodynamic characteristics resemble mean-field behavior for a wide range of parameters. Indeed, such expectations have spurred numerous successful applications of mean-field theories (MFT), collectively known as polymer self-consistent field theory (SCFT),[1–4] for the prediction of the equilibrium morphologies and characteristics of multicomponent polymers. Despite such successes, fluctuation effects have been shown to lead to important corrections to mean-field theories of polymer melts. For instance, such effects lead to a modification of both the temperature and the nature of the order to disorder transitions (ODT) [5, 7–10, 105–107] in monodisperse diblock copolymer systems. In other contexts, fluctuation effects have also been shown to stabilize novel morphologies such as bicontinuous microemulsion phases in blends of block copolymers

[13, 16, 17] and new morphologies in multiblock copolymers.[108, 109] Motivated by such results, there has arisen an interest in understanding the influence of fluctuations upon the equilibrium characteristics of different kinds of multicomponent polymer systems.[110–120]

In this chapter, we are concerned with the interplay between fluctuation effects and polydispersity in diblock copolymer systems. Polydispersity in multicomponent systems can be broadly classified into two categories:

1. MW polydispersity: This represents the case in which there is a polydispersity in the MWs of the copolymer. Such a feature is extremely common, and arises either from imperfections in the synthesis strategies and/or is an inherent outcome of some synthesis techniques.[58, 60, 121, 122] MW polydispersity has shown to significantly alter the ODT and domain spacing in block copolymer melts.[123–130] In this context, our studies are motivated by the experiments of Lynd and Hillmyer which systematically studied the effects of MW polydispersity on the phase behavior and order-disorder transition (ODT) temperature of AB diblock copolymer melts.[123–127] Their work considered the case in which the MW polydispersity was in one of the blocks (which we denote as B in this chapter) and examined copolymer melts containing different average volume fractions of the B component. When the B segments constitute the minority component (i. e. when the average volume fraction of B component, which is denoted as f in this chapter, is such that $f < 0.5$),

they observed that an increase in the MW polydispersity resulted in a decrease in the Flory-Huggins interaction parameter, χ_{ODT}, required for the order disorder transition. Whereas, when the B segments were the majority component ($f > 0.5$), increasing MW polydispersity was seen to result in an increase in the χ_{ODT}. Interestingly, such observations contradicted the predictions of MFTs which suggest that increasing the MW polydispersity should lead to a decrease in the χ_{ODT} for all average compositions (f) of the block copolymer.[131–133]

Spurred by the inconsistency noted between the MFT and experiments of Hillmyer and coworkers, Beardsley and Matsen [128] used lattice Monte Carlo (MC) simulations to study the ODT of polydisperse diblock copolymer melt systems. For a compositionally symmetric copolymer system ($f = 0.5$) their simulation results indicated that the ODT exhibits only a small change with increasing polydispersity, a result which contrasted with MFT predictions,[131–133] but was however qualitatively consistent with the experimental trends noted in Ref. [124]. In a more recent article,[129] they studied *compositionally asymmetric* polydisperse systems and demonstrated a qualitative correspondence with the experimental trends for the ODT behavior as a function of MW polydispersity. Since their MC simulations accounted for fluctuation effects, they concluded that the deviations of experiments from the mean-field predictions arose from the influence of thermal fluctuation effects.

Despite the important insights shed by the study of Beardsley and Mat-

sen, [128, 129] some unresolved issues remain. Specifically, in their MC study for symmetric ($f = 0.5$) copolymers, the χ_{ODT} was found to be practically insensitive to the polydispersity index (PDI) in the range of PDI $= 1.0-2.0$,[128] which contrasted with the results of the experiments in which a slight decrease in the χ_{ODT} with PDI was observed. The more recent simulation study of Beardsley and Matsen,[129] examined only a specific PDI (PDI = 1.5) and fixed invariant degree of polymerization ($\bar{N}$). As a consequence, full clarity on the interplay between PDI, $\bar{N}$ and the average composition (f) of the block copolymer in influencing fluctuation effects of MW polydisperse copolymer systems is still lacking.

Motivated by the above issues, in this paper, we present the results of a more comprehensive examination of fluctuation effects in MW polydisperse systems. Specifically, we probe the interplay between MW polydispersity, average composition and the invariant degree of polymerization of the copolymers in influencing the fluctuation effects. Our results clarify the influence of different parameters on the deviations from MFT predictions and also serve to highlight the influence of the invariant degree of polymerization in influencing the fluctuation effects.

2. Compositional polydispersity: An alternative situation is one wherein the MWs of the copolymers are (approximately) monodisperse, whereas the sequences and the resulting average compositions of individual copolymers display variation among the polymers. Such a situation mostly arises as a consequence of the stochastic nature of the reaction scheme

used in the preparation of the copolymers. In such situations, copolymers are synthesized such that on an average they possess well-defined composition profile, but however, the individual copolymers may exhibit different sequences with differing average compositions. [134–144] There is very little understanding of the interplay between fluctuation effects and such sequence driven compositional polydispersity in copolymer systems.

In this work, we adopt a model of copolymers in which we can explicitly tune the compositional polydispersity to examine its interplay with fluctuation effects in influencing the ODT behavior of such systems. We compare the fluctuation-influenced ODT of an ensemble of sequences of differing compositions (termed as quenched system) with the corresponding mean-field predictions. Additionally, in order to clarify the importance of using such a quenched ensemble of sequences, we compare the fluctuation-influenced ODT of such an ensemble with an "annealed" representation wherein the system consists of an ensemble of chains of single sequence with however a continuously varying composition along the sequence. In the manner, we clarify the interplay between both composition and sequence polydispersity in influencing the effect of thermal fluctuations upon the ODT of diblock copolymers.

The rest of the chapter is arranged as follows. In section 2.2 we briefly discuss the methodology we used to simulate our system and the measures

used to locate the ODT in our simulations. In section 2.3 we present our results for the systems under consideration. In section 2.4 we conclude with a short summary and outlook for future work.

2.2 Simulation Methodology

In this work, we adopted the single chain in mean field (SCMF) simulation methodology proposed by Muller and coworkers[47–53, 145] to study the effects of fluctuations on the ODT and phase behavior of copolymer systems. In essence, SCMF methodology is a MC simulation approach wherein the intramolecular bonded interactions of the polymers are accounted in an exact manner, whereas, the nonbonded pairwise interactions are replaced by inhomogeneous potential fields acting on the polymer monomers. Such potential fields are usually taken to correspond to the mean field limit of the model and is expressed as a function of the spatially varying polymer densities and segmental volume fractions. In the implementation of SCMF, such potential fields are determined on-the-fly using the instantaneous values for the inhomogeneous polymer densities and volume fractions.[47, 48, 146] In the scheme wherein the potentials are updated after each MC move, the SCMF simulation methodology generates configurations consistent with a prespecified Hamiltonian. Due to the absence of direct pairwise intermolecular interactions, SCMF simulations can treat different chains as independent of each other except insofar as the step during which the densities are computed and the potentials are updated. Hence, such methods are computationally efficient and enable

significant parallelization. Such approaches have been used to study the phase behavior of polymer blends,[47, 146] block copolymers,[48, 147–149] polymer nanoparticle mixtures,[150] and semiflexible copolymers.[151]

In relation to the present work, we opted for SCMF approach due to its unique advantage in being able to simulate, without any additional computational cost, ensembles of polymers differing in their molecular weights and/or sequences. In contrast, in some alternative simulations methodologies,[3, 4] studying fluctuation effects in polydisperse systems require significantly more computational effort. Specific advantages of SCMF methodology include the ability to compare to the corresponding mean-field theory results and the ease with which parallelization of the computer algorithms can be achieved. Moreover, by restricting the symmetry of the potential fields, we can study phenomena in a specific spatial dimension. Indeed, since the *qualitative* features of the influence of the fluctuations are expected to be similar in different spatial dimensions, we can expedite our computations to access a wider range of parameters by using two dimensional simulations instead of three dimensional calculations.

2.2.1 Polymer Chain Models

In our SCMF simulations, we considered the following systems:

1. AB diblock copolymer melt with MW polydispersity: We adopted a model which closely mimics the experimental conditions of Lynd and Hillmyer.[123–127] Specifically we assumed that the A block is perfectly

monodisperse and chose the MW of the B blocks based on a Schultz-Zimm distribution.[152, 153] In such a model, the probability $p(N_B)$ that the B-block has N_B segments is given as:

$$p(N_B) = \frac{k^k N_B^{k-1}}{(N_B)_{avg}^k \Gamma(k)} \exp\left(- \frac{k N_B}{(N_B)_{avg}} \right). \tag{2.1}$$

In the above, the parameter k is related to PDI through PDI $= (k+1)/k$ and $(N_B)_{avg}$ is the average number of segments in the distribution. $\Gamma(k)$ denotes the Gamma function.[154] In our study, polymer melts having PDIs $= 1.25, 1.5, 1.75, 2.0$ were considered. The number of segments in A block (N_A) was fixed to 20 and the average composition f was related to $(N_B)_{avg}$ as $f = (N_B)_{avg}/(N_A + (N_B)_{avg})$.

2. Compositionally polydisperse AB diblock copolymer melts: We considered an ensemble of diblock copolymers in which the probability distribution $P(f)$ of the composition of the chain sequences were chosen from:

$$P(f) = \begin{cases} 1 & 0.5 - \Delta \leq f < 0.5 + \Delta \\ 0 & \text{otherwise} \end{cases} \tag{2.2}$$

The parameter Δ quantifies the compositional polydispersity of the melt system. Explicitly, a large (small) Δ corresponds to a system wherein the chain sequences possess a wide (narrow) distribution of average compositions.

The above model corresponds to an ensemble of diblock copolymer chains of varying individual compositions, with however the system possessing an overall average composition of $f = 0.5$. However, we note that the

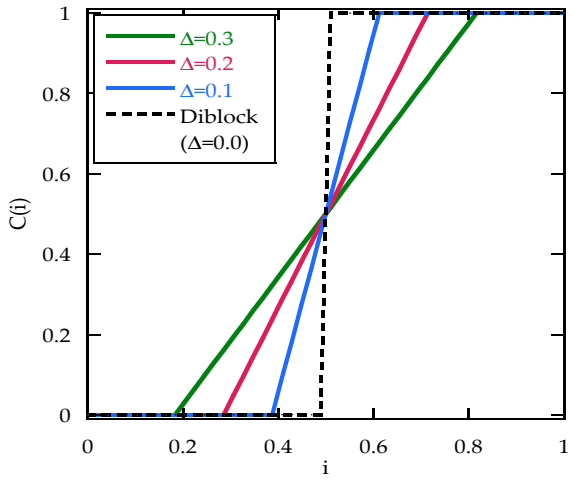

Figure 2.1: Composition profiles for an annealed representation of sequences as a function of Δ. $C(i)$ denotes the average volume fraction of A monomers at a specific location i in the polymer chain. i denotes the segment index (normalized by the total number of segments).

above model can also equally well serve as a more detailed representation for a system of blocky copolymer chains possessing an averaged monomer scale composition profile displayed in Fig. 2.1. Such systems are termed as "tapered copolymers" and have attracted considerable attention due to the opportunities they furnish for tuning the self-assembly characteristics.[155–163] In a number of previous studies, it has been observed that the phase behavior and properties of systems possessing an ensemble of sequences exhibits significant differences compared to that wherein a single averaged sequence is used as a model.[143, 164–167]

In this work, we probe the fluctuation effects on the ODT of an ensemble of sequences (termed in our work as the "quenched" system) exhibiting

compositional polydispersity. We also compare such results with corresponding behavior of tapered copolymers (termed in our work as the "annealed" system). In this manner we clarify the effects arising from the polydispersity in the composition as well as those that can be attributed to the sequence polydispersity effects.

2.2.2 Single Chain in Mean Field Simulation

For our SCMF simulations, we adopted the Gaussian chain model in which each polymer chain is discretized into a collection of N beads connected by $N-1$ harmonic springs. For copolymers having MW polydispersity, N_B is determined by the Schultz-Zimm distribution discussed in earlier section and N is calculated using $N = N_A + N_B$. The bonded and nonbonded interactions are described by the following single chain Hamiltonian:

$$\frac{H[\boldsymbol{r}_i(s)]}{k_B T} = \sum_{s=1}^{N-1} \left[\frac{3}{2b^2} [\boldsymbol{r}_i(s) - \boldsymbol{r}_i(s+1)]^2 + \frac{(2\gamma(s)-1)w(\boldsymbol{r}_i(s)) + \pi(\boldsymbol{r}_i(s))}{N-1} \right], \tag{2.3}$$

where $\boldsymbol{r}_i(s)$ denote the position of the s^{th} monomer on the i^{th} chain and b denotes the effective bond length. In the above, $\gamma(s) = 1$ if the segment s is A monomer and is 0 otherwise. The potential fields $w(\boldsymbol{r}_i(s))$ and $\pi(\boldsymbol{r}_i(s))$ acting on the polymer segments are adopted as the saddle point solutions of the corresponding field theory.[3] Explicitly,

$$w(\boldsymbol{r}) = \frac{\chi N}{2}(\phi_A(\boldsymbol{r}) - \phi_B(\boldsymbol{r})), \tag{2.4}$$

$$\pi(\boldsymbol{r}) = \kappa N(\phi_A(\boldsymbol{r}) + \phi_B(\boldsymbol{r}) - 1). \tag{2.5}$$

where ϕ_α ($\alpha = A, B$) represents the instantaneous local volume fraction of α segments, χ is the Flory-Huggins interaction parameter which describes the incompatibility between A and B segments, and κ is a parameter which is inversely proportional to the isothermal compressibility of the overall system. In the above notation, $w_A = -w + \pi$ and $w_B = w + \pi$ are the fields acting on the A and B monomers respectively.

We used a MC simulation approach in which the Hamiltonian, H, is sampled by Metropolis algorithm.[168] The chain beads are evolved in three dimensions using moves involving displacement of the monomers. The "quasi-instantaneous field" approximation in SCMF refers to the update of external potential fields after a specific number of MC steps. However, strictly speaking, such an approach does not satisfy the detailed balance principle, and its accuracy in reproducing the statistical features of the original Hamiltonian method decreases with increasing number of MC steps between subsequent update of potential fields. Daoulas and Muller[48] systematically quantified the effect of updating frequency upon the accuracy of SCMF simulations. For a homopolymer melt system they reported that the results for the polymer end-to-end distance computed using SCMF methodology showed good agreement ($\approx$ 3% error) with the same calculated using direct MC simulations for updating frequencies less than 1 i.e. the fields were updated after one (or less) MC moves per monomer. They also pointed out that this error between SCMF and MC simulations occur mainly due to the local stretching of bonds whereas, intrachain correlations are not largely influenced by the quasi-

instantaneous field approximation. In our simulations, we update the potential fields $w(\boldsymbol{r}_i(s)), \pi(\boldsymbol{r}_i(s))$ based on the inhomogeneous volume fractions of A and B monomers after one MC step which offers a tradeoff between quality of quasi-instantaneous field approximation and computational efficiency. Some of our simulations were effected in a two-dimensional representation in which the density fields corresponding to the particle locations were averaged over two-dimensions. We used a box size of 64×64 and $64 \times 64 \times 64$ lattice units for two-dimensional and three-dimensional simulations respectively. In all of our simulations, we used $\kappa = 50$ to ensure a nearly incompressible system. The system was equilibrated for 1×10^6 MCS per monomer and thermodynamic quantities (discussed below) were averaged every 50 MCS per monomer.

In some works,[10, 169] it has been common to characterize the effect of fluctuations through a parameter $C = \rho R_g^d/N$ (with d denoting the number of dimensions and $\rho = nN/V$ where n denotes the total number of copolymer chains in the system and V is the system volume in terms of unperturbed radius of gyration, R_g). C is related to the commonly used invariant degree of polymerization, $\bar{N}$, through $C = (\bar{N}/6^3)^{d/2-1}$, and represents the "Ginzburg" parameter for our field theory. A small value of C is equivalent to a small number of polymer chains surrounding each molecule, and hence corresponds to stronger composition fluctuations. The limit of mean-field theories correspond to $C \to \infty$. Some of the experimental results in the context of MW polydisperse copolymer systems correspond to $\bar{N}$ values as low as 300.[124, 129] On the other hand, SCMF-type approaches require a minimum number of monomers

per grid point so that the instantaneous densities are suitably approximated. Probing low values of $\bar{N}$ necessitates decreasing the total number of grid points (i.e. increasing grid spacing). However, such modifications would necessitate a more careful accounting of the errors resulting from discretization effects. Instead, in our simulations we maintain a fixed discretization ($\Delta L = 0.156 R_g$) to ensure comparable discretization errors in the different simulations, thereby enabling us to compare the results for different physical parameters. In this regard we were guided by the work of Daoulas and Muller which introduced a parameter ε to quantify the accuracy of quasi-instantaneous field approximation.[48] Explicitly, they suggested that $\varepsilon \ll 1$ with

$$\varepsilon \equiv \frac{V}{nN^2\Delta L^3} \tag{2.6}$$

ensures the validity of quasi-instantaneous field approximation. In our simulations, the highest value of ε (encountered for lowest C) is $\approx 1.6 \times 10^{-3}$ which ensures that SCMF captures fluctuations. However, our efforts to meet the above criterion with a fixed discretization also limited the lowest C parameters we could probe in our simulations. As a consequence, our studies are limited to C parameter values in the range $10 - 100$ which corresponds to $\bar{N} \approx 2.16 \times 10^4 - 2.16 \times 10^6$.

To quantify the fluctuation effects in our work, we compute the deviation of ODT calculated from SCMF simulations from the mean-field predictions. For the model system considered in this study, the ODT predictions from the random phase approximation (RPA) have been noted to be in good

agreement with SCFT results,[131, 132] and hence we use the former as a measure of the prediction of mean field theories. However, the spatial discretization employed in SCMF simulations is equivalent to a finite range of interaction between the monomers and requires to be accounted within the RPA theories.[145, 170] To incorporate such effects, we employ the approach suggested by Wang[170] to compute the corrected RPA predictions and henceforth we refer to such values as the mean-field ODT results.

2.2.3 Determining ODT

Three different measures were used to discern the location of $\chi_{ODT}N$ for the different systems:

(i) The structure factor of composition fluctuations was calculated as,

$$S(\boldsymbol{q}) = \frac{1}{4nN}\left\langle \left| \sum_{j=1}^{n}\sum_{s=1}^{N}[2\gamma(s)-1]\exp(-i\boldsymbol{q}.\boldsymbol{r}_j(s)) \right|^2 \right\rangle. \tag{2.7}$$

The contribution of dominant wavevectors to $S(\boldsymbol{q})$ is expected to be small in the disordered phase and considerably large in the ordered phase. Based on such expectations, we probed the measure $S_1 = \sum_j S(\hat{\boldsymbol{q}}_j)$ (where j indexes the wavevector, $\hat{\boldsymbol{q}}$ for which $S(\boldsymbol{q})$ is maximum. For instance, if the dominant contribution from 5 wavevectors is considered, $j = 1$ to 5.) and identified the χ at which S_1 undergoes a jump as the ODT.[1] As an alternate measure, we also probed $S_2 = \int S(q)^2 q dq$ which also undergoes a jump near the ODT[128] where $S(q)$ is spherically averaged structure factor. As we demonstrate later

[1]We thank Prof. David Morse for this suggestion.

(cf. discussion in the context of Fig. 2.2) the ODT computed from S_1 and S_2 were found to be in agreement with each other.

(ii) We computed anisotropy parameters f_2, f_4 which are defined as:[16]

$$f_n(q) = \frac{1}{2\pi}\left| \int_0^{2\pi} d\theta |F(\boldsymbol{q})|^2 \exp(in\theta) \right| \tag{2.8}$$

where

$$F(\boldsymbol{q}) = \int \hat{\phi}_A(\boldsymbol{r}) \exp(-2\pi i \boldsymbol{q}\boldsymbol{r}) d\boldsymbol{r}. \tag{2.9}$$

In the above, $\hat{\phi}_A(\boldsymbol{r})$ represents the averaged composition of A monomer (in contrast to the "instantaneous" compositions $\phi_A(\boldsymbol{r})$ in eqns. (6.3) and (6.4)) and $F(\boldsymbol{q})$ represents the fourier transform of such a quantity. The order parameters f_2, f_4 are zero in the disordered phase and are positive in ordered morphologies. For simplicity, we use a single dimensionless number, F_n to quantify the anisotropy parameter:

$$F_n = \frac{\int dq f_n(q)}{\sigma} \tag{2.10}$$

with

$$\sigma = \left[\frac{\int dq q^2 f_n(q)}{\int dq f_n(q)} - \left(\frac{\int dq q f_n(q)}{\int dq f_n(q)} \right)^2 \right]^{1/2}. \tag{2.11}$$

The order parameters F_2 and F_4 are also expected to display a jump near the ODT,[16] and we identified $\chi_{ODT}N$ as the onset of such a behavior.

(iii) We used the occurrence of a sharp change in average internal energy of the system as a function of χ to identify the ODT. We note that the internal energy of the system can exhibit hysteresis in the vicinity of first order

transitions. To account for such phenomena, we started the SCMF simulations from a disordered state and increased χ every 2×10^5 MCS (cooling run) and determined the average energy of the system as a function of χ. We also repeated such a process starting from an ordered state (high χ) by lowering the χ (heating run). In many cases, we observed that the average energy of the system in the heating and cooling runs were indistinguishable within numerical error of 0.25 in terms of χN (i.e. hysteresis loops were imperceptible, cf. Fig. 2.2(c)). We fitted the average energy data to a hyperbolic tangent profile and located the ODT as the χ at which average energy decreased to 20% of its high temperature value.

In Fig. 2.2, we depict a comparison of the results from the different measures used to locate the ODT. For illustrative purposes, we consider the block copolymer melt system having symmetric composition ($f = 0.5$) with different MW PDIs. In Fig. 2.2(a), we display the structure factor measures S_1 and S_2 which are seen to undergo a sharp jump near a critical χ which is identified as the ODT. Figure 2.2(b) displays the normalized anisotropy parameters, F_2 and F_4 which are also seen to undergo a sudden jump in the vicinity of the ODT. In Fig. 2.2(c) we depict the average energy and observe that the hysteresis effects between the heating and cooling protocols are minimal. In Fig. 2.2(d) we compare the ODTs discerned in Figs. 2.2(a-c) and observe that the χ_{ODT} values discerned from the different measures agree within a numerical resolution of 0.25 in χN. In the results below we base our discussion primarily on the ODTs located by the use of the anisotropy parameters F_2 and F_4.

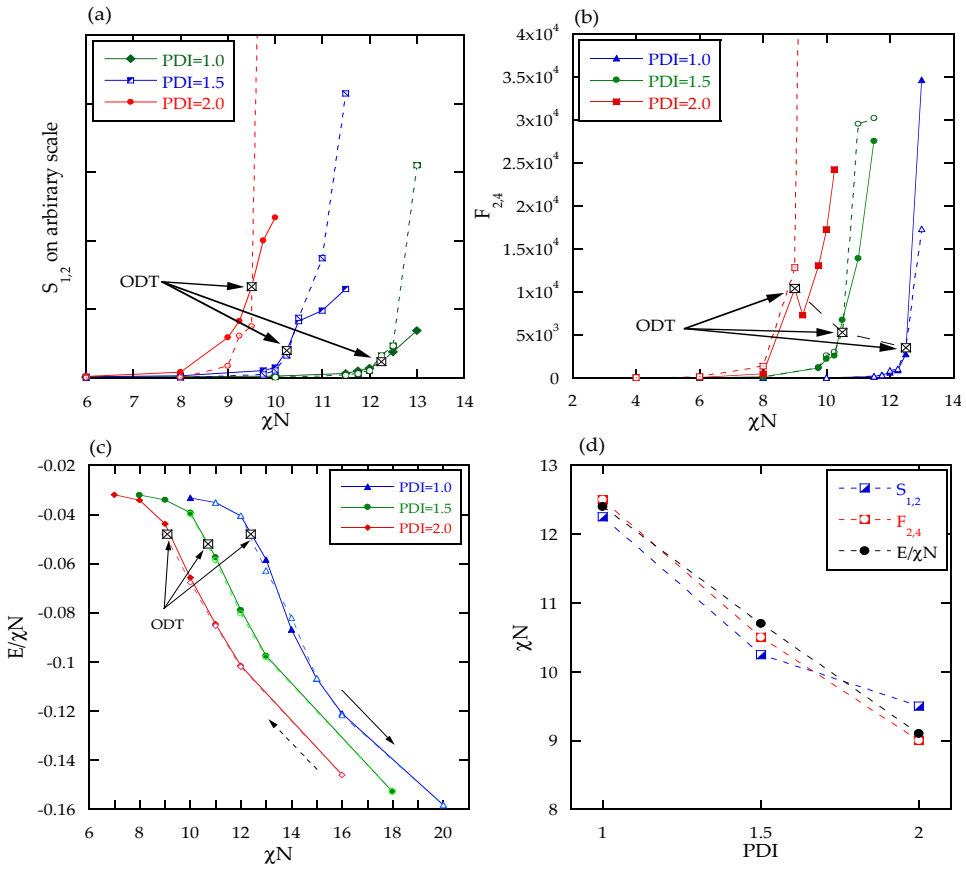

Figure 2.2: (a) Structure factor measures S_1 (filled) and S_2 (hollow) as a function of χN; (b) anisotropy parameters, F_2 (hollow) and F_4 (filled) as a function of χN; (c) Hysteresis loop in the average energy normalized by χN; and (d) Comparison of ODTs discerned by the measures depicted in (a)-(c). All plots correspond to 3D SCMF simulation of symmetric block copolymer melt ($f = 0.5$) for $C = 20$.

2.3 Results

In this section we present results quantifying the effect of fluctuations on the ODT of polydisperse copolymer systems. As a first step, we assess the ability of SCMF simulation method to quantitatively capture the fluctuation effects in (compositionally and MW) monodisperse copolymer melt systems. Subsequently, we present results which characterize the influence of fluctuations on MW and compositionally polydisperse copolymer systems.

2.3.1 Comparison of SCMF with Field-Theoretic Simulations (FTS)

In an earlier work, Daoulas and Muller extensively studied the ability of SCMF to capture fluctuation phenomena in polymeric systems.[48] Explicitly, they probed the structure factor, $S(q)$, in SCMF simulations and compared the results against the predictions of both RPA and the Fredrickson-Helfand (FH) one-loop fluctuation theory.[48, 106] Consistent with the expected influence of fluctuation effects, they found that $S(q)$ (where q^* denotes the wavevector corresponding to maximum in $S(q)$) calculated from the SCMF simulations deviated from the RPA predictions and displayed semi-quantitative agreement with the predictions of FH theory.[106]

While the study of Daoulas and Muller was insightful in clarifying the manifestation of fluctuation effects in SCMF simulations, their comparisons relied upon the FH approximation — a theory which is expected to be valid at only large values of C. To undertake a more rigorous quantification of the ability of SCMF to capture fluctuation effects, especially for smaller C, we

probed the ODT of *monodisperse* diblock copolymer melts within a two dimensional framework of the SCMF approach and compared our results with those reported based on the field-theoretic simulation (FTS) approach.[10] FTS is a methodology which directly samples the field-theory model by using either complex Langevin technique or MC simulation method. FTS has been used successfully in earlier works to study fluctuation effects in diblock copolymers,[10, 171] polymer blends,[16, 17] polymer solutions,[169, 172, 173] and polyelectrolytes.[174] Since FTS makes no approximation to the underlying field theory, a comparison to FTS is expected to be a stronger test of the ability of SCMF to capture fluctuations.

In Fig. 2.3 we display a comparison of the fluctuation-induced shifts in the ODT from the mean field value deduced from FTS and SCMF approaches. It can be observed that the results of SCMF quantitatively tracks the ODTs reported using the FTS methodology. Interestingly, such agreement seems to hold even for $C = 30 - 40$, for which the fluctuation effects are expected to be significant. These results serve to confirm that SCMF can indeed be used as a tool to quantitatively assess the effect of fluctuations upon the ODT of *polydisperse* diblock copolymer melt systems.

2.3.2 Fluctuation Effects in Symmetric Block Copolymers with MW Polydispersity

In this section, we present results for the effect of fluctuations on the ODT of symmetric ($f = 0.5$) block copolymer melts exhibiting MW polydis-

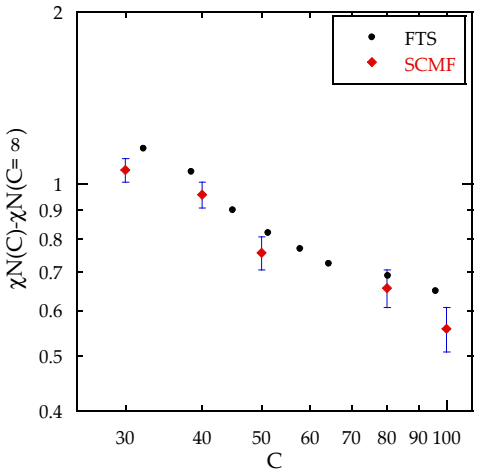

Figure 2.3: The fluctuation induced shift in ODT for symmetric monodisperse diblock copolymer melt as a function of Ginzburg parameter (C) obtained from two-dimensional FTS(•)[10] and SCMF(⧫) simulations. $N = 40$, the simulation box length of $8R_g$ with a discretization of $0.125R_g$ has been utilized for both simulations. The error bars on SCMF data correspond to a deviation of 0.1 in χN from the reported ODT. The error bars for SCMF results correspond to the resolution with which of χ was varied in SCMF simulations for locating χ_{ODT}.

persity. As discussed in the introduction, mean-field theories for MW polydisperse symmetric copolymers predict that an increase in the polydispersity should lead to a decrease in the χ_{ODT}.[131–133] While the experimental trends qualitatively agree with such predictions, significant quantitative discrepancies have been noted. Explicitly, in Fig. 2.4 we display a comparison of the experimental results of Lynd and Hillmyer [124] and the respective mean-field ODTs. Shown alongside are also the corresponding MC simulation results of Beardsley and Matsen which shows the upper and lower bound of hysteresis loops observed for a particular system size.[128] We note that the experimental results used the mean-field value of monodisperse (PDI = 1.0) block copolymers to parametrize χ, and hence the displayed values are only appropriate for examining the influence of PDI on the relative deviation of the ODTs from the MFT predictions. In Fig. 2.4, it can be seen that the experimental results show only a slight decrease in absolute values of the $\chi_{ODT}N$ with increasing PDI, which contrasts with the significant slope exhibited by the mean-field predictions. As a consequence, the deviations between the experimental results and the mean-field predictions are seen to increase with increasing polydispersity. The MC simulation results on the other hand are seen to exhibit an almost constant χ_{ODT} with variations in PDI.[128]

In this section, we present the results of SCMF simulations effected in two dimensions (with the polymer chains evolved in three dimensions) to address the influence of the C parameter upon fluctuation effects. Specifically, we are interested in probing whether the differences between experimental obser-

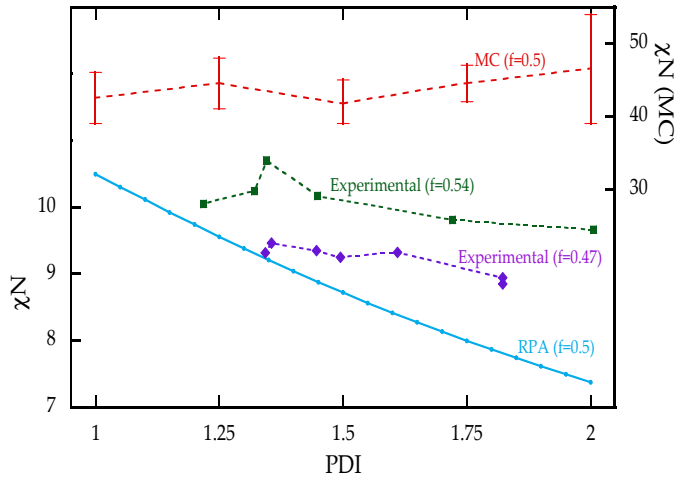

Figure 2.4: Experimental data by Lynd and Hillmyer adopted from Ref. [124] for nearly symmetric (filled diamonds and squares) poly-(ethylene-alt-propylene)-b-poly(DL-lactide) diblock copolymers having polydispersity in one block plotted with respective mean-field ODT. The MC simulation data by Beardsley and Matsen from Ref. [128] for a specific system size ($L = 54$ lattice units) is also shown. The limits of error bars correspond to the upper and lower bound of hysteresis loops presented in Ref. [128]. The lines are meant to be a guide to the eye.

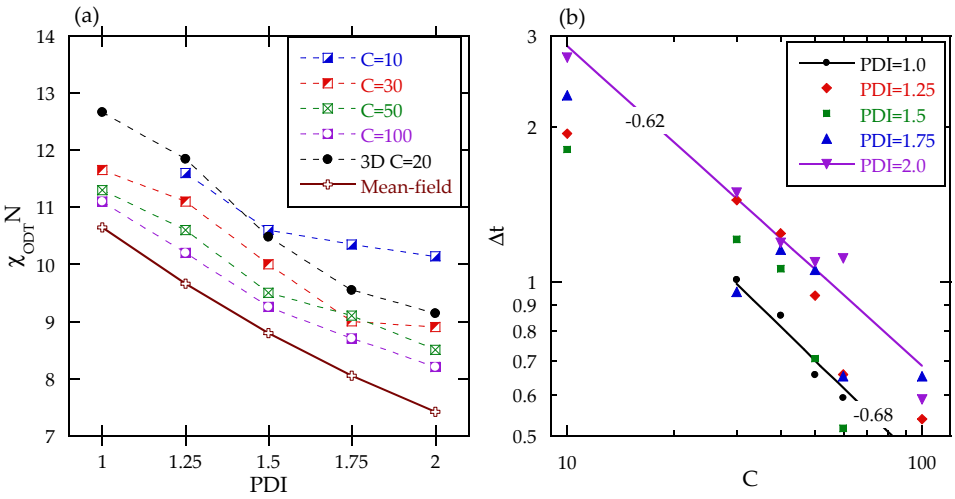

Figure 2.5: (a) Effect of B-block polydispersity for a symmetric melt on χN_{ODT} as a function of PDI as characterized by Ginzburg parameter (C). We also display a result from 3D simulations at $C = 20$ to characterize the influence of dimensionality on the ODT. The lines are guide to the eye. (b) Effect of B-block polydispersity for a symmetric melt on fluctuation induced shift in ODT temperature relative to mean field value (Δt) as a function of Ginzburg parameter (C) for different PDI. Δt approximately follows a power law with respect to C and the power law slopes of these lines (indicated in the figure) are seen to be approximately the same (within statistical error of 0.1 in χN).

vations, mean-field predictions and the simulation results depicted in Fig. 2.4 can be understood as a consequence of the influence of C and fluctuations. Towards this objective, we use the measure Δt which represents the shift of $\chi_{ODT}N$ discerned from SCMF from the corresponding mean-field predictions and probe its dependence upon C.

Figure 2.5(a) displays $\chi_{ODT}N$ as a function of PDI for different C values. We observe that the fluctuation-influenced $\chi_{ODT}N$ decreases with increasing PDI — a trend which is similar to that of the mean-field predictions.

Moreover, we also display a comparison to the results of 3D simulations for $C = 20$, which indicate trends which are semiquantitatively similar to that of 2D simulations. To understand more clearly the influence of fluctuations on the PDI, in Fig. 2.5(b) we display the fluctuation-induced shift of $\chi_{ODT}N$ from the mean field predictions as a function of the Ginzburg parameter, C. Consistent with expectations, the deviations from the mean field predictions are seen to increase with decreasing C parameter. Explicitly, the deviations Δt are seen to follow approximately a power law behavior $C^{-\alpha}$ with $\alpha \simeq 0.62 - 0.68$, which indicates an agreement of SCMF results with the mean-field predictions for $C \to \infty$. More interestingly, fluctuation-induced shifts in the ODT at higher PDI are seen to be generally higher than the corresponding values at lower PDI. As a consequence, we observe that the slopes of the χ_{ODT} vs. PDI curves in Fig. 2.5(a) decrease in magnitude with decreasing C, and there is a gradual flattening of the dependence of the fluctuation-induced ODTs upon the PDI.

The above results (specifically, those presented in Fig. 2.5(b)) indicate that fluctuations have a stronger influence on the $\chi_{ODT}N$ for higher PDI systems. Moreover, the displayed SCMF results are also consistent with the associated experimental observations[124] and indicate a gradual flattening of the χ_{ODT} behavior (as a function of PDI) at smaller C (as discussed earlier, the experimental results correspond to Cs which are smaller than those probed in our simulations). We also note that the above results help rationalizing the discrepancies between the Matsen's simulations results[128] and experiments.[124]

Explicitly, we note that Matsen's simulations correspond to a lower C (corresponding to $\bar{N} = 100$) compared to the experiments ($\bar{N} = 300, 1200$), and hence is expected to exhibit a lower slope of $\chi_{ODT}N$ vs. PDI behavior. Such an expectation is consistent with the results displayed in Fig. 2.4.

2.3.3 Fluctuation Effects in Asymmetric Copolymers with MW Polydispersity

In this section, we present results quantifying the interplay between PDI and C in influencing the ODT of compositionally asymmetric copolymers. As discussed in the introduction, experiments of Lynd and Hillmyer[124] have demonstrated that when the polydisperse block is the majority component ($f > 0.5$), $\chi_{ODT}N$ increases with increasing polydispersity. In contrast, for $f < 0.5$, the $\chi_{ODT}N$ was seen to decrease with PDI, a behavior which was consistent with the situation of symmetric copolymers. Interestingly, the mean field predictions for both $f \leq 0.5$ and $f > 0.5$ indicate a decrease in $\chi_{ODT}N$ with increase in polydispersity. Motivated by such discrepancies, in this section we present the results for the ODT of asymmetric diblock copolymers having MW polydispersity in the majority component ($f > 0.5$). Our objective is to discern the specific roles of C and PDI on the deviations from the mean field predictions and thereby probe whether the deviations from MFT noted in experiments arise as a consequence of fluctuations. We note that previous studies have reported that asymmetric polydisperse copolymer melts may form gyroid/perforated lamellar phases,[123, 124, 129] and hence we used three-dimensional simulations to study the effect of MW polydispersity in

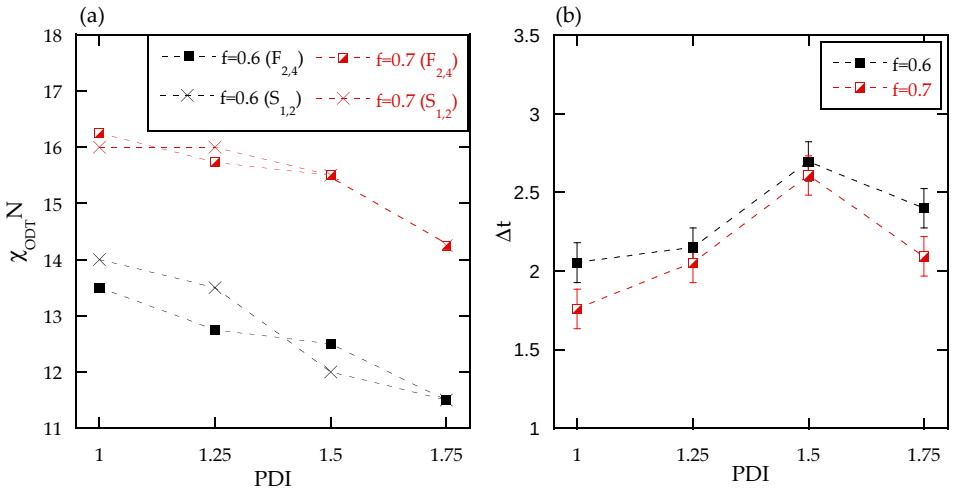

Figure 2.6: Variations in (a) $\chi_{ODT}N$ and (b) fluctuation-induced shift in the ODT (Δt), with PDI. The results correspond to three-dimensional SCMF at $C = 20$. To avoid clutter, we have only plotted the Δt values determined from $F_{2,4}$ measures. The statistical error is of the order of 0.25 in χN. The lines are a guide to the eye.

asymmetric copolymers. Due to the computationally expensive nature of such simulations, most of our results are for a fixed value of Ginzburg parameter corresponding to $C = 20$ (except for $f = 0.7$, as we discuss later).

We display the SCMF results for the ODT of asymmetric copolymers in Fig. 2.6(a) for $f = 0.6$ and 0.7. Overall, for both fs, we observe that $\chi_{ODT}N$ decreases with increasing MW polydispersity. Moreover, from the results displayed in Fig. 2.6(b), we observe that the deviations from the mean-field predictions, Δt, increases with increasing PDI (within numerical error, the Δt results for PDI = 1.75 are comparable to those of PDI = 1.5). Overall, these trends match with the results discussed for $f = 0.5$ in the previous

section.

While the fluctuation effects are seen to be enhanced with increasing PDI, our results for $\chi_{ODT}N$ do not agree with experimental trends discussed in the beginning of the section. Explicitly, despite the stronger fluctuations at higher PDIs we do not observe an increase in $\chi_{ODT}N$ with increasing polydispersity in asymmetric copolymers. We speculate that a possible resolution between our simulation and experiments could be that the invariant degree of polymerization used in our study ($C = 20, \bar{N} = 86.4 \times 10^3$) is higher than that used for experiments ($\bar{N} = 300$) and in other simulations ($\bar{N} = 100$). We recall that results from the previous section indicated that for smaller Cs (or $\bar{N}$) the effect of fluctuations for larger PDIs becomes stronger so as to cause flattening of the slope of $\chi_{ODT}N$ vs. PDI curves. One may speculate that for even smaller $\bar{N}$s the fluctuation effects become even stronger so as to cause an increase in $\chi_{ODT}N$ as a function of PDI.

In support of the above conjecture, we demonstrate that the effect of C on the ODT of asymmetric block copolymers at different PDIs is similar to that observed in the previous section for symmetric copolymers. Towards this objective, we simulated an asymmetric copolymer system ($f = 0.7$) for $C = 10$, and in Fig. 2.7b, we compare the results for the deviation of the ODT from mean-field predictions (Δt) for $C = 10$ and 20. With decreasing C, we observe a larger slope in Δt vs PDI trends, a behavior which is consistent with the increased influence of fluctuations for larger PDI. In turn, such effects manifest as a smaller slope for χ_{ODT} vs PDI (see Fig. 2.7(a)). While we were

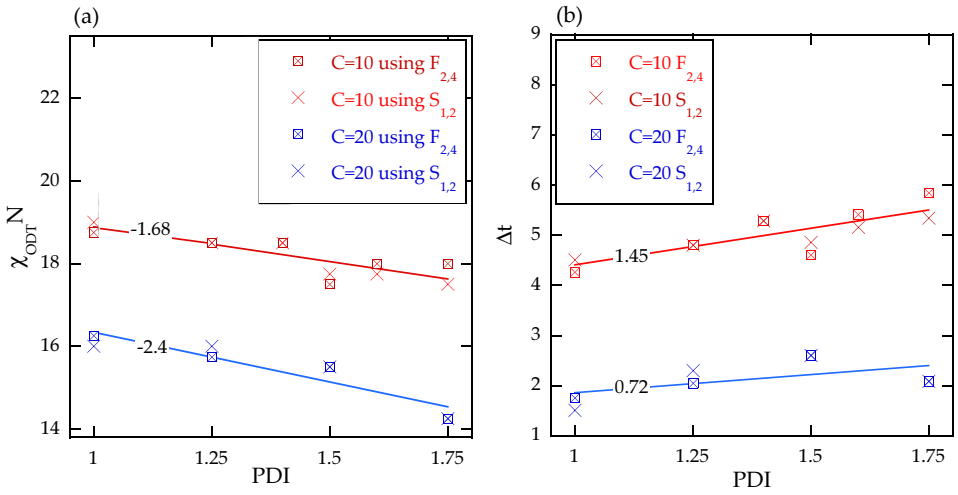

Figure 2.7: Variations in (a) $\chi_{ODT}N$ and (b) Δt with PDI for $f = 0.7$ compared for different C values. The numbers denote the slope of linear fits to the data.

unable to observe an increase in $\chi_{ODT}N$ with PDI at $C = 10$, we note that the corresponding $\bar{N} = 21.64 \times 10^3$ is still considerably larger than the experimental values. Unfortunately, as discussed earlier, probing of even smaller C would require us to more carefully account for discretization effects, and hence we do not embark on such an undertaking in this work. However, the displayed results still supports the hypothesis that experimentally observed trends and the deviations from mean-field could be a consequence of the enhanced influence of fluctuations at smaller C for larger PDI systems. Moreover, our results point to an interesting experimentally testable prediction that for asymmetric copolymers, larger values of invariant degree of polymerization would lead to a decrease in the $\chi_{ODT}N$ with increasing PDI.

2.3.4 Fluctuation Effects in Compositionally Polydisperse Diblock Copolymers

In this section, we present the results for fluctuation induced shift in the ODT in compositionally polydisperse block copolymer melts represented by the composition profiles described in Sec. 2.2.1. We consider only symmetric copolymers ($f = 0.5$) and use the parameter Δ (cf. Sec 2.2.1) to quantify the compositional polydispersity of the sequences. Similar to the approach adopted in the previous section, we identify the influence of fluctuations by comparing the SCMF results with the predictions of RPA theory.

In Fig. 2.8(a) we display the SCMF results for χ_{ODT} for the system of quenched ensemble of sequences. To quantify the effect of fluctuations more directly, in Fig. 2.8(b) we display Δt which represents the deviation of the SCMF results from the mean-field predictions. Overall, we observe that compositionally monodisperse diblock copolymers exhibit the least influence of fluctuations and that the fluctuation-induced shift in the ODT increases with increasing compositional polydispersity (Δ) of the copolymers. Moreover, as observed earlier in case of MW polydisperse block copolymers (cf. Secs. 2.3.2 and 2.3.3), the influence of fluctuations is seen to increase with decreasing C.

As discussed in Sec. 2.2.1, our "quenched" model which contains an ensemble of sequences also serves as a representation for a system of blocky, tapered copolymers with average composition profiles depicted in Fig. 2.1 (annealed system). In this context, we note that the mean-field (RPA) predictions for the quenched and annealed systems exhibit contrasting trends with

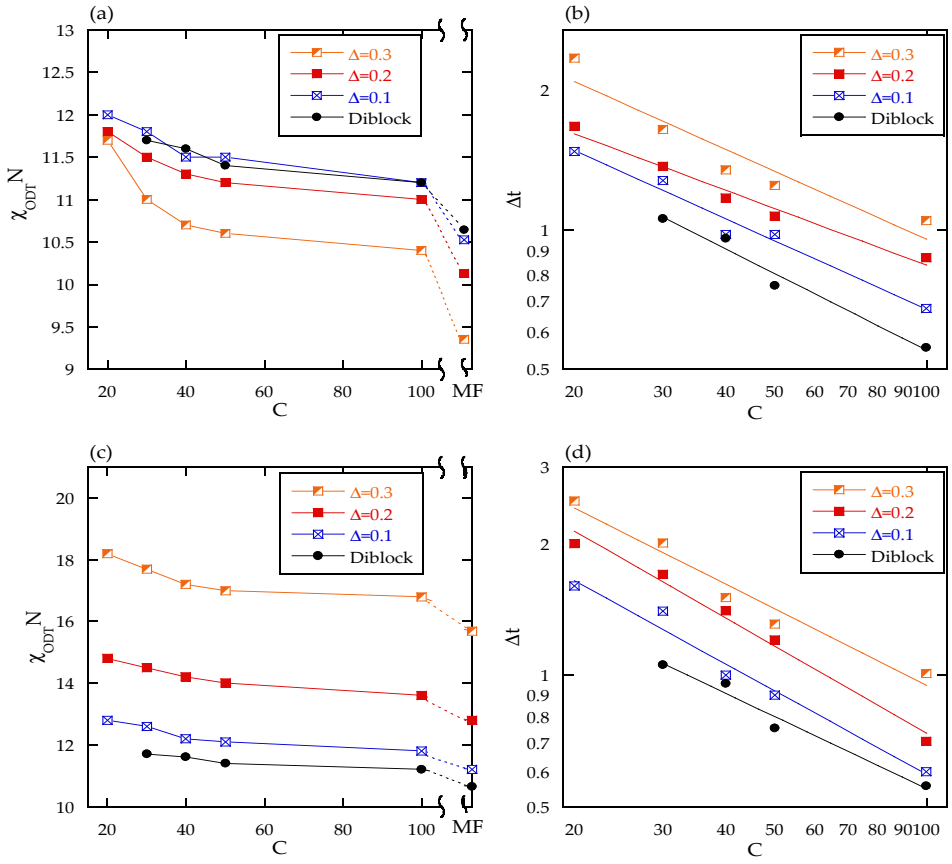

Figure 2.8: Variation in $\chi_{ODT}N$ with Ginzburg parameter, C for (a) quenched and (c) annealed representation of sequence. Fluctuation-induced shift in the ODT of (b) quenched and (d) annealed representation of sequences for compositionally polydisperse block copolymer systems. The statistical error is of the order of 0.1 in χN.

increasing compositional polydispersity. Explicitly, for the system of quenched ensemble of sequences, the mean-field predictions for $\chi_{ODT}N$ are $9.35, 10.13$ and 10.52 respectively for $\Delta = 0.3, 0.2$ and 0.1 (i. e. ODT increases with decreasing Δ). In contrast, for the annealed, tapered copolymer system the mean-field predictions for the $\chi_{ODT}N$ are $15.69, 12.8$ and 11.2 respectively for $\Delta = 0.3, 0.2$ and 0.1 (i. e. ODT decreases with decreasing Δ). Hence, it is of interest to consider the influence of fluctuations upon the annealed model and probe the differences, if any, with the quenched ensemble of sequences.

In Fig. 2.8(c) and (d), we display the corresponding SCMF results for the annealed system of tapered copolymers. Interestingly, despite the contrast in the mean-field dependence of χ_{ODT} upon Δ, we observe that both quenched and annealed ensemble displays similar trends with respect to the influence of fluctuation effects. Specifically, we observe that an increase in Δ (representing the gradient strength of the annealed representation) increases the influences of fluctuations. Moreover, the annealed and quenched systems are seen to exhibit quantitatively comparable magnitudes of deviations in ODT from the corresponding mean-field predictions. Overall, these results suggest that similar fluctuation effects manifest in quenched and annealed systems and indicates that the sequence polydispersity effects play only a secondary role in the influencing the fluctuation effects upon ODT.

2.4 Summary

In this chapter, we presented results quantifying the effects of fluctuations on MW polydisperse (AB diblock copolymers having polydispersity in B block length distribution) and compositionally polydisperse (quenched and annealed ensemble of symmetric gradient copolymer melts) copolymer melts using single chain in mean field simulations. The strength of fluctuations was characterized by the Ginzburg parameter (C) representing the number of polymer chains per unit volume. We demonstrated that both compositional and MW polydispersity can have a significant impact on fluctuations near the order-disorder transition.

For diblock copolymer melts having symmetric composition, MW polydispersity was seen to enhance the strength of fluctuations. For symmetric diblock copolymers, $\chi_{ODT}N$ was found to decrease with increasing PDI which was consistent with experimental observations (cf. Fig. 2.4). Also, the magnitude of the slope of the variation in $\chi_{ODT}N$ with PDI decreased with decreasing C suggesting that the deviations of the ODT from mean-field predictions increase at higher PDI. Such behavior was in agreement with the experimentally observed deviations. For asymmetric diblock copolymers ($f > 0.5$), we observed a decrease in $\chi_{ODT}N$ with increasing MW polydispersity. While this trend does not agree with the experimental observations,[124] we suggested that the increased influence of fluctuations with increasing PDI for lower C values may explain the ODT behavior in experiments. For compositionally polydisperse diblock copolymers, we observed that the compositional polydis-

persity increases the strength of fluctuations. Moreover, we observed similar trends in fluctuation effects for quenched and annealed representation of sequences.

In contrast to the extensive theoretical frameworks which have addressed fluctuation effects in monodisperse block copolymer systems, comparable analytical results do not exist for composition and/or MW polydisperse systems. The simulation results presented in this chapter serve to fill this void by presenting results, albeit numerical, quantifying the influence of fluctuations as a function of the degree of polydispersity. Such results are expected to be useful both in the context of interpreting experiments and in the validation of analytical theories. In a next chapter, we demonstrate that the results presented herein prove useful for the interpretation of fluctuation effects in polymer blends containing different architectures of block copolymer compatibilizers.

Chapter 3

Efficacy of Different Block Copolymers in Facilitating Microemulsion Phases in Polymer Blend Systems

3.1 Introduction

In this work we are concerned with a mixture of two homopolymers (denoted as A and B) of equal molecular weight (MW) mixed with block copolymers. In the case when the ternary blend contains AB diblock copolymers, mean-field theories[175–183] have suggested that the phase behavior of such a ternary system is governed by the following parameters: (i) Ratio of the chain lengths of the homopolymer to copolymer, denoted as α in this chapter; (ii) Total volume fraction of homopolymer, denoted as ϕ_H; (iii) The composition of the copolymer, denoted as f; and (iv) The incompatibility between the A and B monomers characterized by the Flory-Huggins interaction parameter (χ). A schematic phase diagram for the case when the system consists of symmetric ($f = 0.5$) AB copolymers mixed with A + B polymer blend is shown in Figure 3.1. For small homopolymer volume fractions (ϕ_H), ordered lamellar phase is observed at low temperatures. The lamellar microstructure persists for increasing ϕ_H, however with increasing domain sizes. Beyond a critical ϕ_H, the lamellar phase "unbinds" to lead to macrophase segregation.[184] Theoretical

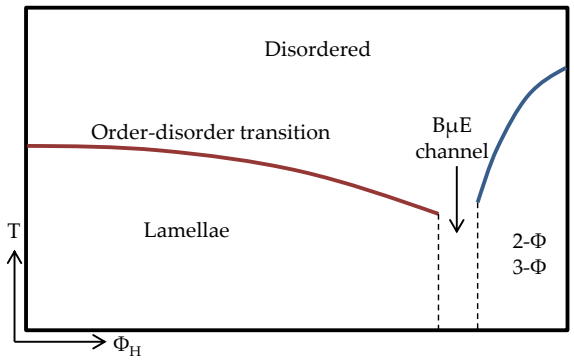

Figure 3.1: Schematic of phase diagram of ternary symmetric blend of homopolymers with copolymer. ϕ_H denotes the total homopolymer volume fraction and T represents temperature.

and experimental results have suggested that between the two-phase (2ϕ) and lamellar region, a narrow channel of bicontinuous microemulsion (BμE) phase is formed as a result of thermal fluctuations.[11–21] Such phases constitute the focus of this chapter.

In contrast to conventional oil-water microemulsions, polymeric BμEs possesses characteristic lengthscales of approximately 100 nm,[185] and large surface areas, rendering them ideal candidates for synthesizing nanoporous materials with uniform pore sizes.[185–188] Not surprisingly, such phases have attracted attention in the context of various applications such as catalysis,[189] gas storage,[190] electronic devices,[191] separations and drug delivery,[192] etc. The first experimental evidence of BμE using block copolymers was found in late 90's by Bates and coworkers.[13–15, 193] However, despite the initial flurry of activity accompanying the discovery of BμE phases,[11, 13–17, 19–

21, 180–182, 194–198] very little progress has been achieved in the systematic design of ternary blend systems which can allow versatile access to such phases.

Polymeric BμE phases owe their origin to thermal fluctuation effects,[14, 16, 17] which are not captured in mean-field approaches such as self-consistent field theories.[2–4] Hence, initial theoretical and computational studies of such morphologies were limited to indirect approaches to identify the optimal formulations for accessing polymeric BμE phases. For instance, Matsen and coworkers used mean-field theories to identify different characteristics of the block copolymer which could optimize the formation of BμE phases in ternary polymer blend systems.[180, 181, 199–201] Specifically, Thompson and Matsen[201] demonstrated that in ternary blends of homopolymers with diblock copolymers, the copolymers form inflexible monolayers which tend to attract each other. Moreover, if the attraction is significant, they suggested that the copolymer monolayers tend to expel the homopolymer and lead to macrophase segregation. By using mean-field calculations,[2–4] Thompson and Matsen predicted that introducing polydispersity in block copolymers can overcome the attraction between the copolymer layers and also endow them with appropriate flexibility to improve the formation of polymeric BμE phases. In a different context, Fredrickson and Bates[12] have used mean-field theories to identify the location (in the $\chi - \phi_H$ space) of the transition between lamella and two phase region to suggest strategies to improve the formation of polymeric BμE phases.

Recently however a number of computational approaches have been de-

veloped to study fluctuation effects in polymeric systems[3, 4, 16, 17, 47, 48, 111, 118–120] which have enabled the study of polymeric microemulsion phases. For instance, Duchs and coworkers,[16, 17] used field theoretic simulation (FTS)[3, 4] methodology effected in two-dimensions to study fluctuation effects in the ternary homopolymer/diblock copolymer blend system. Their results for order-disorder transition (ODT) showed qualitative agreement with the experimental phase diagram. Moreover, they found evidence of a narrow channel of BμE phase consistent with the experiments. More recently, Sun and Guo[202, 203] studied the phase behavior and interfacial properties of the ternary homopolymer/gradient copolymer blends using Monte Carlo simulations. Their studies suggested that the gradient copolymers possessing a larger width of composition distribution are capable of forming soft monolayers and are more efficient in forming BμE phases.

Inspired by the above developments, in this work we use the computational methodology of single chain in mean field (SCMF) approach to study directly the efficacy of different copolymer formulations in promoting the formation of polymeric BμE phases in ternary blend systems. Specifically, we consider the following classes of compatibilizers:

(a) Monodisperse diblock copolymers (D): Most of the research related to the formation of BμEs has been focussed on diblock copolymers having (approximately) monodisperse MW distribution. In this work, we consider monodisperse diblock copolymers: (i) To use the existing results in the context of such copolymers to validate our simulation method and analysis; and (ii)

To compare the efficacy of such systems against other copolymer architectures (discussed below).

(b) Diblock copolymers having bidisperse MW distribution (BDL): Study of this system has been motivated by the work of Thompson and Matsen[200] which indicated that MW polydisperse block copolymers are more efficient in forming BμE phases. We seek to examine the correlation between interfacial properties and the onset of BμE formation in such systems and compare the efficacy of BDL system as compared to D system.

(c) Diblock copolymers having polydispersity in one of the blocks (PD): MW polydisperse copolymers have been predicted to be better compatibilizers compared to monodisperse diblock copolymers, as they create a more gradual interface which suppresses the attractive interactions between diblock monolayers.[200] In contrast however, experiments found a shift in the BμE channel towards higher copolymer volume fractions[20]. We simulate the PD system and compare our results with experimental observations and probe whether diblock copolymers with MW polydispersity in a single block do exhibit better propensity to form BμEs.

(d) Diblock copolymers having bidisperse composition (BDC): We simulate a mixture of diblock copolymers having monodisperse MWs but different compositions (f). Using bidispersity in composition have shown to greatly influence the interfacial properties in case of random copolymers.[204] We seek to examine if imparting similar compositional polydispersity in block copolymers could also lead to improvement in the formation of BμE.

(e) Gradient copolymers (G): Gradient copolymers possess a gradual change in the composition along the chain length[68, 69]. Such systems have recently attracted significant attention due to their promising interfacial properties. Prior studies have confirmed that gradient copolymers in homopolymers preferentially phase segregate to the interface and stabilize the blend.[64, 202] Sun and Guo [203] recently reported that the copolymers having larger width of gradient composition occupy larger interfacial area and form softer monolayers and are more efficient in forming BμEs. Motivated by such observations, in this work we study the effect of different sequence distributions of gradient copolymers in influencing the formation of BμE phases.

An "optimal" formulation of copolymer can serve to aid in the formation of BμE phases by two means: (i) Ensure that the BμEs are formed with the minimum amount of copolymers. Since the copolymer is typically the most expensive component in the blend, this issue has important implications in rendering the process economically feasible; and (ii) Increase the overall area of phase diagram occupied by the BμE phases to allow access to such morphologies for a wider range of parameters. Motivated by such considerations, in this work we use SCMF methodology to study both the onset of formation of BμE and the width of the BμE region for the different compatibilizer systems. We hypothesize that the property (i) above is likely to be related to the interfacial activity of the compatibilizer in a polymer blend system,[180, 199–201] and use polymer self-consistent field theory to quantify the interfacial activity of the different copolymer formulations and thereby

understand the trends observed in the onset of formation of BμE phases. We propose that the property (ii) is more closely related to the influence of thermal fluctuations in ternary blend systems, and use considerations relating to fluctuation effects in the corresponding copolymer systems to justify the roles of different compatibilizers.

The rest of this chapter is arranged as follows. In Section 3.2, we describe the models used for the systems considered in this study and outline the details of our simulation framework including the methodology used to identify BμE phases. In Section 3.3, we present results for the interfacial tension and the phase diagrams of ternary blend. We discuss the observed phase boundaries of BμE in terms of the interfacial activity and the fluctuation effects in the respective systems.

3.2 Simulation Details

3.2.1 Model Copolymer Systems

The following presents the model details and the terminology of the different copolymer systems we have studied in the context of ternary homopolymer/copolymer blend system. In all cases, the copolymer chain length was fixed at $N = 50$.

1. **D**: Monodisperse diblock copolymer having symmetric composition, $f = 0.5$.

2. **BDL**: Bidisperse diblock copolymers containing equal number of long ($N_1 = 70$) and short ($N_2 = 30$) symmetric diblock copolymers each with a fixed composition $f = 0.5$.

3. **PD**: Polydisperse diblock copolymer having MW polydispersity in B block. We choose a polydispersity index, PDI= 1.5 and possessing a symmetric composition ($f = 0.5$) on an average. We chose the MW of the B blocks based on a Schultz-Zimm distribution.[152, 153] In such a model, the probability $p(N_B)$ that the B-block has N_B segments is given as:

$$p(N_B) = \frac{k^k N_B^{k-1}}{(N_B)_{avg}^k \Gamma(k)} \exp\left(- \frac{kN_B}{(N_B)_{avg}} \right). \tag{3.1}$$

In the above, the parameter k is related to polydispersity index (PDI) through PDI $= (k+1)/k$ and $(N_B)_{avg}$ is the average number of segments in the distribution; and $\Gamma(k)$ denotes the Gamma function.[154] The number of segments in A block (N_A) is fixed to 25 and the average composition f is related to $(N_B)_{avg}$ as $f = (N_B)_{avg}/(N_A + (N_B)_{avg})$.

4. **BDC**: MW monodisperse diblock copolymer containing a 50-50 mixture of diblock copolymers having compositions; $f_1 = 0.75$ and $f_2 = 0.25$.

5. **G1**: Symmetric ($f = 0.5$) gradient copolymer exhibiting tangent hyperbolic composition profile. To model such systems, we considered an *ensemble* of sequences such that the average composition of the ensemble $f(i)$ at the segment index i ($= 1 \cdots N$) follows a tangent hyperbolic

profile of the form,

$$f(i) = \frac{1}{2}\left[1 + \tanh\left(A\pi(\frac{i}{N} - \bar{f}^*)\right)\right]. \tag{3.2}$$

In the above expression $\bar{f}^*$ is a parameter chosen such that the overall average composition of B monomers in the melt matches the specified average composition (f). The parameter A controls the steepness of the gradient profile. Systems corresponding to large A values are referred to as strong gradient copolymers, whereas, those possessing small A values are termed as weak gradient copolymers. In our earlier work,[205] we pointed out that in consideration of such ensembles of sequences, the blockiness of the sequences (denoted as λ, $0 \leq \lambda \leq 1$) emerges as an additional important parameter. In physical terms, λ is a nondimensional parameter which quantifies the correlations along a single polymer chain and represents the size of continuous sequences of the monomers of the same chemical identity. In other words, a large (small) λ corresponds to an ensemble of sequences consisting of chains which possess large (small) blocks of A and B segments.

In the present work, we seek to quantify the effects of compositional gradient and sequence blockiness of the copolymeric system upon the phase behavior of ternary homopolymer/copolymer system. In this context, we use $\lambda = 0.1$ and 0.7 for $A = 1$ as a model for polymers possessing weak compositional gradient, and having non-blocky and blocky sequences respectively. To generate sequences of gradient copolymers having specified

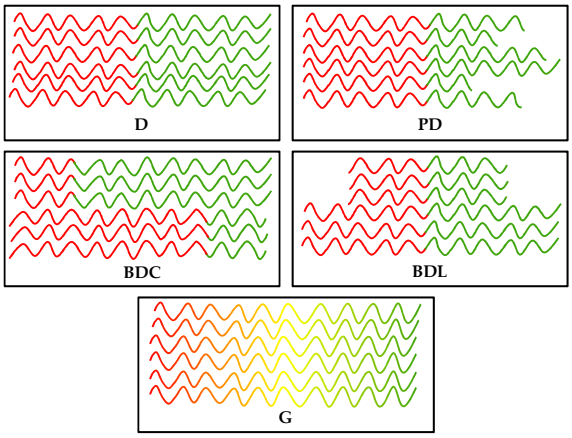

Figure 3.2: Schematic representation of polydisperse copolymer sequences utilized in this study.

composition profile and blockiness, we adopt the methodology proposed in our earlier work.[205]

The schematic representation of ensembles of the above model copolymer systems is depicted in Figure 3.2.

3.2.2 SCFT and Interfacial Tension

The formation of BμE phases has typically been associated with ultralow interfacial tensions of the homopolymer/copolymer blend system.[206] Based on such considerations, we speculate that the onset of formation of BμE phases are likely to correlate to the interfacial activity of the copolymers. In this work, we use the changes in the interfacial tension of polymer blend resulting from the addition of copolymers as a measure of the interfacial activity of the compatibilizer. Strictly speaking, a quantification of interfacial activity

also requires consideration of properties such as bending modulus, saddle-splay modulus, etc.[199, 200, 207] However, since we mainly propose to use such measures to qualitatively understand the phase behavior of the ternary blend, in this work we restrict our considerations to just interfacial tension as a measure of interfacial activity.

Quantifying interfacial tension requires free energy of the ternary blend system, a quantity whose calculation is computationally involved in fluctuation based approaches.[208] In this work, we instead opt to use the mean-field framework of polymer self-consistent field theory (SCFT). The details of our SCFT model closely resemble to that used in Matsen's studies [199, 207] to examine the interfacial properties of diblock copolymers. In our previous publication[205], we outlined the manner in which such SCFT formalism can be extended to compute the interfacial tension in systems containing an ensemble of chains of different characteristics. In a nutshell, the presence of an ensemble of MW or compositionally polydisperse sequences, requires us to modify the underlying field theory to incorporate the nature of individual sequence. At a practical level, this entails the solution of the diffusion equations arising in SCFT for each of the different chains.

3.2.3 Single Chain in Mean Field Simulations

To study the phase diagrams of ternary blend of homopolymer/copolymer systems, we used the single chain in mean field (SCMF) simulation methodology proposed by Muller and coworkers[47–53]. In SCMF methodology, the

intramolecular bonded interactions of the polymers are accounted in an exact manner, whereas, the nonbonded pairwise interactions are replaced by inhomogeneous potential fields acting on the polymer monomers. Such potential fields are expressed as a function of the spatially varying polymer densities and are determined instantaneously using inhomogeneous polymer densities.[47, 48, 146, 209] When the potentials are updated after each MC move, the SCMF simulation methodology generates configurations consistent with a prespecified Hamiltonian. SCMF-type approaches have been used to study the phase behavior of polymer blends,[47, 146, 209] block copolymers,[48, 147–149, 210] polymer nanoparticle mixtures,[150] and semiflexible copolymers.[151] In a recent study, we used SCMF methodology to probe the fluctuation effects in MW polydisperse block copolymer melts.[210] In order to test the capability of SCMF method to capture fluctuations, we also compared the fluctuation-induced shifts in order-disorder transition (ODT) of monodisperse diblock copolymer melts arising in the SCMF and field-theoretic simulation (FTS) methods. The comparison showed excellent agreement which suggested SCMF to be a suitable methodology for studying fluctuation phenomena in polymeric systems.

In this work, we adopted the SCMF approach because it provides a straightforward approach to study the equilibrium behavior of an ensemble of polymer chains differing in MW and/or sequence distributions without any additional computational cost relative to a monodisperse system. In this respect, SCMF offers advantages over other computational methods such as field

theoretic simulations.[3, 4] Moreover, due to the absence of direct pairwise intermolecular interactions, SCMF simulations can treat different chains as independent of each other (except at the step of updating the potential field). Hence, such methods enable significant parallelization and are computationally efficient compared to full scale MC simulations with pairwise interactions.[47]

In our SCMF framework, the polymer chain is represented by a Gaussian chain model having $N-1$ bonds per polymer. The bonded and non-bonded interactions are described by the following single chain Hamiltonian:

$$\frac{H[\boldsymbol{r}_i(s)]}{k_BT} = \sum_{s=1}^{N-1}\left[\frac{N-1}{4R_g^2}[\boldsymbol{r}_i(s)-\boldsymbol{r}_i(s+1)]^2 + \frac{(2\gamma(s)-1)w[\boldsymbol{r}_i(s)]-\pi[\boldsymbol{r}_i(s)]}{N-1}\right], \tag{3.3}$$

where $\boldsymbol{r}_i(s)$ denote the position of the s^{th} monomer on the i^{th} chain and R_g denotes the unperturbed radius of gyration, $R_g = b\sqrt{N/6}$, where b is the segment length. In the above, $\gamma(s) = 1$ if the segment s is A monomer and is 0 otherwise. The potential fields $w(\boldsymbol{r}_i(s))$ and $\pi(\boldsymbol{r}_i(s))$ acting on the polymer segments correspond to the saddle point solution of the corresponding field theory and are given by,[4, 48]

$$w(\boldsymbol{r}) = \frac{\chi N}{2}(\phi_A(\boldsymbol{r}) - \phi_B(\boldsymbol{r})), \tag{3.4}$$

$$\pi(\boldsymbol{r}) = \kappa N(\phi_A(\boldsymbol{r}) + \phi_B(\boldsymbol{r}) - 1). \tag{3.5}$$

where ϕ_α ($\alpha = A, B$) represents the instantaneous local volume fraction of α segments, χ denotes the Flory-Huggins interaction parameter which describes the incompatibility between A and B segments, and κ is a parameter inversely

proportional to the isothermal compressibility of the overall system.[48] In the above notation, $w_A = -w + \pi$ and $w_B = w + \pi$ are the fields acting on the A and B segments respectively.

The single chain Hamiltonian, $H[\boldsymbol{r}_i(s)]$ (Eq. 6.1), was sampled by MC simulation approach using Metropolis algorithm.[168] The monomer positions were evolved in three dimensions using random displacement MC moves. After every MC step (i.e. one MC attempt per monomer), we updated the fields $w(\boldsymbol{r}_i(s)), \pi(\boldsymbol{r}_i(s))$ based on the inhomogeneous volume fractions of A and B monomers. Additional details of the algorithm are described elsewhere [48].

As discussed in the introduction, the formation of BμE phases is driven by thermal fluctuation effects. Such fluctuation effects are in general influenced by the degree of overlap between monomers, which in turn is quantified by a parameter given as,[211]

$$C = \frac{Rg^3}{N} \sum_j \frac{n_j N_j}{V} \tag{3.6}$$

where n_j represents number of polymer chains of species j each having N_j segments and V represents the volume of the system. The parameter "C" is referred to as the "Ginzburg" parameter[3, 4, 10, 212] and for one component polymer systems its related to the commonly used invariant degree of polymerization, $\bar{N}$ as, $C \propto \bar{N}^{d/2-1}$ (with d denoting number of dimensions). In this work, we fixed the value of Ginzburg parameter, $C = 10$ and examined the influence of the architecture of the compatibilizer on the formation of BμE.

In our simulations, the ratio of chain length of homopolymer to copoly-

mer ($\alpha = N_h/N$), was fixed at 0.2. This value of α was motivated by our earlier study on fluctuation effects in ternary blend of homopolymer/block copolymer using FTS methodology[16]. Since the *qualitative* features of the influence of the fluctuations are expected to be similar in different spatial dimensions,[16, 210] we used simulations in two dimensions which allows access to a wider range of parameter space. Considering the longer lengthscales involved in the formation of BμEs, we utilized a simulation box size of $40R_g$ (which corresponds to 8×10^5 monomers for $C = 10$) and computational grid of 128×128. In all of our simulations, we used $\kappa N = 50$ to ensure a nearly incompressible system. The system was equilibrated for 1×10^6 MCS per monomer and thermodynamic quantities were averaged every 50 MCS per monomer for another 1×10^6 MCS.

3.2.4 Identifying Phase Boundaries

The phase behavior of the ternary blend of homopolymers and block copolymer considered in this work exhibits disordered, ordered lamellar, BμE and macrophase segregated morphologies for appropriate χs and volume fractions of the homopolymer. We used the structure factor of composition fluctuations, defined as,[48]

$$S(\boldsymbol{q}) = \frac{1}{4nN}\left\langle \left| \sum_{j=1}^{n}\sum_{s=1}^{N}[2\gamma(s)-1]exp(-i\boldsymbol{q}.\boldsymbol{r}_j(s)) \right|^2 \right\rangle, \tag{3.7}$$

as the primary quantity to identify the phase boundaries between disordered/ordered/BμE/macrop segregated morphologies (n is the total number of polymer chains in the system).

Macrophase segregation is observed when the wavevector q^* corresponding to the peak in spherically averaged $S(\boldsymbol{q})$ is identically zero.[18, 21] However, due to periodic boundary conditions in our simulations, macrophase segregation manifests as a small q^* which is close to zero. In contrast, transition from BμE and microphase separation into lamellar phase manifests in a peak at a finite q^*. To distinguish between the lamellar and BμE phases, we fit $S(q)$ to the Teubner-Strey functional form,[213]

$$S(q) = \frac{1}{w + gq^2 + cq^4} \tag{3.8}$$

and extract the coefficients w, g and c. Regimes in which $w > 0, q < 0, c > 0$ and $4wc - g^2 > 0$ are identified as BμE phases[213] and regimes for which these inequalities are not fulfilled is taken to correspond to lamellar morphologies. To illustrate, in Figure 3.3(a) we display representative q^* for two systems, D and BDL as a function of ϕ_H at $\chi N = 14$. We observe that for high ϕ_H systems, $q^* \backsimeq 0.4$ which corresponds to the macrophase segregated regime. For smaller ϕ_H systems, we observe a transition to a larger q^*. The boundaries between disordered/lamellar phase$-$BμE phase, and BμE$-$macrophase separated regions as deduced using the Teubner-Strey fit is displayed in the plot as dashed lines.

We note that in some other works, amphiphilicity factor[214–216] defined as,

$$f_a = \frac{g}{\sqrt{4wc}} \tag{3.9}$$

is used as a measure to identify the BμE phases. Specifically, $f_a < -1$ is

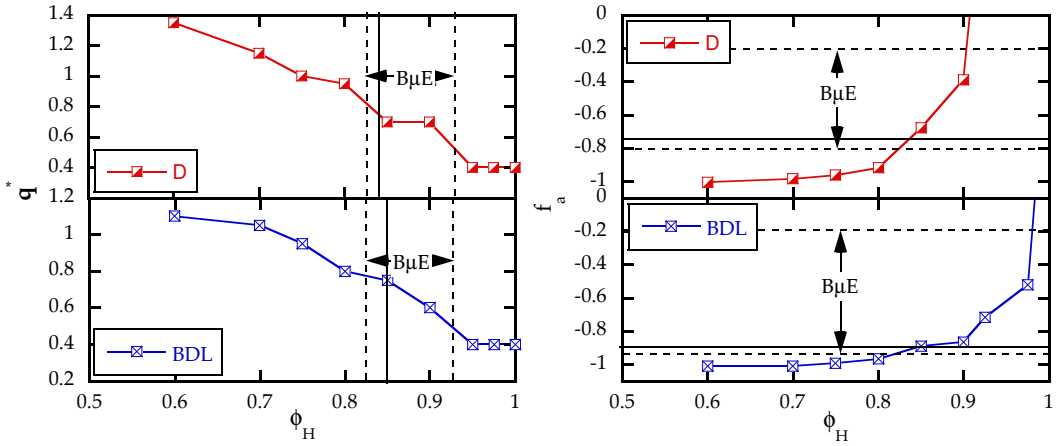

Figure 3.3: (a) The variation in the peak position of $S(q)$, q^* and (b) amphiphilicity factor, f_a with homopolymer volume fraction, ϕ_H for the homopolymer blend with copolymer corresponding to the model systems: D and BDL at χN=14. The dotted lines denote the approximate phase boundary of BμE phase determined using Teubner-Strey fit. The solid lines denote the phase boundary determined using graphical measure, D_c discussed in the text.

taken to correspond to a lamellar phase, whereas, BμE phases are identified as $-1 < f_a < 0$. In Figure 3.3(b) we present results for the Teubner-Strey fit in terms of the amphiphilicity factor as a function of ϕ_H and also depict the phase boundaries of Figure 3.3(a). It is seen that, the BμE phase boundaries determined by q^* (and Teubner-Strey fit) (Figure 3.3(a)) match closely with the BμE regimes suggested by amphiphilicity factor.

In addition to the structure factor measures, we also used a graphical analysis of the averaged volume fraction profiles to identify the BμE phase boundary on the copolymer rich side. To implement this approach, we convert

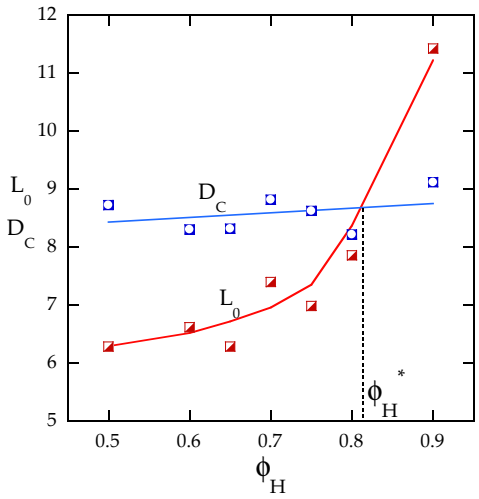

Figure 3.4: Variation in preferential lengthscale, L_0 and mean curvature diameter, D_C with homopolymer volume fraction, ϕ_H for BDL copolymer system at χ_N=14. The lines are guide to the eye.

the averaged composition profile, $\bar{\phi}_A(\boldsymbol{r})$ to a black and white image by assigning the white pixels to correspond to $0 \leqslant \bar{\phi}_A \leqslant 0.5$ and the black pixels to correspond to $0.5 < \bar{\phi}_A \leqslant 1$. We then calculate the mean curvature diameter given as,[17]

$$D_C = 2\left[\frac{1}{L_C}\int dx \left|\frac{d\boldsymbol{t}}{dx}\right|^2\right]^{1/2}. \tag{3.10}$$

In Eq. 3.10, L_C is the sum of all contour lengths of the microdomain boundaries and $\boldsymbol{t}$ is the tangent vector at a given position x along the contour. It was proposed by Duchs et al.[17] that the transition from lamellar to BμE phases manifests at the volume fraction ϕ_H at which the structural length scale, $L_0 = 2\pi/q^*$ becomes greater than the mean curvature diameter, D_C.

Figure 3.4 depicts the results for the length scale, $L_0 = 2\pi/q^*$, and

the mean curvature diameter, D_C, as a function of the homopolymer volume fraction, ϕ_H, for BDL copolymer system at χN=14. It can be seen that L_0 gradually increases with ϕ_H, whereas D_C is approximately a constant over the range of ϕ_H examined. These trends can be understood by noting that at moderate-high ϕ_H, the copolymers segregate mainly to the interface between the microdomains. Since the curvature is induced by the copolymers, the mean curvature diameter, D_C, remains independent of amount of homopolymers as long as the interface is saturated. In contrast, the structural lengthscale, L_0 increases with increasing ϕ_H due to the associated swelling of lamellae. In this framework, the transition between lamellar and BμE phase, ϕ_H^*, is identified as the point of intersection of D_c and L_0. In Figure 3.3 we display the so-determined boundaries as solid black lines. It can be seen that there is an excellent agreement between the boundaries determined using the D_c, L_0 approach and the S(q) measures. In the following section, we base our discussion mainly on the results obtained using Teubner-Strey fit.

3.3 Results and Discussion

In this section we present the results for the interfacial activity and the corresponding phase diagrams of ternary blend of homopolymers A and B having equal chain length ($N_A = N_B = \alpha N_{AB}$) with different model copolymers described in Section 3.2.1. Since we are primarily concerned with the BμE phases, we focus only on the homopolymer rich side of the phase diagram and restrict our results to the region, $0.6 < \phi_H < 1.0$.

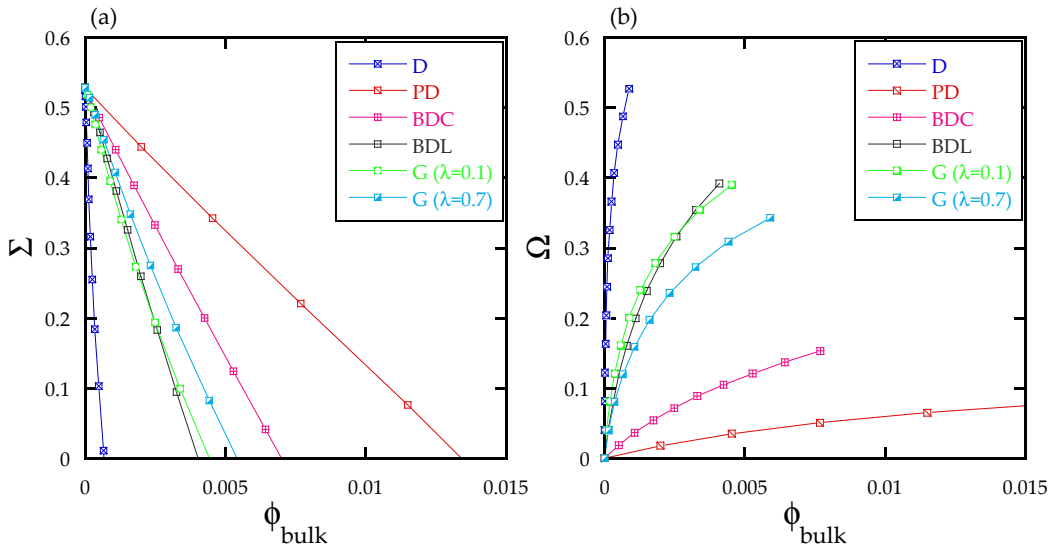

Figure 3.5: (a) Interfacial tension, $\sum$ versus bulk concentration of copolymer, ϕ_{bulk} and (b) excess copolymer, Ω versus ϕ_{bulk} for the model copolymer systems (cf. Section 3.2.1) considered in this study.

In Figure 3.5 we present the results for the interfacial tension of the homopolymer/model copolymer blend for the different compatibilizer architectures. Specifically, in Figure 3.5(a) we display the variation in the interfacial tension ($\sum$) with concentration of the copolymer dissolved in the bulk phase (ϕ_{bulk}), and in Figure 3.5(b) we display the interfacial excess copolymer (Ω) as a function of the bulk copolymer concentration. We observe in Figure 3.5(a) that diblock copolymers (D) require the minimum amount of bulk copolymer to saturate the interface (i.e. corresponding to $\sum = 0$). In contrast, diblock copolymers having polydispersity in one block (PD) and diblock copolymers having bidisperse composition (BDC) display the lowest interfacial activity

(with the activity of PD < BDL) requiring the largest ϕ_{bulk} for achieving a saturated interface. Gradient copolymers (G) and diblock copolymers having bidispersity in length (BDL) are seen to display an interfacial activity intermediate between D, BDL and PD.

The above results can be understood by considering the interfacial excess, Ω as a function of ϕ_{bulk} displayed in Figure 3.5(b). It can be seen that Ω displays a direct correlation to the interfacial activity. Explicitly, the D copolymer exhibits the largest Ω, whereas, PD displays the lowest Ω for a specific ϕ_{bulk}. This correspondence between $\sum$ and Ω can be understood by noting that the interfacial activity is expected to be correlated to the amount of compatibilizer at the interface. Since PD and BDC copolymers contain an ensemble of chains, some of which are individually enriched in A or B components, the resulting partitioning of such enriched chains to the respective homopolymer domains is expected to result in a reduced propensity for interfacial segregation in such systems (relative to a compositionally monodisperse system). In the case of PD copolymers, due to the MW polydispersity, there is additionally expected to be a population of short chains which experience reduced driving force for interfacial segregation. Hence, for a given ϕ_{bulk}, PD chains can be expected to display an even lower Ω compared to BDC. Gradient copolymers are seen to display Ω values which are intermediate between D and PD copolymers. G copolymers also have a significant number of copolymer chains which are enriched in either A or B monomers, and hence they also experience a propensity for segregation to the respective homopolymer phases.

However, due to the stochastic nature of sequences in such polymers, they are likely to experience more unfavorable interactions during their dissolution in the corresponding homopolymer phases. Hence, there is a stronger driving force for the adsorption of G copolymers on the interface relative to PD and BDC copolymers.

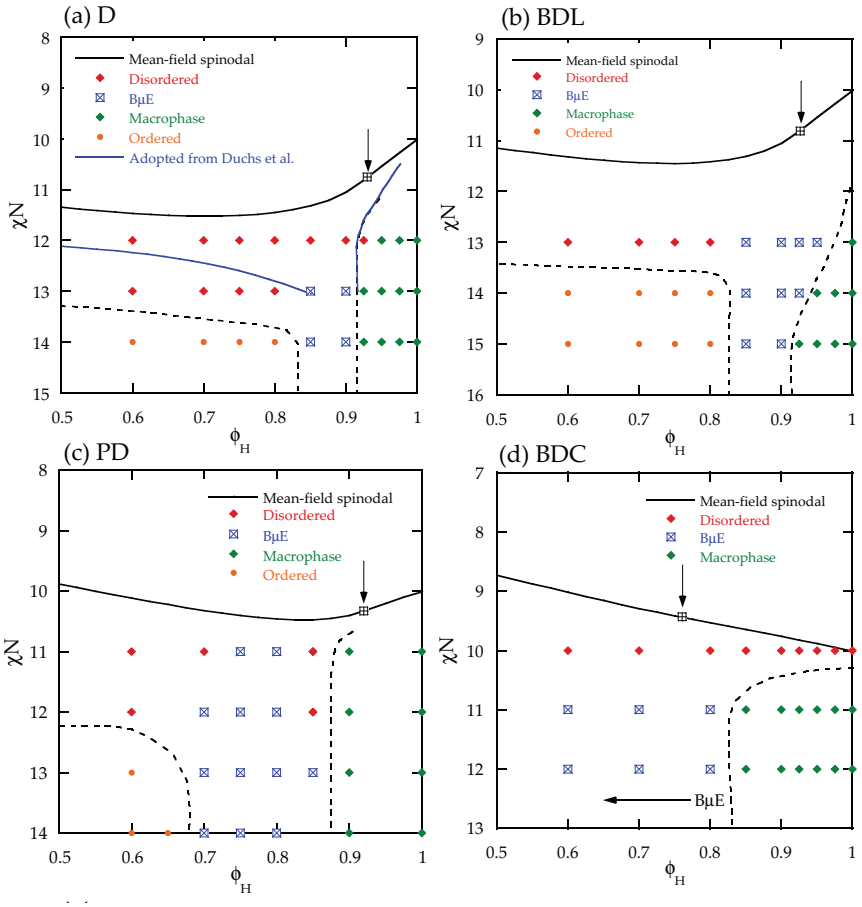

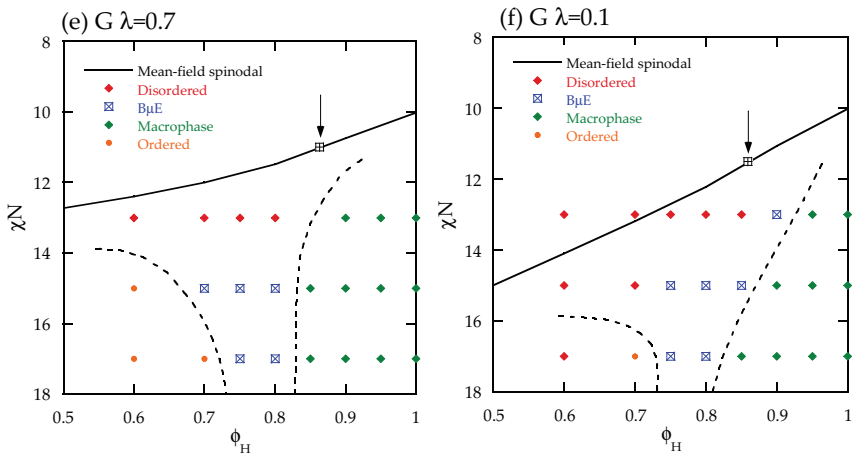

Figure 3.6: Phase diagrams of homopolymer blend with (a) diblock copolymer (D), (b) diblock copolymer having bidisperse length (BDL), (c) diblock copolymer having polydispersity in one of the blocks (PD), (d) diblock copolymer having bidisperse composition (BDC), (e) gradient copolymer (G) having $A = 1$ and $\lambda = 0.7$, and (f) gradient copolymer having $A = 1$ and $\lambda = 0.1$. The square marker on the mean-field spinodal indicated by the arrow represents the location of the Lifshitz point predicted by random phase approximation. The black dotted lines are only guide to the eye and do not depict real boundaries of BμE phase.

Based on the results of Figure 3.5, one would expect that D copolymers, as a consequence of possessing the highest interfacial activity, would require the least amount of copolymers to form BμE, followed in that order by BDL and G systems. In contrast, for PD and BDC systems, based on the results for $\sum$, one would expect the onset of formation of BμE phase to require larger copolymer volume fractions. Below, we test such expectations against explicit results of the phase behavior.

Figure 3.6(a-f) display the phase diagrams for the model copolymer systems described in Section 3.2.1. Figure 3.6(a) shows the phase diagram for homopolymer blend with monodisperse diblock copolymer (D). The phase boundaries reported by Duchs et al.[16, 17] for the same system obtained in two-dimensions at $C = 50$ using FTS methodology are also depicted in Figure 3.6(a). Our BμE phase boundaries are seen to be in qualitative agreement with the phase diagram reported by Duchs et al.[17] Surprisingly, we observe that despite the difference in C parameter, the width of the BμE channel of our results agrees approximately with that of Duchs's results. However, the phase boundaries in our study (dotted lines) are seen to shift towards higher χN values as compared to Duchs's phase diagram. Such a result is a consequence of the stronger fluctuation effects which result due to the lower C parameter used in our study. These results serve to validate the SCMF simulation method and the measures used in this work for identifying phase boundaries.

In comparing the behavior of the different compatibilizers, we observe that all the copolymers considered in our study exhibit BμE phases. From Fig-

ure 3.6(a-b) we observe that, D and BDL systems form BμE with the lowest amount of copolymer, a trend which is consistent with the highest interfacial activity exhibited by these copolymers (cf. Figure 3.5). On the other hand, the PD, BDC and G systems are seen to require larger content of copolymer to stabilize the BμE phase. We note that such shift of BμE channel towards higher copolymer volume fraction observed in PD systems relative to D system is consistent with experiments of Ellison et al.[20] While above observations broadly agree with the interfacial activities for these copolymers (cf. Figure 3.5), some small discrepancies are seen. Specifically, while the interfacial activity of G copolymers is seen to be comparable to that of BDL system in Figure 3.5, in contrast, the onset of formation of BμE phase is seen to be at higher copolymer volume fractions in G copolymers compared to BDL copolymers. Moreover, while PD systems exhibited lowest interfacial activity among the different compatibilizers, the onset of the actual BμE phase boundary is seen to occur at lower copolymer volume fraction in PD systems compared to the BDC and G systems which exhibited higher interfacial activity. Hence, the interfacial activity of copolymers is seen to be at best only a qualitative predictor of the efficacy of copolymers in forming BμE phases.

A second quantity of interest in the phase diagrams of Figure 3.6 is the width of homopolymer volume fractions of the regions where BμE phases are formed. While the onset of BμE phases were seen to be broadly correlated to the interfacial tension, the width of BμE channel is more likely to be related to the influence of fluctuation effects, and hence proves less straightforward to

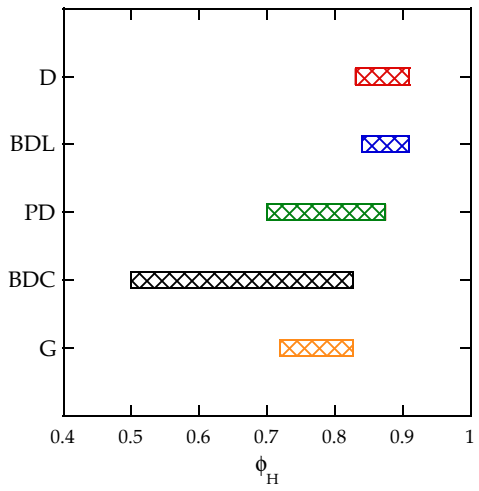

Figure 3.7: The BμE phase boundary (hatched region) of the ternary homopolymer/copolymer blend phase diagram for various model copolymer systems. The BμE phase boundaries are identified at the highest χN probed for each system assuming the width of the channel does not change substantially. Note that these boundaries are approximate as we studied the phase behavior at large intervals of homopolymer volume fraction, ϕ_H.

rationalize. To explicitly compare the effects of the compatibilizer architecture on the width of BμE channel, in Figure 3.7 we consider the highest χN probed for each system and display the ϕ_H range over which BμE phases are observed in the compatibilizer systems. From Figure 3.7 we observe that the width of the BμE regions in BDL and D systems are approximately same (cf. Figure 3.6(a-b)), indicating the MW bidisperse systems and monodisperse block copolymers are comparably efficient in forming BμE phases, a result which contrasts with the prediction of Thompson and Matsen.[200] However, we note that our study effected SCMF simulations for only one set of bidisperse length copolymers ($N_1 = 70, N_2 = 30$) and hence it is not evident if the comparison between D and BDL copolymers hold in general. For PD systems (cf. Figure 3.6(c)), we observe that despite the larger amount of copolymer needed to form BμE phases, the width of the resulting BμE region is larger than that for D and BDL copolymer systems. More interestingly, bidisperse composition diblock copolymers (BDC cf. Figure 3.6(d)), BμEs are seen to exhibit widest BμE channel as compared to other copolymer systems. Also, the BμE channel in G system is seen to form over approximately same range of homopolymer volume fractions for high and low blockiness copolymers (cf. Figure 3.6(e-f)), hence both high and low blockiness copolymers are denoted as "G" in Figure 3.7 and is seen to exhibit a width which is comparable to PD system.

To understand the results of Figure 3.7, we note that the different copolymer systems differ by at least two factors in their ability to promote/sustain BμE phases. On one hand, the thermal fluctuations which are responsible for

the formation of BμE phases are likely to have different influences on the phase behavior of the copolymer systems. On the other hand, in systems such as BDC and PD, the presence of asymmetric copolymers in the ensemble is likely to promote the formation of interfaces with different spontaneous curvatures. For instance, a SCFT study of interfacial properties by Muller and Gompper[207] suggested that the spontaneous curvature imparted by a mixture of asymmetric block copolymers lowers the bending rigidity of polymer blend interfaces. Such effects are likely to enhance the propensity to form BμE phases.

As a step towards understanding the trends noted in Figure 3.7, we consider the influence of fluctuations on the phase behavior of the corresponding copolymer systems. In a recent study, we examined the fluctuation-induced shift in the ODT of block copolymers having MW polydispersity in one of the blocks (PD) and compared such results with monodisperse length block copolymers.[210] We observed that the influence of fluctuations increased with increasing MW polydispersity. We believe that such stronger influence of fluctuations in PD systems in conjunction with the spontaneous curvature effects discussed above allows stabilization of BμE morphologies over broader range of homopolymer volume fraction as compared to monodisperse diblock copolymers (D).

In order to investigate if the above explanation can also rationalize the trends seen in case of BDL, BDC and G copolymers, we examined the effects of fluctuation-induced shift in the ODT of these copolymers. In our previ-

ous article,[210] we have presented an elaborate discussion of the methodology used to determine ODT and hence we refrain from repeating the details here and present only the final results. In Figure 3.8 we compare the fluctuation-induced shift, Δt, in the ODT of D, BDL, BDC and G copolymer melts from the respective mean-field predictions as a function of the C parameter. From the results for $C = 20$ and $C = 30$, it can be seen that D and BDL systems exhibit the smallest influence of fluctuations (the results for $C = 10$ are harder to resolve within the numerical accuracy we probed). Additionally, due to symmetric nature of the copolymers in D and BDL systems, the spontaneous curvature effects are expected to be absent. These considerations rationalize the narrower channel of BμE phase in the D and BDL systems. On the other hand, it is evident that gradient copolymers (both high and low blockiness) exhibit stronger influence of fluctuations which manifest as a larger shift of ODT than diblock copolymers. Moreover, due to the presence of fluctuations in spontaneous curvature in such systems, the BμE channel is expected to be wider in G copolymers as compared to the D system. In comparing BDC system with other copolymers, we observe that the BDC system exhibit highest strength of fluctuations as compared to D, BDL and G systems. Moreover, due to the presence of copolymers of significantly different compositions in BDC systems, there is expected to be significant local spontaneous curvature fluctuations induced by the presence of the copolymers of the different compositions at the polymer blend interface. Together we believe that such fluctuation and spontaneous curvature effects aid in stabilizing the BμEs over large range of

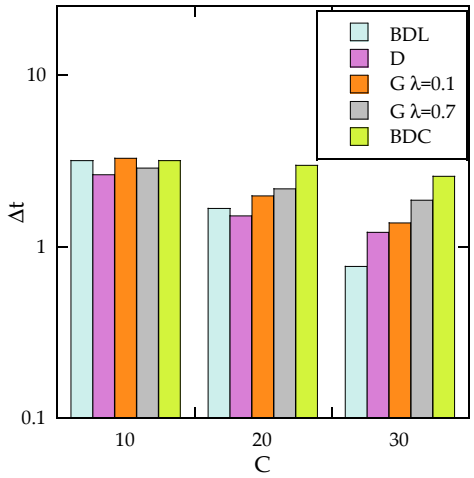

Figure 3.8: The fluctuation-induced shift in the ODT of copolymer melts from the mean field prediction ($\Delta t = \chi N(C) - \chi N(C = \infty)$) as a function of C parameter.

homopolymer volume fractions in BDC ternary blends.

3.4 Summary

We studied the phase behavior of ternary blend of symmetric homopolymers with various polydisperse copolymers using single chain in mean-field simulations. Specifically, we identified the phase boundaries of BμE region to clarify the role of different compatibilizing copolymers in forming BμE phases. Moreover, using self-consistent field theory, we calculated the interfacial tension in our model systems to examine correlation between the BμE phase boundaries and the interfacial activity of the copolymers.

We observed that monodisperse diblock copolymers and bidisperse (length)

diblock copolymers were the most efficient in forming BμEs as they require least amount of copolymer to form BμE. However, the area of phase diagram occupied by BμEs was seen to be narrow in such systems as compared to polydisperse copolymer systems. MW polydispersity in one of the blocks of a diblock copolymer was seen to shift the BμE channel towards copolymer rich side of the phase diagram. However, the BμEs were formed over a wider range of homopolymer volume fraction as compared to monodisperse and bidisperse (length) block copolymers. Diblock copolymers having compositional polydispersity were seen to exhibit widest BμE channel among all model copolymer systems. However, they also required the largest amount of copolymer to stabilize BμEs. Gradient copolymers showed an intermediate behavior between monodisperse diblock copolymers and compositionally bidisperse diblock copolymers.

In summary, our results suggest that compositionally polydisperse copolymers serve as more efficient compatibilizers for stabilizing BμE morphologies over wider homopolymer concentration. Whereas, MW polydisperse copolymers exhibit better interfacial activity and form BμEs with low amount of copolymer. Broadly, our results for the interfacial tension were seen to be correlated with the efficiency of copolymers to form BμE whereas, the influence of fluctuations on the corresponding copolymer system was seen to be correlated with the width of BμE channel. We believe these findings can be used as a rule of thumb for experimental design of BμE morphologies using polydisperse copolymers.

Chapter 4

Phase Behavior of Gradient Copolymer Solutions

4.1 Introduction

With the development of advanced polymerization techniques, it is now becoming possible to exercise significant control over polymer properties by controlling their physicochemical characteristics such as molecular weight, chain architecture, sequence chemistry etc.[54–57] As a consequence, synthesis of new classes of copolymers, such as gradient copolymers, comb copolymers, star copolymers etc. is now becoming common.[58–61] In this chapter we focus on a class of such polymers which has recently attracted significant attention in the context of interfacial modifiers, termed *gradient copolymers*.[62–67] Gradient copolymers are random copolymers which exhibit a gradual change in monomer composition along the length of the polymer.[68, 69] A number of other uses have also been proposed for such a class of polymers, which include applications as reinforcement agents,[70] damping materials[71] and thermoplastic elastomers.[72][73]

The equilibrium properties of gradient copolymers are expected to be intermediate between the behavior of diblock copolymers, which exhibit a

step change in composition, and that of random copolymers, which possess a uniform composition profile.[217–220] For instance, Okabe *et al.*[217, 218] observed micelle formation and microphase segregation in semi-dilute aqueous solution of gradient copolymers and block copolymers using small-angle neutron scattering and dynamic light scattering (DLS). The micelle size for gradient copolymer was found to decrease gradually with temperature and less ordered micelle structures were observed as compared to block copolymer solutions. The work reported in the chapter is motivated by recent experimental results of Gallow *et al.*[142, 144] which examined the effect of monomer sequence distribution on the cloud point of dilute solutions of gradient copolymers. They synthesized a series of 2-hydroxyethyl methacrylate and 2-(dimethylamino)ethyl methacrylate gradient copolymers having prespecified composition profiles. In dilute aqueous-buffered solutions, these copolymers exhibited aggregation and phase separation phenomena whose onset was sensitively dependent on the details of monomer sequence distribution. Moreover, based on the combined results of DLS and cloud point observations, a two-step aggregation mechanism for solutions was proposed, in which the initial stages of phase separation involves the local collapse of the chains (intramolecular aggregation) followed by strong interchain aggregation which manifests as macroscopic clouding.

A number of prior theoretical studies have considered the phase behavior of gradient copolymer systems, but mostly in the regime of melt-like conditions.[50, 221–225] Such studies have examined the interfacial properties,[226]

the self-assembly morphologies[50, 221–225] and the conformations of polymer brushes[227] using polymer self consistent field theory. Despite this significant body of literature, the phase behavior of gradient copolymers in solution conditions remains unexplored. In the chapter, we report results of Monte Carlo simulation studies exploring the phase behavior of gradient copolymer solutions. Our work seeks to address the influence of the sequence distribution of the gradient copolymers upon their phase separation characteristics in poor solvent conditions. To quantify the phase separation characteristics, we examine the size and organization of the clusters formed during phase separation and quantify the relative roles of inter and intramolecular aggregation. Specifically, we would like to address: (i) the origin of the gradient strength dependence of the critical temperature; and (ii) whether the sequence of aggregation events indeed correspond to that hypothesized in experiments.

A second, related issue we probe in this chapter is the influence of the "randomness" of the gradient copolymer sequences. Specifically, much of the prior theoretical studies[50, 221–224, 227] have used an "annealed" representation of the gradient copolymer (albeit, exceptions do exist[225]). In such a model, all the copolymers are assumed to possess the same sequence, with however, the identity and the interactions of each monomer chosen to be representative of the "averaged" identity of the monomer. While this is a reasonable first step, a more realistic model for such systems, and one that we primarily focus on in this work, is to use an ensemble of "quenched" sequences, whose compositions on an average mimic the experimentally synthesized conditions of

the gradient copolymers. For instance, recent work has demonstrated that the chemical sequence of copolymer compatibilizers can significantly influence the dynamics of phase separation of immiscible binary homopolymer blends.[67] Other studies[143, 164–166] have demonstrated that the use of the more realistic quenched sequences for grafted copolymers can lead to novel phenomena and effects which cannot in general be captured by the annealed sequences. Motivated by such considerations, we compare the phase separation characteristics of annealed sequences with the behavior of the more realistic, quenched sequence model of gradient copolymer systems.

The rest of this chapter is arranged as follows. In Section 4.2, we outline details of our simulation methodology, the quenched and annealed models of the linear gradient copolymer systems and the framework used for cluster analysis. In Section 4.3, we present our results in both the annealed and quenched systems for the phase transition temperature and the characteristics of the micelle-like structures formed below the phase separation temperature. We discuss our results in connection with the above-cited experimental observations.

4.2 Simulation Details

4.2.1 Bond Fluctuation Model

Monte Carlo lattice models has been used extensively to study the equilibrium properties for a variety of copolymeric systems.[67, 107, 225, 228–238] In this chapter, we use the Bond Fluctuation method (BFM) of Carmesin and

Kremer[239] to study the phase separation process in gradient copolymer solutions.[240] Many prior studies have demonstrated BFM simulation approach as a convenient method to study both the equilibrium and dynamical properties of polymer melts and solutions. For instance, earlier studies have applied the BFM approach for the study of issues such as phase separation of polymer blends,[241] interdiffusion of polymers,[239] the static and dynamical properties of block copolymers[242] and the transport properties of penetrants in polymer matrices.[243, 244]

In BFM, a polymer chain is represented by cubes (each monomer occupying 8 lattice sites) on a lattice, with a maximum occupancy for each lattice position restricted to a single monomer in order to model excluded volume interactions. The monomers are connected by bond vectors whose magnitudes l lie in the range $2 \leq l \leq 10$. The latter constrains the bond vectors to the set [200][210][211][221][300][310] and their permutations and sign inversions. An elementary move in BFM consists of choosing a monomer at random and displacing it by one lattice unit. If the move leads to a bond vector contained in the admissible bond vector set and if excluded volume conditions are satisfied, the move is accepted according to the Metropolis criterion based on the energetic differences.[168] The original BFM simulation limits the MC moves only among the 6 directions around the monomer to ensure bond non-crossability. However, we use a modified version of the BFM algorithm proposed by Wittmer *et al.*[245] where attempts to displace the monomer are effected in the 26 available directions. Such a modification helps in reducing

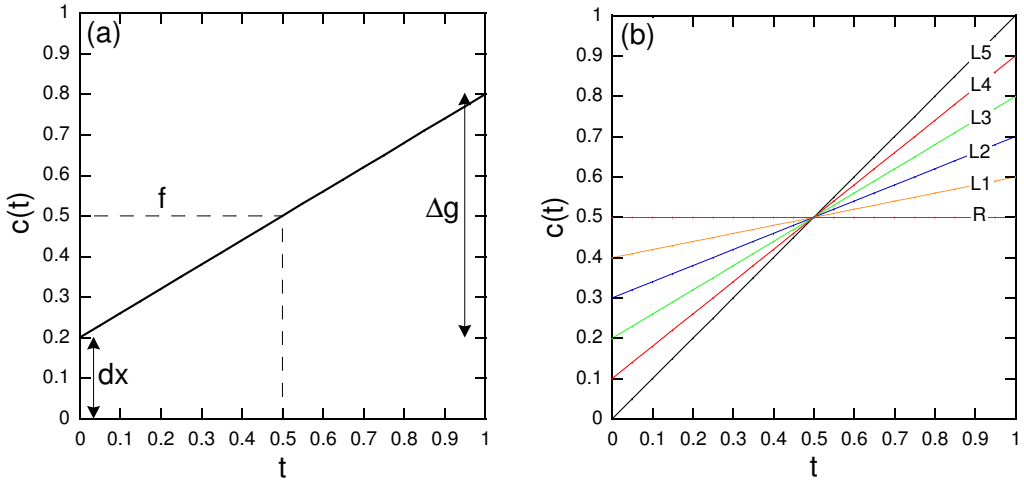

Figure 4.1: (a) A depiction of the linear composition profiles adopted for the polymer chains in our simulation. The figure also defines the gradient strength, Δg, a quantity which constitutes the focus of our study. (b) Composition Profiles: R ($\Delta g = 0$), L1 ($\Delta g = 0.2$), L2 ($\Delta g = 0.4$), L3 ($\Delta g = 0.6$), L4 ($\Delta g = 0.8$), L5 ($\Delta g = 1.0$).

the relaxation time for the system, and is especially convenient for probing equilibrium properties.

4.2.2 Modeling Linear Gradient Copolymer Solutions

We consider linear gradient copolymers comprising A (hydrophilic) and B (hydrophobic) monomers. The average compositions of such linear gradient copolymers are modeled through a continuous composition function $c(t)dt$, where t (index along polymer backbone) varies from 0 to 1. Explicitly,

$$c(t) = 2(f_A - dx)t + dx, \tag{4.1}$$

where f_A is the average of composition over the chain, $dx = f - \Delta g/2$ represents the lowest composition of A monomer and Δg is the gradient strength of the copolymer and is defined as the largest difference in the instantaneous composition along the backbone of copolymer.[142] The composition profile of such linear gradient copolymer is pictorially depicted in Figure 4.1(a).

In the experiments discussed in the introduction,[142, 144] gradient copolymers were synthesized by a semi batch polymerization process wherein one monomer is loaded and the comonomer flow rate is continuously monitored. While the monomeric sequences generated by the experiments are expected to possess complex correlations along the chain, in an effort to account for the chain-to-chain variability in the sequences, we adopt a stochastic approach relying on an ensemble of many chains to mimic the compositional profiles depicted in Figure 4.1(b). Explicitly, for each chain, a specified monomer t is probabilistically chosen to be as either an A or a B monomer based on the average composition at that location. Since the average composition changes along the backbone, the chemical identity of the specified monomers also varies gradually along the backbone (albeit, in a probabilistic manner). To contrast with the phase behavior of random copolymer solutions, we also consider the behavior of a pure random copolymer solution (denoted as R in our results). In the latter, the polymer chains are populated by random, uncorrelated sequence of A and B monomers.

To study the phase behavior of a system of above copolymers in solution conditions, we treat the solvent molecules (S) in an implicit manner

as the "vacancies" or holes in our system. Following the parametrization of Khokhlov *et al.*[230], we set both ε_{AB} and ε_{AA} identically to zero, where ϵ_{ij} refers to the interaction energy parameter between i and j species. In other words, we limit A-A and A-B interactions to just the excluded volume steric interactions. To mimic the hydrophilic and hydrophobic behaviors of the A and B monomers, we impose $\varepsilon_{AS} < 0$, $\varepsilon_{BS} > 0$ and $\varepsilon_{BB} < 0$. Two non-bonded monomers are considered to be interacting if their distance vectors belongs to the set $(2,0,0) \bigcup (2,1,0) \bigcup (2,1,1)$ (and their permutations and sign inversions) which covers 54 lattice sites around the randomly selected monomer. The maximum number of monomer-monomer contacts for this interaction range is 26, whereas the number of corresponding monomer-solvent contacts is 98. Consequently, we use the following simple parametrization and assume that $-98/26\varepsilon_{AS} = 98/26\varepsilon_{BS} = -\varepsilon_{BB} = \varepsilon$, where ϵ represents a measure of temperature in the system and constitutes the parameter that is varied in our study. The interaction parameter, ε is proportional to inverse temperature in case of systems exhibiting upper critical solution temperature (UCST) behavior. However, the experimental results of Gallow *et al.*[142, 144] correspond to a lower critical solution temperature (LCST) system. To avoid confusion while comparing the simulation results with experiments, we identify ε to be proportional to temperature, although the same analysis can be easily extended to UCST systems.

All our simulations were carried out for a chain length corresponding to the number of monomers N set to $N = 128$, and for the case where the

volume fraction of the polymer chains corresponded $\phi = N \times m \times 8/L^3 \approx 0.03$, where m is number of copolymer chains of length N. Moreover, we fixed the average composition of the A and B monomers as $f_A = f_B = 0.5$. Our study is primarily concerned with the influence of the "gradient strength" upon the phase separation behavior of copolymer solutions. For this purpose, we study the phase separation behavior of five linear gradient copolymers which are depicted in Figure 4.1(b) and are labeled in the increasing order of gradient strengths. Henceforth in this chapter, we will use the terminology L1 - L5 (Figure 4.1(b)) to identify the system to which the results correspond.

As mentioned in the introduction, a second objective of this work is to examine the impact of using an annealed model representation of the gradient copolymer solutions. In pursuit of this, we consider the two extreme compositional profiles, $L1$ and $L5$ in Figure 4.1(b), and consider an annealed representation of the sequences. Explicitly, in such simulations, the monomers are treated as partially resembling both A and B in character, but with however each chain in the ensemble possessing the same sequence. The interaction energies experienced by a monomer t is then calculated as:

$$E_t = c(t)(-\frac{98}{26}\varepsilon_{AS}n_s) + (1 - c(t))(\frac{98}{26}\varepsilon_{BS}n_s - \varepsilon_{BB}\sum_{i=1}^{M}(1 - c_i(t))), \qquad (4.2)$$

where n_s denotes the the number of solvent molecules and M labels the polymeric monomers present in the interaction range of the monomer t. In the above, $c(t)$ denotes the probability of the monomer t being A (cf. Figure 4.1(a)).

4.2.3 Parallel Tempering Algorithm

To study the phase separation behavior of the gradient copolymer solutions in computer simulations, we employed a parallel tempering (PT) algorithm (replica exchange).[246] Many earlier studies[232–234] have demonstrated that PT provides an efficient approach to sample the phase space and acquire better statistics during polymer collapse and phase separation processes. In this methodology, M non-interacting replicas of the system are simulated in parallel at different temperatures. After a pre-specified number of Monte Carlo steps within the given temperature, (in this work, PT moves were performed at a frequency of one PT move per one hundred MC sweeps of the system), a swap move is attempted between the configurations of neighboring replicas. Such swap moves are accepted based on the Metropolis criterion:[247]

$$p(t_i \leftrightarrow t_{i+1}) = min\{1, exp[-(\beta_i - \beta_{i+1})(U_i - U_{i+1})]\} \tag{4.3}$$

where

$$\beta_i = 1/k_B T_i \tag{4.4}$$

where U_i is the total energy of the replica system at the temperature T_i. Exchange of configurations between replicas offers an efficient way to overcome the energy barriers encountered at low temperatures and thereby facilitate the system to reach equilibrium.

In our work, we used a modified PT algorithm to make the algorithm efficient for parallel computing. Explicitly, in PT, the only inter-processor

communication occurs while attempting a swap. In MPI (Message Passing Interface) implementation, a master thread randomly chooses the replicas which will participate in exchange and broadcast the information to all threads. This involves global synchronization, a procedure which is computationally expensive. Instead, we implement a decentralized parallel tempering algorithm[248] using SPRNG 4.0 (Scalable Parallel Random Number Generator) library.[249] SPRNG library provides independent random number streams for parallel processes which are deterministic and reproducible. Thus identical random number streams (starting with same seed) can be spawned on each processor to decide which replicas are participating in the swap. The latter eliminates global synchronization and thus speeds up computation. In addition to these global random number streams (restricted to replica exchange moves), we need to maintain independent random number streams local to the processor to determine Metropolis acceptance for MC moves. The pertinent details of the algorithm have been provided elsewhere.[248]

We use $M = 36$ replicas for our simulations. As we are interested in collapse and phase separation transition, we mainly focus on the temperature regime around the phase separation temperature of the system. The M replicas are first equilibrated for 1×10^6 MC cycles to get the initial configurations, and then subsequently, parallel tempering is carried out for 5×10^6 MC cycles. The system is further equilibrated for 2×10^6 MC cycles and various thermodynamic quantities are averaged each 100 MC cycles for 3×10^6 MC cycles.

4.2.4 Cluster Analysis Algorithm

At low temperatures, amphiphilic gradient copolymers are expected to exist in a homogeneous disordered state in solution. However, upon increasing the temperature, there is expected to be an enhancement in the B-S repulsion and the A-S and B-B attractions. These features are expected to lead to a high temperature state wherein the B monomers of the different chains aggregate to form micelle-like structures. In the snapshots displayed in Figure 4.2, such considerations are indeed seen to be borne out in our simulations. Interestingly, bigger clusters are seen to be formed in case of L5 (highest gradient strength)(Figure 4.2(a)) with as compared to the L1 Figure 4.2(c) sequences. These microsegregated structures are not strictly micelles as they lack the typical core-shell structure due to linear composition profile, but for brevity of notation henceforth we address these structures as micelles.

To compare and contrast (pictorially) the behavior of the quenched sequence model with that of the annealed sequences, we also display the snapshots for the high temperature structures in annealed sequences in Figure 4.2(b) and Figure 4.2(d). For clarity, annealed sequences are colored in a manner such that the monomers when $c(t) < 0.5$ are identified as B whereas when $c(t) > 0.5$ the monomers are identified as A. In comparing the results in Figure 4.2(b) and Figure 4.2(d) with Figure 4.2(a) and Figure 4.2(c), we observe that the annealed model displays structures that are substantially different from the quenched model. Specifically, for the annealed case, the sizes of clusters are seen to increase with decreasing gradient strength, which is

opposite the behavior noted for the quenched model. These results can be understood by noting that for the symmetric case ($f_A = f_B = 0.5$) considered in this study, lowering the gradient strength would render the annealed copolymer system similar to a homopolymer system retaining only the attractions between the hydrophobic monomers (Section 4.2.1). Such interactions would lead to the formation of macroscopic aggregates instead of micelles in the case of annealed L1 polymers, which is consistent with the observed trends in the sizes of the clusters.

A specific objective of this work is to quantify the characteristics of the aggregates (micelles) formed during the phase separation processes in gradient copolymer solutions. In situations involving regular multiblock copolymer solutions, identification of "micelles" proves straightforward since all the hydrophobic monomers are expected to be confined to the core. In such cases, labeling the B monomers and identifying their connectivities would serve to quantify the micellar size and numbers. In contrast, in quenched gradient copolymers, due to the linear composition profiles along the backbone (and the stochastic nature of sequences), there is expected to be a non-zero fraction of hydrophobic monomers which exist outside the "core" of the micelle. To illustrate this feature, in Figure 4.3(a), we display a snapshot of the collapsed structures formed during the phase separation of quenched gradient copolymers L5 ($\Delta g = 1$). It is clearly evident that there are B monomers present outside the cores of the micelles in the case of gradient copolymers.

To overcome the above issue and identify the micelles formed during

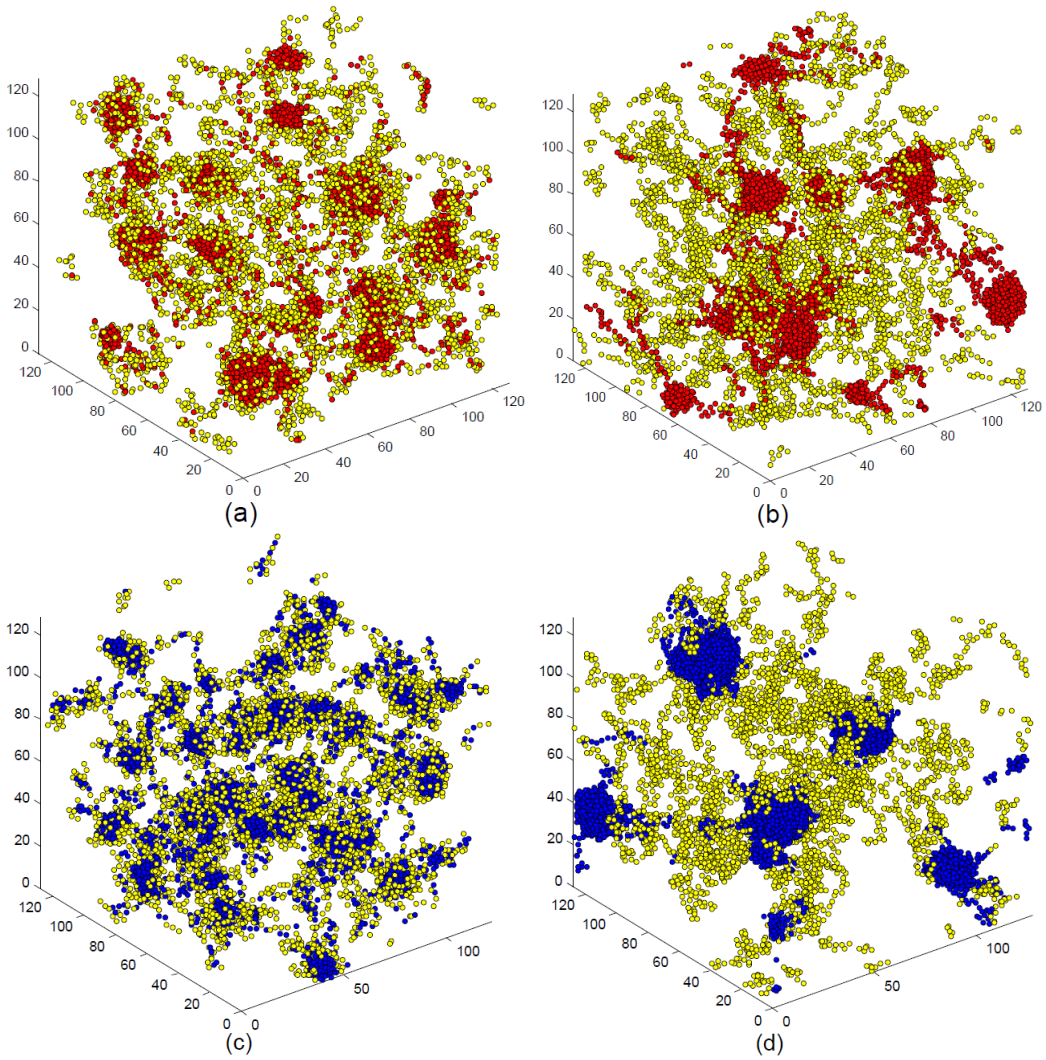

Figure 4.2: Snapshots at (a) L5 at $\epsilon = 0.7$ ($\Delta g = 1.0$) quenched model (b) L5 at $\epsilon = 0.7$ ($\Delta g = 1.0$) annealed model; Snapshots at (c) L1 at $\epsilon = 1.0$ ($\Delta g = 0.2$) quenched model (d) L1 at $\epsilon = 1.7$ ($\Delta g = 0.2$) annealed model.

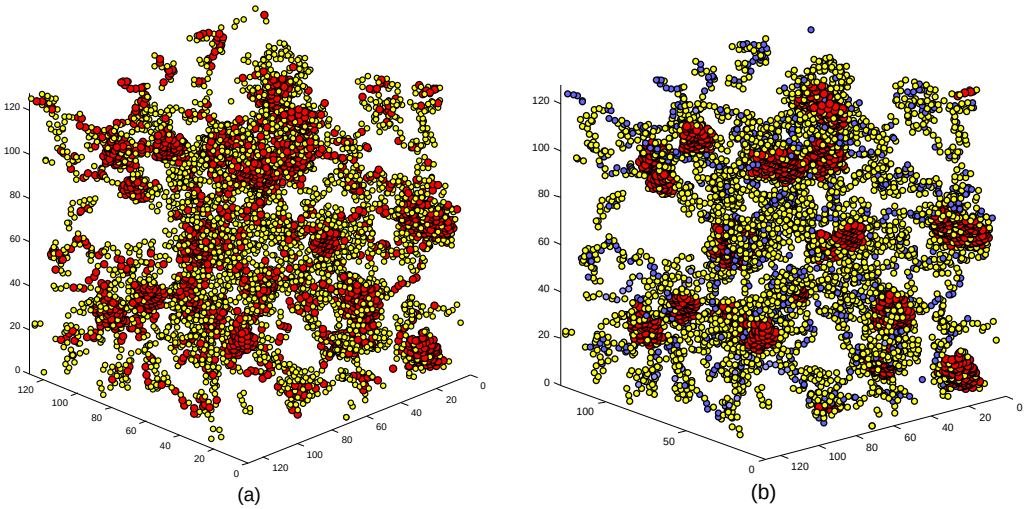

Figure 4.3: (a) Snapshots of collapsed micellar structure for L5 ($\Delta g = 1$). The hydrophilic monomers (in yellow color) are intentionally pictured smaller than hydrophobic monomers so as to make it easier to identify micelle cores. (b) Same system with the core of the micelles identified using proposed algorithm. The monomers discarded as a consequence of not belonging to the clusters is indicated by blue color.

the phase separation of gradient copolymers, we employ a two step procedure by adapting connectivity and cluster identification algorithms used in our prior studies.[250–253] Explicitly, we identify the connectedness between monomers based on whether the monomers are nearest neighbors of each other. To discard the non-core B monomers, we first identify the *biggest cluster in each chain* and identify the monomers in this cluster temporarily as the core of a micelle. As the second step, we color all the other B monomers connected to these micelle cores. To accomplish the latter step, we identify all B monomers which fall in the interaction range of already colored monomers. The latter is achieved by an iterative process to ensure that every monomer belonging to interaction range of colored monomers is included. In Figure 4.3(b) we depict the cores of micelles identified by this procedure. Our approach correctly identifies the micellar structures while eliminating the non core B monomers. Subsequently, we quantify the statistics of the so-identified clusters and study their dependencies upon the gradient strengths.

For structures employing annealed sequences, the B monomers cannot be recognized explicitly, since each monomer is partially A and partially B. Thus, we identify the *biggest cluster in each chain* irrespective of whether the monomers are A or B. Then we color all the monomers (A and B) connected to these clusters. This approach correctly captures the onset of interchain aggregation which is one of the main objectives of this study. However, as a consequence of this coloring process much higher aggregation numbers are expected for the annealed sequences as compared to that of the quenched

sequences.

4.3 Results and Discussion

In this section, we present a quantitative discussion of the results of our computer simulation studies. Our specific parametric studies were motivated by recent experiments which examined the phase separation characteristics of gradient copolymers as a function of the gradient strength.[142, 144] Inspired by the results of the experimental study we address the following issues:

(i) Is it possible to define a specific temperature for the transition from the low temperature disordered phase to the high temperature micellar phase? If so, how does the transition temperature depend upon the gradient strength? This issue is motivated by the experimental results which found that the cloud point discerned in the experiments exhibited a linear dependence on the gradient strength of the copolymers.

(ii) What is the sequence of aggregation events accompanying the transition between the low and high temperature phases? Specifically, we are interested in probing the onset of intra and intermolecular aggregation and their dependence on gradient strength.

(iii) How do the size, number and other characteristics of the micellar structures formed during the phase separation of the system depend on the gradient strength?

(iv) To what extent does annealed model of sequences can capture the

behavior predicted by the more realistic, quenched model?

4.3.1 Phase Transition Temperature

To quantify the transition from the low temperature to the high temperature phase, we probed the temperature dependence of both the average internal energy and the average fluctuations in the internal energy of the system in our simulations (Figure 4.4 and Figure 4.5). From Figure 4.4(a), we observe that the upon lowering the temperature the system undergoes a steep, albeit continuous, decrease in energy signifying the formation of collapsed micellar phases at high temperatures. More pertinently, we observe that the energy fluctuations in the system (Figure 4.4(b)) displays a peak at a specific interaction strength, which indicates a transition to an aggregated phase at a critical interaction strength.[228, 232, 233] A similar trend in energy and energy fluctuations are also observed for simulations employing annealed sequences (Figure 4.5(a)(b)). We note that due to the finite size of the chains used in our simulations, our results for the critical interaction strength are expected to depend on the chain length N of the copolymers. Moreover, for the same reason our results are not sufficient to draw conclusions regarding the order of the phase transition occurring in these systems. Despite these limitations, the peaks in the energy fluctuations are discernible for almost all cases; hence, we use the corresponding temperature (ϵ_c) as a measure of the phase transition temperature in the system. Furthermore, in the following section, we present results for the temperature dependence of the intermolecular aggregation and

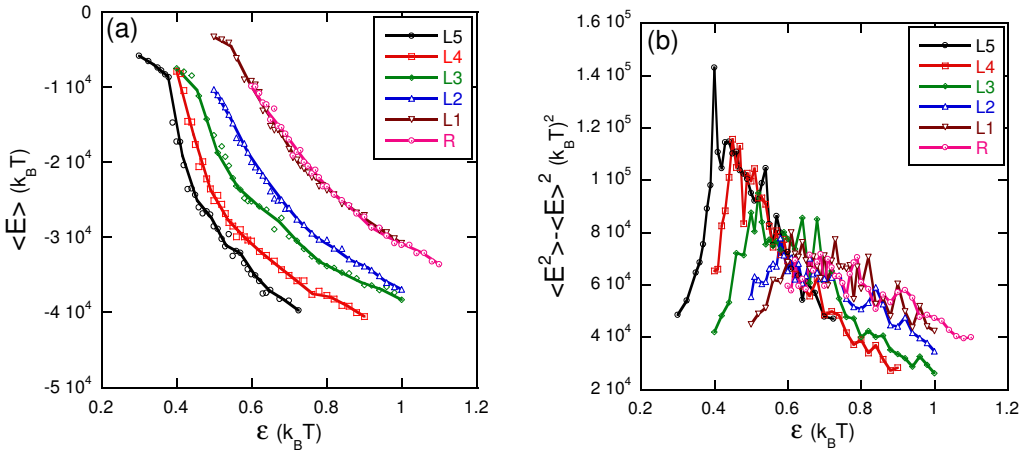

Figure 4.4: Quenched model: (a) average energy and (b) average fluctuations in energy as a function of interaction parameter ε: R ($\Delta g = 0$), L1 ($\Delta g = 0.2$), L2 ($\Delta g = 0.4$), L3 ($\Delta g = 0.6$), L4 ($\Delta g = 0.8$), L5 ($\Delta g = 1.0$). Lines are just a guide to the eye.

micelle sizes, wherein it will be demonstrated that such quantities also undergo a sharp transition at ϵ_c, thereby confirming that ϵ_c as deduced through the energy fluctuations can be identified as the phase transition temperature from a disordered phase to the micellar phase.

In Figure 4.6 we display ϵ_c for different sequences as a function of the gradient strength in the copolymer. We observe that for the quenched model, the critical interaction strength (critical temperature) decreases linearly with an increase in the gradient strength of the copolymers. We note that such a trend agrees *quantitatively* with the linear dependence of the cloud point temperature as a function of the gradient strength found in the experiments of Gallow *et al.* [142, 144] In the experiments, the cloud point was determined

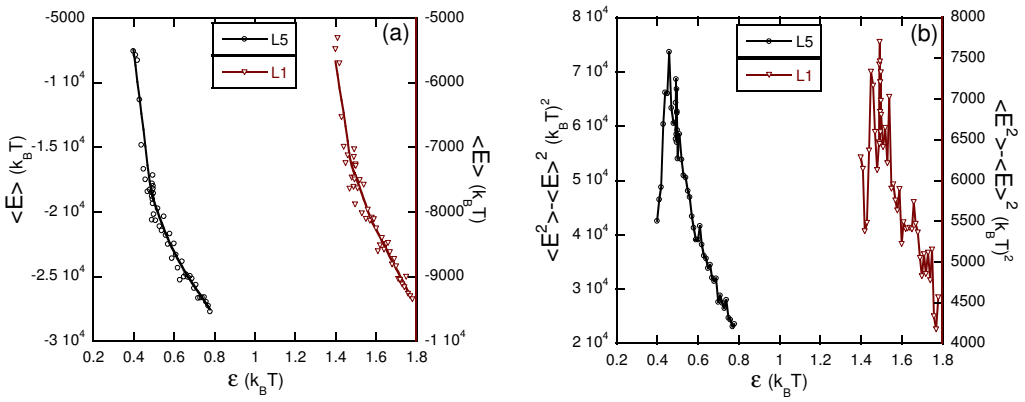

Figure 4.5: Annealed model: (a) average energy and (b) average fluctuations in energy as a function of interaction parameter ε: L1 ($\Delta g = 0.2$), L5 ($\Delta g = 1.0$.) Lines are just a guide to the eye.

as the temperature at which the polymer solution underwent a transition from a transparent to turbid solution. Based on the similarities in the gradient strength dependence noted between our simulation results and the experiments, we conclude that the transition noted in the experiments indeed corresponds to a change from the homogeneous solution to an aggregated micellar phase.

In comparing the results for the annealed model against the quenched polymers, we observe that significantly higher critical interaction energies are required to collapse copolymers having annealed sequences. Such a result is easy to understand since the annealed model smears out the interactions between the monomers (Figure 4.2) and hence much stronger effective interactions are needed for chain collapse. This feature becomes more prominent at lower gradient strengths, since, in such a limit the identity and the interac-

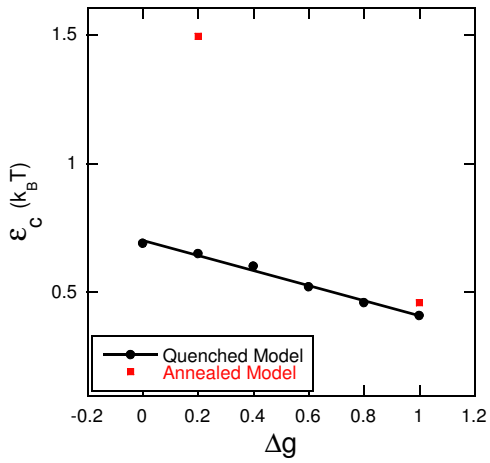

Figure 4.6: Effect of gradient strength on phase transition temperature. The continuous line represents a linear fit to the data.

tions of the monomers becomes more uniform ($f \approx 0.5$, cf. Figure 4.1(b)) in the annealed model and hence much higher interaction strengths are required to achieve aggregation. In contrast, the quenched model retains the specific identities and interactions of the monomers, and thus some chains possess long enough sequences of B segments to cause the collapse of the chains at much smaller interaction strengths.

What is the origin of the above-observed dependence of the critical temperature on the gradient strength ? We note that the average compositions of the different copolymers considered in our study are identical and hence a mean-field (Flory-Huggins) like theory would actually predict no difference in the transition temperatures for the different systems. The latter suggests that the observed simulation results arise from correlation effects embodied

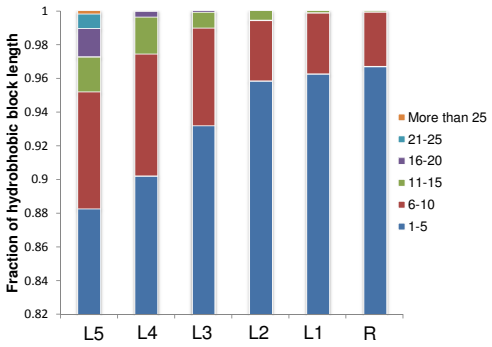

Figure 4.7: Hydrophobic block length distributions for linear gradient copolymers of varying gradient strengths.

in the sequences of our different gradient copolymer systems. Specifically, we hypothesize that copolymers with larger gradient strengths are more likely to possess longer sections of hydrophilic and hydrophobic groups at their ends. The presence of such longer sections of the groups would facilitate easier intermolecular aggregation of the chains and hence require only weaker interaction energies. In contrast, copolymers with weaker gradient strengths are expected to possess shorter sections of the hydrophilic and hydrophobic groups, such that aggregation would result in energetically unfavorable contacts between A and B monomers, thereby requiring stronger interaction strengths to facilitate phase separation.

In Figure 4.7 and Figure 4.8, we provide quantitative evidence supporting our above hypothesis. Specifically, in Figure 4.7 we display the distribution of the number of blocks of continuous hydrophobic or hydrophilic monomers as a function of the gradient strength of the copolymer sequences. It can be

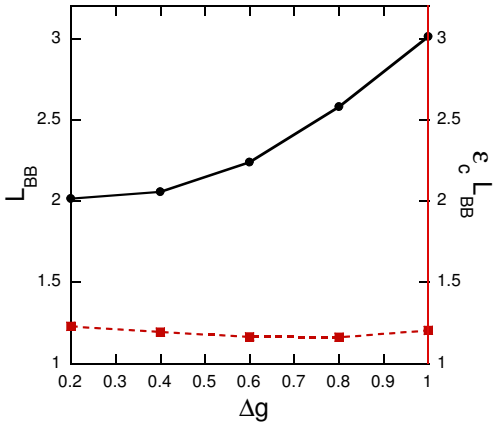

Figure 4.8: Variation of average hydrophobic block length (L_{BB}) and $\epsilon_c L_{BB}$ (dotted lines) with gradient strength for linear gradient copolymers. Lines are just a guide to the eye.

seen that with an increase in the gradient strength, the overall distribution develops a more prominent tail towards larger blocks of continuous hydrophobic monomers. In Figure 4.8 we provide a more direct measure of the block length distributions by depicting the average hydrophobic block length L_{BB} for the different polymers considered in our study. It is seen that indeed the average hydrophobic block length increases with increasing gradient strength (with the minimum occurring for $\Delta g = 0$ in the case of purely random copolymer).

To probe whether the above trends can quantitatively explain the behavior of the critical interaction strengths observed in our simulations, in Figure 4.8 we display the product of critical interaction energies and the average hydrophobic block length of such continuous hydrophobic segments. It is seen that to a good degree of approximation, such a product is independent of the

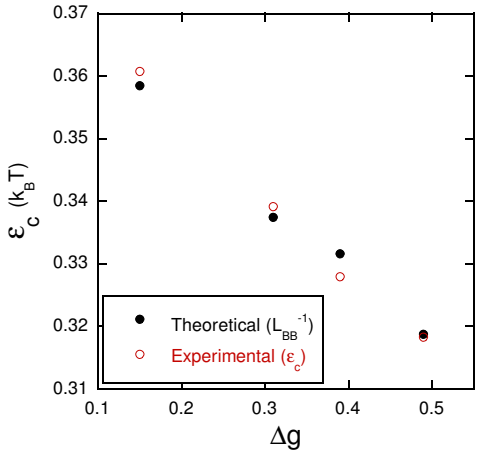

Figure 4.9: Experimental and theoretical data for linear composition profile with gradient strength. Hollow points correspond to experimental data[144] normalized to fit the scale assuming $\epsilon_c = a + bT_c$ for LCST systems. The theoretical data for ϵ_c correspond to inverse of average hydrophobic block length (L_{BB}).

gradient strength, suggesting that the linear dependence of the critical interaction temperature upon the gradient strength arises purely as a consequence of the variations in the average hydrophobic block length as a function of the gradient strength.

Motivated by the success of the ability of L_{BB} to quantitatively predict our simulation results for the critical interaction strengths, we probe whether similar considerations can also be used, at a quantitative level, to rationalize experimental observations. To probe this hypothesis in the context of the linear gradient copolymers studied in the experiments, we generated sequences corresponding to the experimental conditions ($f \backsimeq 0.65$) and computed the L_{BB} corresponding to such sequences. In Figure 4.9, we display a comparison

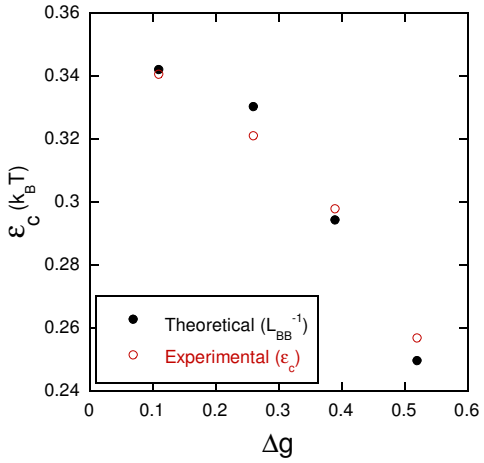

Figure 4.10: Experimental and theoretical data for hyperbolic composition profile with gradient strength. Hollow point correspond to experimental data[144] normalized to fit the scale assuming $\epsilon_c = a + bT_c$ for LCST systems. The theoretical data for ϵ_c correspond to inverse of average hydrophobic block length (L_{BB}).

of the L_{BB}^{-1} and the critical temperatures observed in the system (we assume that the cloud point temperature of the experiments T_c can be translated to an interaction parameter ϵ_c through $\epsilon_c = a + bT_c$, where a and b are temperature, gradient strength independent constants). In Figure 4.9, it is seen that there is remarkably good agreement between T_c and the average length of the hydrophobic segments in the sequences. This quantitative agreement between the experimental work and our simulations points to the fact that L_{BB} is directly correlated with the experimentally tunable variable of gradient strength.

Experimental studies cited in the introduction have observed that a strong dependence of cloud point with gradient strength held true even for copolymers containing hyperbolic composition profiles.[144] Despite the fact that the correlation deduced in our simulations was for linear gradient copolymeric systems (and compared to the corresponding experiments above), we probe whether similar considerations ($\epsilon \propto L_{BB}^{-1}$) hold true even when other composition profiles are considered. To achieve this, we again generated sequences corresponding to the experimental conditions of the hyperbolic gradient composition profiles and computed L_{BB} for such systems. In Figure 4.10, we display a comparison of the L_{BB} and the critical temperatures observed in the system. Yet again, there is seen to be an excellent agreement between T_c and the average length of the hydrophobic segments in the sequences, suggesting that the quantity L_{BB} serves more generally as a quantitative predictor of the cloud point temperature for gradient copolymer solutions.

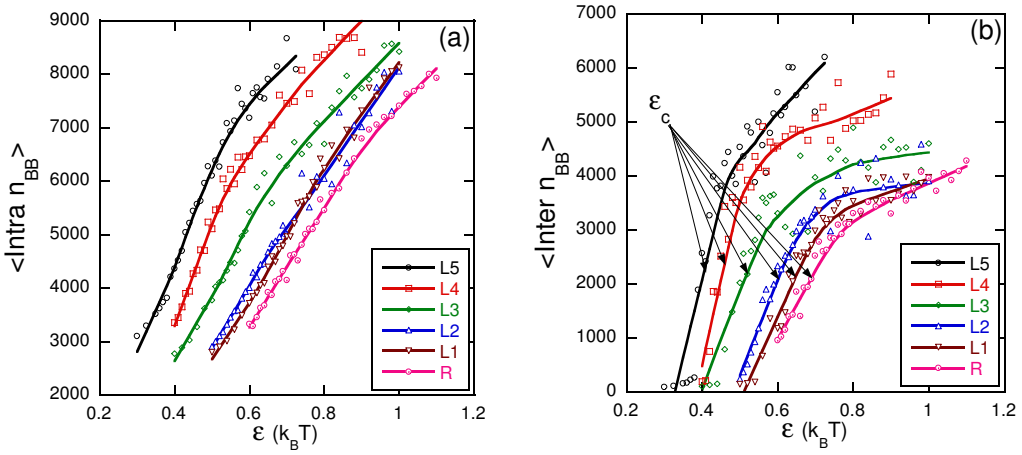

Figure 4.11: Average number of BB contacts for quenched model: (a) Intramolecular (b) Intermolecular as a function of interaction parameter ε: R ($\Delta g = 0$), L1 ($\Delta g = 0.2$), L2 ($\Delta g = 0.4$), L3 ($\Delta g = 0.6$), L4 ($\Delta g = 0.8$), L5 ($\Delta g = 1.0$). Lines are just a guide to the eye.

4.3.2 Intra- and Intermolecular Aggregation

The results presented in the preceding section provides evidence for the occurrence of a phase transition in the gradient copolymer systems. While the low temperature phase in the different copolymeric systems is well-defined as corresponding to a solution of homogeneous non-aggregated chains, the morphology of the high temperature "aggregated" systems corresponds in fact to a variety of states, ranging from a few micelles to a large network of micellar cores linked by bridges. Of interest are the questions, what is the sequence of aggregation events accompanying phase transition ? Specifically, does intramolecular aggregation precede intermolecular aggregation or vice versa ? Is there a dependence of such features on the gradient strength? For instance, in the

experiments discussed in the introduction,[144] the phase transition phenomena in gradient copolymer solutions were studied by two different techniques: DLS and turbidity measurements. The former was argued to be sensitive to intrachain aggregation, whereas the latter was more sensitive to larger scale, interchain aggregation. Based on systematic differences between the aggregation temperature and the macroscopic cloud point temperature extracted from DLS and turbidity measurements, respectively, phase separation in gradient copolymer solutions was found to proceed in a two step manner wherein the intrachain aggregation occurs at a much lower temperature compared to the interchain aggregation. A specific objective of this section is to quantify the aggregation events in our simulations of gradient copolymer solutions and verify the hypothesis presented in the experimental context.

To study the above issues, we probed the temperature (interaction parameter) dependence of inter- and intramolecular BB contacts (Figure 4.11) for the quenched and annealed models (not displayed). From the data in Figure 4.11, it is seen that even at the lowest ε we probed, a substantial number of intrachain contacts are already present. Moreover, with an increase in ε, there is a gradual enhancement of intrachain BB contacts. In contrast, the number of interchain BB contacts are negligible at the lowest temperatures and exhibits a sharp jump at around the critical (cloud-point) temperature. Interestingly, the results for the intra- and intermolecular BB contacts for the annealed model also exhibited trends similar to that noted for the quenched model (not displayed).

The above results are qualitatively consistent with the hypothesis presented in the corresponding experiments.[144] Indeed, our results confirm that the phase transition phenomena discerned in the previous section (which we argued to correspond to the turbidity of the solution) does indeed coincide with the onset of significant interchain aggregation. However, within the limited temperature range we probed, we did not see any sharp jump in the intrachain contacts. In contrast, since the intrachain aggregation and contacts are significant even much prior to the phase transition temperature, one may conclude that the onset of intrachain aggregation occurs at a much lower ε, as was deduced through the experimental DLS measurements.

4.3.3 Interaggregate Bridges

The preceding two sections provided evidence for the influence of the gradient strength upon the phase transition temperature and the nature of the accompanying transition. In this final section, we discuss the influence of the gradient strength on the nature of the aggregates and the larger lengthscale structures formed subsequent to the phase separation. The results presented in this section are motivated by the results of experimental transmittance studies which revealed a larger breadth of transition (i.e. temperature interval over which the copolymer solution changes from transparent to turbid[142]) for higher gradient strength copolymers. We hypothesize that such results arise from the fact that lower gradient strength copolymers possess shorter sequences of hydrophobic (B) groups (Figure 4.8), and also are more likely

to possess B groups towards the middle and A-rich regions of the chains. As a consequence, we propose that the lower (higher) gradient strength copolymers tend to form smaller (larger) sized aggregates, but with substantially more (less) intermicellar connections (bridges). Since the formation of bridges corresponds to the growth of larger length scale structures, we associate the breadth of the transition noted in the transmittance experiments to the number of bridges as a function of temperature and gradient strengths. To corroborate these hypotheses, in this section we present results which characterize the micellar aggregates through two measures: (i) Their aggregation numbers (i.e. number of monomers in the micellar core); and (ii) The bridging number, which quantifies the number of chains forming bridges between micelles relative to the total number of chains. A chain is identified as forming a bridge if its hydrophobic monomers belong to at least two different micelle cores.

In Figure 4.12(a), we display the results for aggregation number of the micelles as a function of the gradient strength in the copolymers. Consistent with the hypothesis presented above, we observe indeed that the aggregation numbers decrease with decreasing gradient strengths. To compare these results with the behavior of annealed model copolymer sequences, we also display the aggregation numbers for L1 and L5 using the annealed model in Figure 4.12(b). In contrast to the trends noted for the quenched model, the aggregation numbers are found to increase with decreasing gradient strength in the annealed model. These results are easy to understand in the context that the annealed model becomes akin to a homopolymer solution (in a poor solvent) in the limit

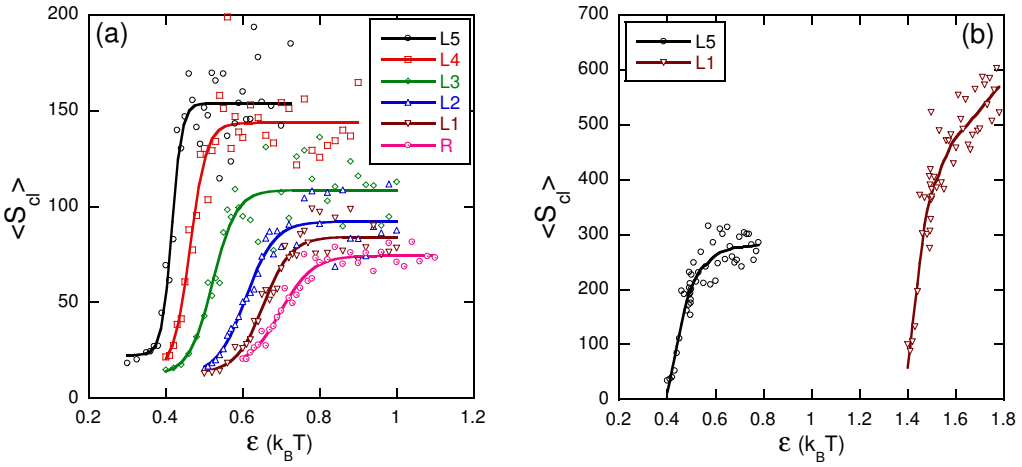

Figure 4.12: (a) Change in average size of micelle core with interaction parameter ε: R ($\Delta g = 0$), L1 ($\Delta g = 0.2$), L2 ($\Delta g = 0.4$), L3 ($\Delta g = 0.6$), L4 ($\Delta g = 0.8$), L5 ($\Delta g = 1.0$). (b) Size of cluster for annealed model as a function of interaction parameter ε: L1 ($\Delta g = 0.2$), L5 ($\Delta g = 1.0$). Lines are just a guide to the eye.

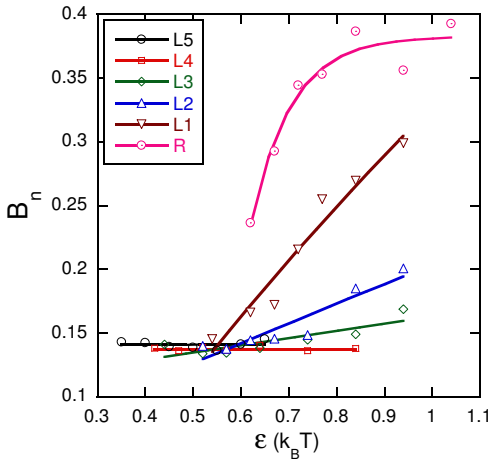

Figure 4.13: The variation in bridge number, B_n with gradient strength, Δg. Lines are just a guide to the eye.

of weak gradient strengths of the copolymer. Hence, at interaction strengths greater than the critical value, the system undergoes macroscopic phase separation characterized by the formation of a large aggregates which represent intermediates in the path towards a completely segregated system.

In Figure 4.13, we display the bridging numbers in the micelles as a function of the gradient strength of the copolymers. In accord with our hypothesis above, it can be seen that both the number of chains forming bridges, as well as the sharpness of the temperature dependence of the number of bridges, correlates inversely with the gradient strength of the copolymer solutions sequences. This result is physically intuitive since the weakest gradient copolymers are more likely to possess smaller blocks of hydrophobic monomers which are distributed over the entire backbone (Figure 4.8). Such blocks are

more likely to become involved in independent aggregation events with other chains and result in the formation of bridges among neighboring chains. Indeed, the stronger gradient copolymers resemble diblock copolymers due to their blocky ends, and hence the number of chains forming bridges are substantially lowered in such systems.

4.4 Summary

By using Monte Carlo simulations and a parallel tempering algorithm, we have studied the phase behavior of amphiphilic linear gradient copolymers for both quenched and annealed model of sequences. Under poor solvent conditions, the copolymer chains collapse to form micelle like structures. With quenched model, we found a linear trend for transition temperature with gradient strength which agrees with the results reported by Gallow *et al.*[142] We argued that such trends arise from the average length of the hydrophobic segments L_{BB} in the gradient copolymer sequences. After validating this hypothesis against our simulation results for linear gradient copolymers, we demonstrated that L_{BB} provides a quantitative means to predict the cloud point temperatures of gradient copolymer solutions even for other composition profiles.

As a second aspect of this work, we probed the statistics of the aggregates formed during the phase separation process and confirmed the two step sequence of aggregation hypothesized in experiments. Specifically, interchain interactions were found to undergo a sudden jump around the critical (cloud

point) temperature, whereas the onset of intrachain aggregation occurred at a much lower interaction strengths, consistent with the observation of a unimer-to-aggregate transition via DLS at temperatures below the macroscopic cloud points. A strong dependence of the resulting micellar properties upon the gradient strength of copolymers was also observed.

In this work, we also contrasted our results for the quenched model of gradient copolymer against that of the annealed model. In the latter situation, due to smearing of interactions, the copolymer collapse occurred at significantly higher interaction strength as compared to quenched model. While the annealed model exhibited a similar sequence of aggregation events as quenched model, much of the behaviors upon varying the gradient strengths either disappeared or contrasted with the quenched model due to the lack of sequence correlations in the annealed model.

Chapter 5

Computer Simulations of Dendrimer and Polyelectrolyte Complexes

5.1 Introduction

The increasing need for effective gene delivery vectors have motivated the design of novel polymeric materials to enhance the efficiency of drug delivery and gene therapy systems. In this context, charged dendrimers have shown great promise as they exhibit desirable binding with drug/genetic material.[40–46] In support of the utility of dendrimers for gene delivery applications, a number of experimental studies have reported the formation of nanoscale complexes/aggregates in the dilute solution of charged dendrimers and DNA molecules.[77–89] Subsequent studies have also shown that such complexes, termed as "dendriplexes," can penetrate the cell membrane and deliver genetic material.

Recent experiments have highlighted the influence of different parameters in influencing the DNA-dendrimer complexation and drug delivery. "Charged dendrimers" (henceforth referred to as "dendrimers" in the text) are regularly branched macromolecules carrying charged groups which are capable of dissociation in the presence of a solvent.[78] Such macromolecules comprise of linear

chains called spacers stemming out from one/two central monomers comprising the 0^{th} generation of the dendrimer. The spacers attached to the end groups of 0^{th} generation forms the 1^{st} generation and so on. The functionality of dendrimer denotes the number of spacers connected to each branch point whereas the generation number controls the spread or size of the molecule. A number of studies have illustrated the effect of dendrimer size/generation on the size of the clusters and on the uptake of such clusters by various types of cells. Specifically, experiments by Chen et al. found that higher generation dendrimers (4^{th} and 5^{th}) form more stable complexes in solutions with oligodeoxynucleotides (as characterized by higher zeta potential).[77] Also, the cell intake was seen to be better for complexes synthesized using 4^{th} and 5^{th} generation dendrimers as compared to those arising from lower generation dendrimers.[77] Kabanov et al. also confirmed that the solubility of clusters formed using dendrimers with generations four and five significantly differs from the dendrimers with smaller generations $(1-3)$.[254] A number of other studies have also characterized the effect of dendrimer to DNA ratio (expressed as dendrimer surface groups to DNA base pairs) and found better binding for charge ratios close to or greater than unity.[85] These experiments have raised significant interest in gaining a fundamental understanding of the influence of different parameters on polyelectrolyte-dendrimer complexation phenomena.

Motivated by the above observations, in the past decade, several theoretical and simulation studies have examined the conformational properties of the complexes formed by electrostatic binding between dendrimer and linear

polyelectrolytes (LPE).[90–104] For instance, Welch and Muthukumar used Monte Carlo simulations to examine the conformation of complexes formed between dendrimers with terminally charged groups and oppositely charged polyelectrolyte.[96] They observed different possible conformations of complexes, involving cases where a dendrimer may completely encapsulate the LPE, or situations in which the LPE can interpenetrate the dendrimer. Lyulin and coworkers used Brownian Dynamics simulations to explore the effect of dendrimer/nucleic acid charge ratio on the overall charge of the complex.[97–100]

Most of the above studies focus on a single dendrimer interacting with one (or a few) LPE molecules. Recently however, progress has been made in the context of simulating multiple dendrimers interacting with multiple LPEs.[255–257] For instance, Posocco et al.,[256] studied the self-assembly of spermine-functionalized dendrones and their aggregation with DNA using dissipative particle dynamics simulations. They found that first generation dendrones yield aggregates with higher charge density which makes them more effective in binding to DNA as compared to second generation dendrones. Eleftheriou and Karatasos used Molecular Dynamics (MD) simulation to study the effect of strength of electrostatic interactions upon the formation of complexes between dendrimers and oppositely charged linear polyelectrolytes and concluded that the chain length of polyelectrolytes and the strength of electrostatic interactions are key parameters in determining the structure of the resulting complex.[257]

While the above studies have led to several useful insights, there are still some unresolved issues. Namely, very few studies have embarked on a detail characterization of the statistical features of aggregates and clusters which result in dendrimer-LPE systems. Also, as far as we are aware, none of the earlier theoretical studies have considered the influence of parameters such as the relative concentrations of the dendrimer, LPEs and the length of the LPEs upon the resulting complexes. From a modeling perspective, many of the theoretical studies have incorporated only a screened Coulomb potential of the Debye-Huckel type. Results in other contexts have shown that such an approximation to electrostatic interactions may prove inadequate for predicting the structure and properties of charged polymers.[258] Moreover, most of the prior studies were limited to lower generation dendrimers (3^{rd} generation) containing few charge groups (≤ 24 per dendrimer). In contrast, dendrimers used in experiments are typically of higher generations, and containing larger number of surface groups — features which are expected to significantly influence the complexation phenomena.

Motivated by above issues, in this work we adapt the single chain in mean field (SCMF) simulation method to study the complexation between LPE and dendrimers. SCMF is a hybrid methodology combining Monte Carlo (MC) and polymer self-consistent field theory and provides a straightforward means to incorporate complex polymeric architectures while still enabling study of equilibrium properties of dense systems.[47–53] Moreover, study of complexation process in oppositely charged systems requires accounting for

fluctuation phenomena,[259] effects which are naturally present in SCMF framework.[210] Another advantage of SCMF type approach in contrast to competing methodologies such as field-theoretic simulations (FTS)[259] is the fact that the conformational aspects of the molecules are directly accessible in SCMF simulations, and hence quantification of cluster characteristics of the resulting complexes is much more straightforward in the latter framework.

In this study, we carry out a systematic analysis of the structures formed as a result of electrostatic interactions between peripherally charged cationic dendrimers and negatively charged LPE chains. We specifically aim to probe the effects of dendrimer generation, LPE length, salt concentration and charge ratio (i.e. concentration of charges on the LPE relative to those on the dendrimers) on the structure of the resulting aggregate. We also explicitly compare our results with the series of studies by Linse and co-workers which have systematically examined similar effects in the context of macroion-LPE mixtures.[260–265]

The outline of the rest of the chapter is as follows: In Section 5.2 we describe the nomenclature and simulation method employed in this study and a brief description of the simulation methodology and the different measures used to characterize clusters. In Section 5.3, we first present some results which validate the use of SCMF for studying electrostatic phenomena in polymeric systems. Subsequently, we present results for the effect of LPE length, addition of salt and charge ratio on the structure of the resulting complexes. We summarize our results in Section 5.4.

5.2 Simulation Method

In this section, we discuss the model and terminology used to describe the dendrimer-polyelectrolyte mixture. As mentioned in the introduction, we adopt the single chain in mean field simulation framework to model the equilibrium behavior of our system. In a nutshell, the SCMF methodology proposed by Muller and co-workers[47–53] is a MC simulation approach in which the bonded interactions between the polymer molecules are accounted in an exact manner, whereas, the nonbonded interactions are accounted through one-body interactions of polymer segments with external fluctuating potential fields. The explicit functional form of such potential fields is usually derived from the mean-field limit of the corresponding field-theory model[4] and typically leads to a framework in which the potential fields are determined by the instantaneous values of inhomogeneous densities and volume fractions. SCMF-type approaches treat different non-bonded segments of the polymer chains as independent of each other except in so far as the step of computing the potential and density fields from the coordinates of the molecules. As a consequence, such methods facilitate significant parallelization of computation and is especially suited for dense systems. Moreover, the electrostatic interactions can be efficiently quantified by solving the Poisson equation using a grid-based implementation. Further, since the molecular coordinates are retained, such a method allows for straightforward characterization of cluster features.

Our model system is comprised of dendrimers and linear polyelectrolyte molecules (LPEs) in the presence of counterions and monovalent salt ions. We

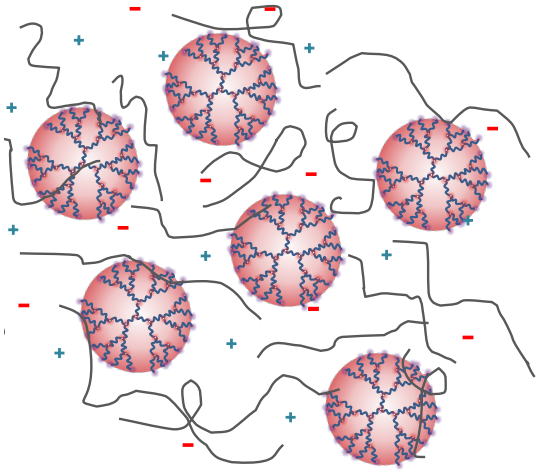

Figure 5.1: Schematic of the model system comprising of 3^{rd} generation dendrimers having functionality of 3, LPE chains and counterions.

consider a mixture of n_{DEN} peripherally charged dendrimers (i.e. only the end groups on the periphery of the dendrimer are charged) and n_{LPE} oppositely charged linear polyelectrolytes of N_{LPE} segments in a system of volume V. In this study we consider trifunctional dendrimers ($f = 3$) having generations in the range $G = 3 - 5$, with spacer length of 5. Figure 5.1 presents the schematic of our model system. The 0^{th} generation is comprised of one core monomer and the spacers attached to it. We have depicted a dendrimer with a functionality of 3 in which three spacers stem out of the core monomer. The next generation is comprised of the spacers attached to the end groups of the earlier generation and so on (the dendrimers shown in Figure 5.1 are third generation dendrimers). The total number of monomers (N_{DEN}) comprising

a dendrimer is given as:

$$N_{DEN}(G) = \frac{nf((f-1)^{G+1}-1)}{f-2} + 1 \tag{5.1}$$

where f denotes the functionality, n represents spacer length and G denotes the generation of the dendrimer. The terminal groups (i.e. monomers at the periphery of the dendrimer) are assumed to carry a positive charge, $z = 1.0$, whereas the LPE monomers are negatively charged each carrying $z = -1.0$ charge. We assume a quenched charge model for our charged monomers wherein all the charged groups on the dendrimer and LPE are completely dissociated and the charge does not vary as a function of solution conditions.

Our mean field model closely resembles the model used by Fredrickson and co-workers to study polycation-polyanion complexation.[259] We use a Gaussian chain model to characterize the connectivity between the monomers of both the LPE chain and the dendrimers. The intramolecular (bonded) energy for the dendrimer-LPE system is given by:

$$\beta U_b(\boldsymbol{r}) = \frac{3}{2b^2}\Bigg(\Bigg[\sum_{i=1}^{n_{DEN}}\sum_{g=0}^{G}\sum_{j=1}^{f(f-1)^g}\sum_{s=1}^{n-1}[\boldsymbol{r}_{i,DEN,g,j}(s+1) - \boldsymbol{r}_{i,DEN,g,j}(s)]^2\Bigg] + \Bigg[\sum_{k=1}^{n_{LPE}}\sum_{s=1}^{N-1}[\boldsymbol{r}_{k,LPE}(s+1) - \boldsymbol{r}_{k,LPE}(s)]^2\Bigg]\Bigg) \tag{5.2}$$

where $\boldsymbol{r}_{m,n}$ denotes the coordinates of m^{th} monomer of n^{th} species. b represents the length of each statistical segment which is assumed the same for the dendrimers and LPEs. In such a notation, the radius of gyration of the LPE chain of length N is given as $R_g = b\sqrt{N/6}$.

To quantify the non-bonded monomer-monomer interactions, we use an implicit solvent model and the interaction between the different LPE and dendrimer segments are represented by an excluded volume potential,

$$\beta U_{ev}(\boldsymbol{r}) = \frac{u_0}{2} \int d^3\boldsymbol{r} \rho^2(\boldsymbol{r}) \tag{5.3}$$

where u_0 is the excluded volume parameter which is assumed to be the same for both LPE and dendrimer segments and $\rho(\boldsymbol{r})$ denotes the sum of concentration of dendrimer and LPE monomers.

The electrostatic interactions between charges in the system is given by,

$$\beta U_{el}(\boldsymbol{r}) = \frac{1}{2} \int \int d^3\boldsymbol{r} d^3\boldsymbol{r}' \rho_c(\boldsymbol{r}) \frac{l_B}{|\boldsymbol{r} - \boldsymbol{r}'|} \rho_c(\boldsymbol{r}') \tag{5.4}$$

where $l_B \equiv \beta e^2/\epsilon$ is the Bjerrum length and e denotes the elementary charge of an electron. In the above, the total microscopic charge density field $\rho_c(\boldsymbol{r})$ as

$$\rho_c(\boldsymbol{r}) = z\rho^+_{DEN}(\boldsymbol{r}) - z\rho_{LPE}(\boldsymbol{r}) + z\rho_+(\boldsymbol{r}) - z\rho_-(\boldsymbol{r}) \tag{5.5}$$

where $\rho^+_{DEN}(\boldsymbol{r}), \rho_{LPE}(\boldsymbol{r}), \rho_+(\boldsymbol{r}), \rho_-(\boldsymbol{r})$ represents the microscopic charge density of terminal monomers of dendrimers, LPE monomers, positive and negative counterions respectively.

In SCMF simulations, the polymer and charge densities are expressed via actual particle coordinates and the pairwise interactions of a polymer segment with the surrounding segments is replaced by the interaction of the polymer segment with a fluctuating potential field.[48] The explicit expression for

such potential fields are derived by a transformation of the particle based representation to a field based representation.[4] In our model, these potential fields account for the excluded volume interactions between segments ($w(\boldsymbol{r})$) and the electrostatic interaction between charged species ($\Phi(\boldsymbol{r})$) and are given as:[259]

$$w(\boldsymbol{r}) = u_0\rho(\boldsymbol{r}) \tag{5.6}$$

$$\bigtriangledown^2\Phi(\boldsymbol{r}) = -4\pi l_B\rho_c(\boldsymbol{r}) \tag{5.7}$$

Using rescaled variables according to $\boldsymbol{r}/R_g \rightarrow \boldsymbol{r}, V/R_g^3 \rightarrow V, Nw \rightarrow w, Nz\Phi \rightarrow \Phi$ the system can be described using a set of dimensionless variables,[259]

$$C = \frac{(n_{LPE}N_{LPE} + n_{DEN}N_{DEN})R_g^3}{NV}, \quad B = \frac{u_0N^2}{R_g^3}, \quad E = \frac{4\pi l_B z^2N^2}{R_g}. \tag{5.8}$$

In the above, C , B and E represents respectively the nondimensionalized chain concentration, excluded volume parameter and Bjerrum length. In such a notation, the potential fields can be written as,

$$w(\boldsymbol{r}) = BC\phi(\boldsymbol{r}) \tag{5.9}$$

$$\bigtriangledown^2\Phi(\boldsymbol{r}) = -EC_c\phi_c(\boldsymbol{r}) \tag{5.10}$$

where ϕ, ϕ_c denotes the total volume fraction of monomers and volume fraction of charged species respectively. In the above,

$$C_c = \frac{R_g^3}{N}\sum_i \frac{n_iN_i}{V} \tag{5.11}$$

where i runs over the number of charged species in the system. Using above representation, the system's total Hamiltonian can be expressed as,

$$\beta H(\boldsymbol{r}) = \beta U_b(\boldsymbol{r}) + \sum_{i=1}^{N} (w(\boldsymbol{r_i}) \pm \Phi(\boldsymbol{r_i})). \tag{5.12}$$

In the above equation, the sign before the electrostatic field corresponds to the charge carried by the monomer. If the monomer is uncharged, it is only acted upon by the $w(\boldsymbol{r})$ field. Our counterions are assumed to be point particles and hence, they are only acted upon by the $\Phi(\boldsymbol{r})$ field. Such a representation is reasonable as the size of counterions is much smaller than the coarse grained polymer and dendrimer segments. Consequently, previous studies have also employed such an approach in the context of polymeric charged systems.[104, 266].

The conformations of LPE-dendrimer solution given by Eq. 5.12 were sampled using Monte Carlo simulations by using Metropolis algorithm.[168] The monomers and counterions were enclosed in a cubic simulation box with periodic boundary conditions in three dimensions. In order to compute the local volume fraction of polymer segments, contribution to eight neighboring grid points surrounding a polymer segment was considered. The potential acting at any location was derived using linear interpolation from the potential acting on eight grid points enclosing the position.

5.2.1 Simulation Details

The SCMF simulation framework is comprised of two steps repeated in a cyclic manner. In the first step, the polymer conformations are evolved under

constant external potential fields ($w(\boldsymbol{r})$ and $\Phi(\boldsymbol{r})$) for a prespecified number of MC moves. In the second step, the potential fields are updated using the instantaneous polymer and charge densities. More frequent updates of potential fields results in a framework which more effectively captures fluctuation effects.[48] Updating the potential field $w(\boldsymbol{r})$ requires only local computations and hence we update $w(\boldsymbol{r})$ after every accepted MC move. In contrast, updating the electrostatic field $\Phi(\boldsymbol{r})$ requires the solution of the Poisson equation and is hence prohibitively expensive to effect after every MC move. We use the symbol ν to denote the updating frequency, which is defined as the number of MC steps (each MC step comprises of one attempted MC move per monomer) executed in between each update of electrostatic field. Almost all our results in the subsequent sections correspond to the case of $\nu = 1$. However, for some of the cases we have repeated the simulations for a number of updating frequencies $\nu = 0.25, 0.5$ and for the set of results reported in this study, we did not notice any significant deviations in the results for charge correlations (see also Section 5.3.1).

Our simulations were initiated with random configurations of the dendrimer, LPE molecules and counterions. The initial equilibration of these polymers was effected for 1×10^5 MC steps in conditions under which all the external potential fields were absent. Subsequently, we turned on the potential fields and equilibrated for another 1×10^6 MC steps. The relevant equilibrium properties were averaged subsequently for another 1×10^6 MC steps. The trial moves involved random displacement of monomers and counterions in three

dimensions. To solve for $\Phi(\boldsymbol{r})$, the Poisson equation was solved using Fast Fourier Transform (FFT) implementation on a $128 \times 128 \times 128$ grid covering the simulation box of length $40R_g$.

The Bjerrum length in our simulations is set equal to the length of polymer segments (b) which is equal to $0.7nm$, corresponding to the Bjerrum length of water. The reduced excluded volume parameter B is set equal to 10 for all simulations (corresponds to a segment radius of approximately $0.2nm$). We did not undertake a study of the influence of these parameters on the cluster properties. The number of dendrimers, n_{DEN} for all simulations was fixed to 30 which approximately corresponds to $0.02, 0.04, 0.09$ M solutions of $G = 3, 4, 5$ dendrimers respectively. We chose this concentration in order to stay well below the overlap concentration. Moreover, most of the studies in the context of complexation behavior have been carried out in the similar concentration regime which makes it easier to compare our results with previous reports.[257, 266]

The results for complexation in dendrimer-LPE solution are divided into three sections wherein we study the effect of LPE length ratio, ionic strength and charge ratio between LPE and dendrimer respectively. The simulation details pertaining to each section are summarized in Table 5.1. The ionic strength is defined as $I = 0.5 \sum_i z_i^2 c_i$ where z_i and c_i are the charge and molar concentration of species i respectively.

In order to confirm that the resulting conformations are true equilibrium configurations, we examined the root mean squared displacement of cen-

Table 5.1: System parameters

G	Effect of LPE Length		Effect of Ionic Strength			Effect of Charge Ratio		
	N_{LPE}	n_{LPE}	N_{LPE}	n_{LPE}	I (M)	N_{LPE}	n_{LPE}	I (M)
3	12,24,48	60,30,15	24	30	0.005-0.1	24	1,15,30,45,60	0.005
4	24,48,96	60,30,15	48	30	0.005-0.1	48	1,15,30,45,60	0.005
5	48,96,192	60,30,15	96	30	0.005-0.1	96	1,15,30,45,60	0.005

ter of mass of dendrimers and LPE molecules. On an average, the dendrimers and LPE molecules were seen to travel $1.6R_g$ and $3R_g$ respectively during each set of 500 MC cycles. This shows that the macromolecules do exhibit substantial displacement during the simulation and suggests that the aggregates we obtain are expected to be of equilibrium nature.

5.2.2 Cluster Analysis

The objective of this study is to quantify the aggregation characteristics of complexes formed in solutions of dendrimer-LPE mixtures. Towards this objective, we carried out a systematic cluster analysis which is adapted from a procedure originally proposed by Sevick et al.[250, 252, 253, 267] In brief, the distribution of particle clusters is analyzed through a connectivity matrix which accounts for direct contact between components of the mixture. This matrix is then further modified to account for indirect connectivity, i.e., particles connected through other particles in the cluster. In our work, two particles

are assumed to be directly connected if the distance between them is less than the grid spacing employed in our simulations. Although this choice of cut off distance is arbitrary, we believe it is still a reasonable choice given the fact that correlation effects smaller than the grid spacing are ignored. From this procedure, we probe the following aspects of cluster statistics: (i) The average radius of gyration of cluster, $< R_{g,cl} >$, where the radius of gyration of a cluster containing n particles is given as:

$$R_{g,cl}(n) = \frac{1}{n} \sum_{i=1}^{n} (\boldsymbol{r}_i - \boldsymbol{r}_{com})^2 \tag{5.13}$$

where $\boldsymbol{r}$ and $\boldsymbol{r}_{com}$ are the coordinates of particle within the cluster and center of mass of the cluster respectively; (ii) The probability distribution of cluster size, $P_{cl}(r)$ representing the fraction of clusters of radius of gyration r; (iii) The cluster charge distribution which quantifies the net charge Q_{cl} distribution as a function of radial distance from the center of mass $\boldsymbol{r}_{com}$ of a cluster; (iv) Bridging fraction, B_f, defined as the average number of LPEs connected to more than one dendrimer. (v) We also probe the dendrimer center-to-center radial distribution function which quantifies the aggregation propensity of dendrimers.

5.3 Results and Discussion

In this section we present results for complex formation in our model system of multiple dendrimers and multiple LPEs in presence of counterions. As a first step, we validate the qualitative ability of our simulation framework

to capture structural features of systems containing charged macromolecules. For this purpose, we study the model of a mixture of positively and negatively charged LPEs, and compare the results with existing theoretical predictions. Subsequently, in the context of dendrimer-LPE solutions, we study the effect of (i) dendrimer sizes, (ii) LPE length, (iii) salt concentration and (iv) charge ratio on the complexation behavior.

5.3.1 Validation of Simulation Method

A number of past studies have used a variety of simulation methods, ranging from particle based MC, MD simulations,[94, 98, 101, 258, 268–270] field theoretic[208, 259] and mean field simulations,[104, 271–276] theoretically informed coarse grained simulations, etc.,[277, 278] to study charged polymeric systems. However, to our knowledge the present report is the first study to examine charged systems using the SCMF approach. In this section, we present some selected results of studies we undertook on simpler systems to validate the simulation framework, its ability to reproduce the physics underlying electrostatic interactions.

The system considered in this section is a mixture consisting of equal volume fraction of identical homopolymers carrying positive (polycations) and negative charge (polyanions). Each monomer carries either a $+z$ or $-z$ charge and the monomers are fully dissociated at all solvent qualities. We specifically probe the charge structure factor $S_{cc}(q)$ for such a system and compare against the corresponding theoretical predictions. We note that an identical system

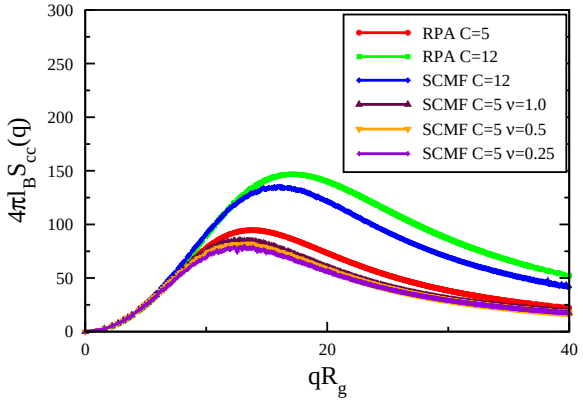

Figure 5.2: Charge structure factor computed using the simulation framework employed in this study for $E = 3600$ and $C = 5, 12$. Comparison to RPA prediction is also displayed.

has been studied by Fredrickson and co-workers using the field theoretic simulation methodology to examine the influence of fluctuation effects.[259] For the parameters $C = 12$, and E in the range $900 - 19600$, they found that the charge structure factors from FTS were in good agreement with predictions based on random phase approximation (RPA). In such a framework, the charge-charge correlation $S_{cc}(q)$ is given by

$$\frac{4\pi l_B}{q^2} S_{cc}(q) \approx \frac{CE\hat{g_D}(q^2R_g^2)}{q^2R_g^2 + CE\hat{g_D}(q^2R_g^2)}. \tag{5.14}$$

The parameters C and E are defined in Eq. 5.8. $\hat{g_D}(q^2R_g^2)$ is the Debye scattering function for an ideal Gaussian chain:[279]

$$\hat{g_D}(x) = \frac{2}{x^2}[\exp(-x) + x - 1]. \tag{5.15}$$

In Figure 5.2 we display the charge structure factor calculated using our framework for $E = 3600$ and $C = 5, 12$, alongside the RPA predictions for

same parameters. We observe that the simulation results are able to match most of the aspects of the theoretical predictions. Specifically, both the location of the peak and the trends arising from changing C are seen to be well-captured within our simulation framework. Quantitatively, we do observe deviations in the magnitude of the charge correlations especially at large wave vectors, which likely arise from the grid framework and coarse-graining inherent in SCMF simulations. The dependence of the results on the updating frequency, ν, for solution of Poisson's equation is also indicated. The charge structure factor is seen to have only a small dependence upon the updating frequency of electrostatic potential. While the influence of updating frequency is seen to be more pronounced for higher values of E, the qualitative effects are seen to be captured even with updating frequency equal to unity. Thus, for the set of parameters considered in this short assessment of our simulation framework, we observe that our simulation method qualitatively captures the charge correlations in polymeric systems.

5.3.2 Complexation in Dendrimer-LPE Solutions

5.3.2.1 Effect of LPE Length

The binding mechanism between charged dendrimer and linear polyelectrolytes is largely dominated by electrostatic attractions. Hence, modifications in the number of charges carried by one of the components of the solution is expected to have a strong influence on the structure of the resulting complexes. Since we assume that the fractional charge carried by the monomers is

fixed, we use LPE length as a parameter to vary the charge carried by individual LPE. We quantify the effect of LPE length using a parameter α defined as the ratio of actual LPE length to LPE length required to balance the charge on the dendrimer.

$$\alpha = \frac{N_{LPE}}{N_{LPE,0}} \tag{5.16}$$

where $N_{LPE,0}$ represents the LPE length required to balance the opposite charge on a dendrimer. For $G = 3, 4, 5$ dendrimers used in this study $N_{LPE,0} = 24, 48, 96$ respectively, and the systems we considered correspond to $\alpha = 0.5, 1.0, 2.0$. However, the number of LPEs were adjusted so that the net negative charge on the LPEs is balanced by the net positive charge on dendrimers. The simulation results presented in this section are carried out at a constant low ionic strength at conditions in which the salt was absent and counterions were included.

Figure 5.3 shows configurations from the simulations for system containing $G = 5$ dendrimers having (a) $\alpha = 0.5$ and (b) $\alpha = 2.0$. We observe that several independent clusters are formed for shorter LPEs corresponding to $\alpha = 0.5$, whereas large clusters connected by LPE molecules are visible for longer LPEs with $\alpha = 2.0$. We note that Linse and coworkers have used MC simulations to study the effect of LPE length on the complex formation between proteins and LPE molecules[266] and observed that shorter LPEs showed less propensity for protein-protein aggregation as reflected in the formation of small clusters, in contrast, larger clusters were seen to form in systems with longer LPEs. Our results displayed in Figure 5.3 are seen to be

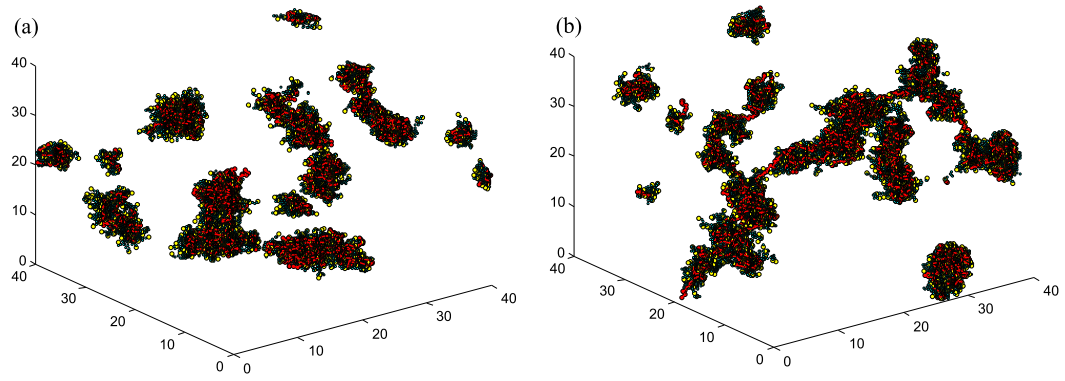

Figure 5.3: (a) Snapshots from simulation for $\alpha = 0.5$ and (b) $\alpha = 2.0$ for $G = 5$ dendrimer. The uncharged dendrimer monomers are shown in blue whereas charged dendrimer monomers are shown in yellow. For clarity, uncharged dendrimer monomers are drawn smaller than charged dendrimer monomers. The LPE monomers are colored in red connected with thick red line.

consistent with such earlier results. In the following text, we quantify our observations using the analysis tools described in Section 5.2.2.

To quantify the organization of the dendrimers within the clusters, we present the dendrimer center-to-center radial distribution functions (rdfs), $(g_{DEN-DEN}(r))$, for $G = 3, 4, 5$ in Figure 5.4. The $g_{DEN-DEN}(r)$ for the case with no electrostatic interactions for $\alpha = 1.0$ is also shown for comparison. The neutral case is seen to display a trend in which the $g_{DEN-DEN}(r)$ gradually increases from zero till unity, characteristic of the presence of only excluded volume interactions between the soft dendrimer cores. In contrast, all the charged systems are seen to display a large peak in $g_{DEN-DEN}(r)$ characteristic of aggregation between the dendrimers. The peak in $g_{DEN-DEN}(r)$ is seen to increase with increasing LPE length ratio α which suggests a higher propensity

for dendrimer aggregation with increasing LPE lengths. Moreover, the overall peak in the $g_{DEN-DEN}(r)$ is seen to shift towards higher separation distances with increasing size/generation of dendrimer.

The above results can be rationalized based on the understanding that the primary driving force for complexation phenomena in dendrimer-LPE systems is the presence of electrostatic interactions between the dendrimer and the LPEs. An increase in α increases the number of dendrimers which can be complexed by a single LPE (below, we present results for the bridging fractions which supports this hypothesis), and thereby serves to bring more of the dendrimers together within a single cluster. Such an effect serves to enhance the peak in the dendrimer-dendrimer radial distribution function $g_{DEN-DEN}(r)$. On the other hand, the location of the peak in the $g_{DEN-DEN}(r)$ reflects a balance between the excluded volume repulsions between the charged dendrimer cores and their aggregation mediated by the LPEs. It is seen to be relatively insensitive to the LPE lengths and occurs at a distance of the order of the radius of gyration of the dendrimer (for instance, the peak for $G = 5$ dendrimers occurs at approximately $1.2R_g$), a feature which is consistent with the dilute dendrimer concentrations in our simulations.

The above results provide insights into the nature of the dendrimer packing within the aggregates, but do not shed light on the nature of the aggregates themselves. To quantify further the nature of the clusters that form in our simulations, in Figure 5.5 we display the probability distribution of cluster sizes $P_{cl}(r)$ for the dendrimer-LPE solution. Figure 5.6(a) displays

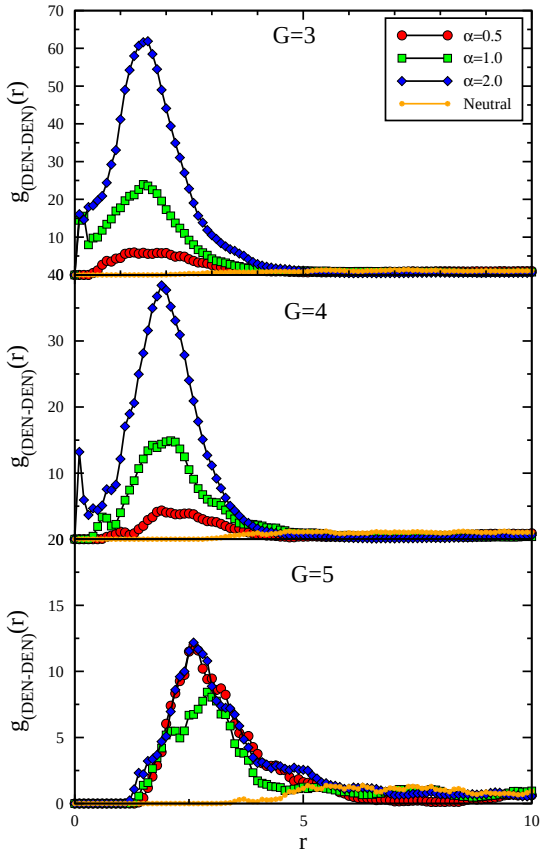

Figure 5.4: Dendrimer center to center radial distribution function, $g_{DEN-DEN}(r)$, for dendrimer generations $3, 4, 5$ as a function of α. The neutral case represents the $g_{DEN-DEN}(r)$ for $\alpha = 1.0$ without electrostatic interactions.

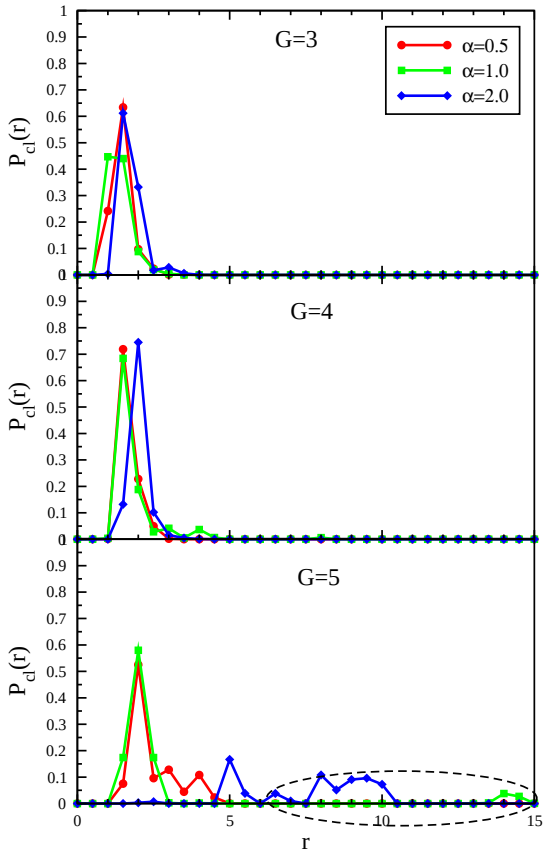

Figure 5.5: Probability distribution of cluster size, $P_{cl}(r)$, as a function of LPE length ratio, α for dendrimers of different generation. The lines are guide to the eye.

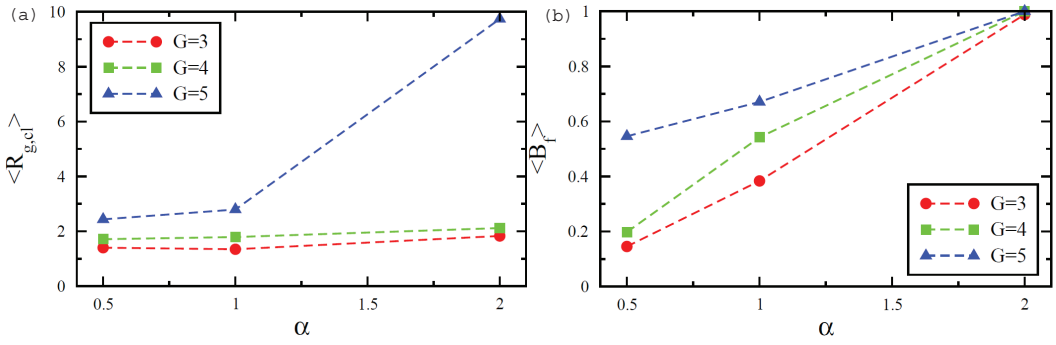

Figure 5.6: (a) The average size of clusters as a function of α for different dendrimer generations. (b) The bridging fraction B_f as a function of α for different dendrimer generations. The lines are guide to the eye.

the corresponding average cluster sizes of the aggregates as a function of α and G. Overall, we observe that with an increase in α there is a shift from a narrowly peaked distribution (at small sizes) to one which exhibits an increased tendency for clusters of larger sizes. Correspondingly, the average cluster size is seen to increase with both the dendrimer generation and the LPE lengths.

The above dependencies of the cluster statistics on the LPE lengths can again be rationalized as a consequence of the propensity for longer LPE chains to "bridge" and thereby complex with more than one dendrimer. Such an effect is expected to lead to a shift of the cluster size distributions to larger clusters. To provide evidence for this effect, in Figure 5.6(b), we display the bridging fraction, B_f, defined as the fraction of LPE monomers complexed with more than one dendrimer. Consistent with our expectations, we observe that longer LPE molecules (higher α) exhibit larger B_f values.

The dependencies of the cluster statistics upon the dendrimer genera-

tion can generally be rationalized as a simple consequence of the larger size of the dendrimers themselves. Consistent with such a reasoning, we observe that for larger G, the cluster distributions are peaked at larger cluster sizes and are indeed characterized by larger average sizes (Figure 5.6(a)). Interestingly, the results for $G = 5$ display trends which are somewhat distinct from $G = 3$ and 4. Explicitly, for $G = 5$ we observe that the cluster size distributions show a pronounced influence of α (large clusters as big as $16R_g$ are evident for $\alpha = 2.0$, as indicated by the dotted lines in Figure 5.5), and correspondingly we observe that the average size of clusters display a pronounced jump for $\alpha = 2.0$. We believe that such trends arise from the fact that our dendrimers are terminally charged, and hence, a larger generation dendrimer which possesses a larger surface area furnishes a stronger possibility for clusters in which different LPEs complex with different portions of a single dendrimer. This would lead to the formation of a loosely packed aggregate of dendrimers which however span a substantial physical extent as reflected in Figure 5.5. The snapshots displayed in Figure 5.3b are seen to be consistent with this picture. Moreover, we also observe that the $g_{DEN-DEN}(r)$ for $G = 5$ displayed in Figure 5.4 are relatively insensitive to α which supports our hypothesis of a dispersed cluster of dendrimers.

The overall charge on the dendrimer-LPE complex has been speculated to play an important role in the uptake of complexes by cells. Motivated by such considerations, in Figure 5.7 we display the average integrated charge distribution, $< Q_{cl} >$ (with reference to the center-of-mass of the cluster) for

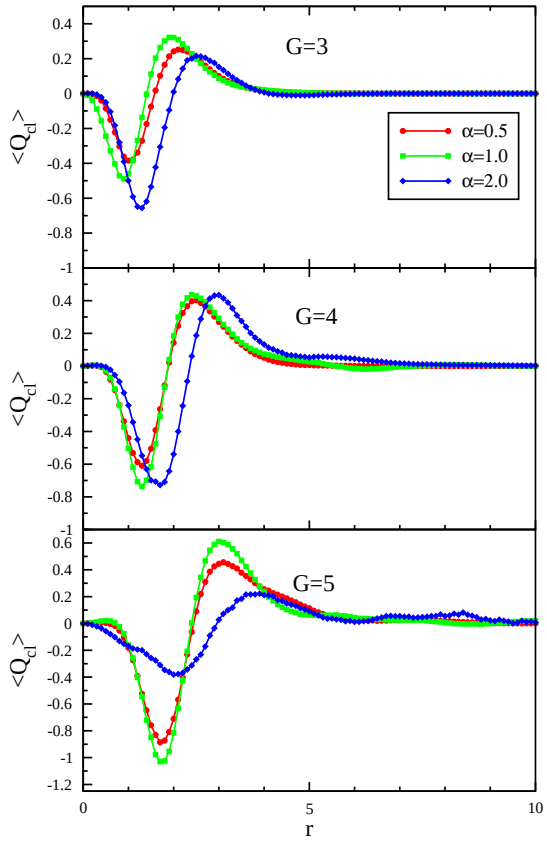

Figure 5.7: Average cluster charge distribution, $< Q_{cl} >$, as a function of dendrimer generation for varying α. The lines are guide to the eye.

the dendrimer-LPE clusters. We observe the dendrimer-LPE complex develops a net negative charge near the center of the cluster which is akin to an overcharging-like effect of the LPEs. At further distances, there is an increased positive charge (Figure 5.7) arising from the neighboring dendrimer molecules. With increasing α, we observe a broader charge distribution which is consistent with increase in average cluster sizes (see Figure 5.6(a)). More interestingly, we observe that the peak in the charge distributions show a nontrivial interplay between the generation numbers and the LPE lengths. Explicitly, for $\alpha = 0.5$ and 1.0 we observe that peak in the charge distributions display larger magnitudes for higher Gs. Such a trend is consistent with the larger (positive) charges possessed by the individual dendrimers for higher Gs. However, for the case of $\alpha = 2.0$ we observe that the peak in $G = 5$ is lower than the corresponding value for $G = 4$. The latter can be understood based on our results of cluster size distributions which indicated the formation of loosely packed clusters for $G = 5$.

In general, from a cell uptake perspective, positively charged complexes are more desirable due to the inherent electrostatic interactions with the cell membranes. Our above results are consistent with the work by Chen et al.[77] which used zeta potential measurements to show an increase in the stability of dendrimer-DNA complexes and their uptake with increasing dendrimer generation. However, our results go beyond such simple considerations also indicate that the effect of generation alone cannot be relied upon as a unique quantity to determine the efficacy of dendrimer-LPE complexes. Indeed, for

appropriate combinations of G and α, lower generations may possess a higher positive charge and efficiency for interactions with the cells. Such insights require detailed characterization of the cluster size and charge distributions such as effected in this work.

5.3.2.2 Effect of Ionic Strength

We now present results for the effect of salt concentration on the dendrimer-LPE complexation characteristics. Since electrostatic interactions are the main driving force for complexation, an increase in the salt concentration is expected to lead to less propensity for complexation. For instance, Linse and co-workers have studied similar effects for LPE-macroion systems and have shown that dissolution of the complexes can be achieved by the addition of appropriate concentrations of salt.[262] For this section, we consider a dilute solution of LPE and dendrimers at stoichiometric charge ratios for dendrimer generation $3-5$ for ionic strengths in the range $I = 0.005 - 0.1M$. The screening length, $\kappa = (4\pi l_B \sum_i z_i^2 c_i)^{-0.5}$ corresponding to the ionic strength values are in the range $\kappa = 4.28 - 0.96$ nm. Since we simulate dendrimer and LPEs at stoichiometric charge ratio, we have only included salt ions (no counterions) for this case. Thus, only salt ions contribute to the ionic strength of the solution.

In Figure 5.8 we display $g_{DEN-DEN}(r)$ for $G = 3, 4, 5$ for different values of ionic strength ($I = 0.02, 0.06, 0.1$). We have also presented the $g_{DEN-DEN}(r)$ for the neutral case where there is an absence of dendrimer aggregates. We observe that with increasing ionic strength, the peak in $g_{DEN-DEN}(r)$

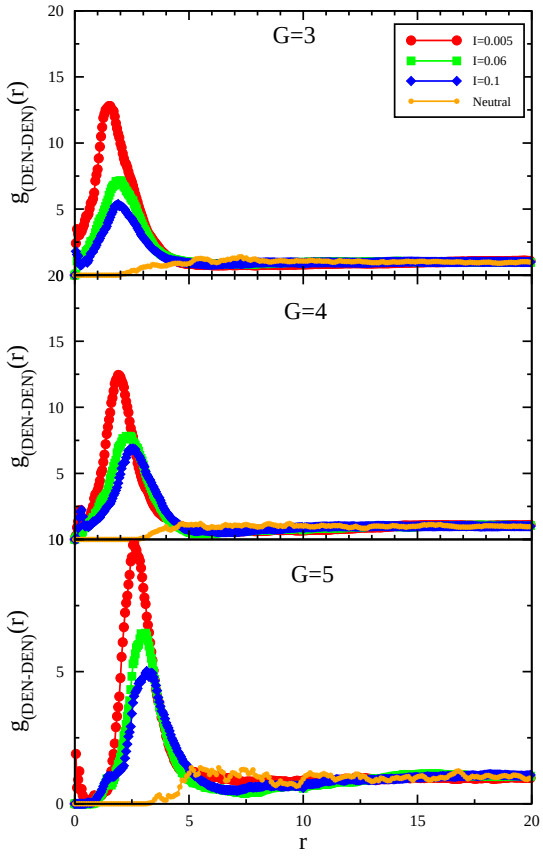

Figure 5.8: Dendrimer center to center radial distribution function, $g_{DEN-DEN}(r)$, for dendrimer generations $3, 4, 5$ as a function of ionic strength.

decreases. Such a trend is consistent with the expectation that increasing ionic strength should decrease the propensity for complexation. As a consequence, we also expect the interpenetration between dendrimers to decrease, a behavior which is reflected in the small but noticeable increase in the average separation between dendrimers.

Interestingly, we see that the aggregation between dendrimers becomes less pronounced with increasing generation/size of the dendrimer at low ionic strength, whereas, for higher ionic strengths the peak in $g_{DEN-DEN}(r)$ is seen to be higher for larger dendrimers. This behavior suggests that larger dendrimers require a larger concentration of salt to facilitate their dissolution. This is expected since the number of charges carried by dendrimers increase with increasing size/generation.

The corresponding cluster size distributions for $G = 3, 4, 5$ are shown in Figure 5.9. Interestingly, we observe that for all dendrimer generations, a preferred cluster size exists which is independent of salt concentration. With the increase in salt concentration, the number of clusters at the most probable size is seen to reduce. With further addition of salt, we expect the trend to continue and lead to dissolution of clusters. In some cases (see results for $G = 5$) we observe the formation of larger clusters at higher ionic strengths. These results may be speculated to be a consequence of increased salt ions which may reduce the electrostatic repulsion between clusters and allow them to merge into larger ones. Alternatively, these results may just be an artifact of our procedure for classifying overlapping monomers as belonging to the same

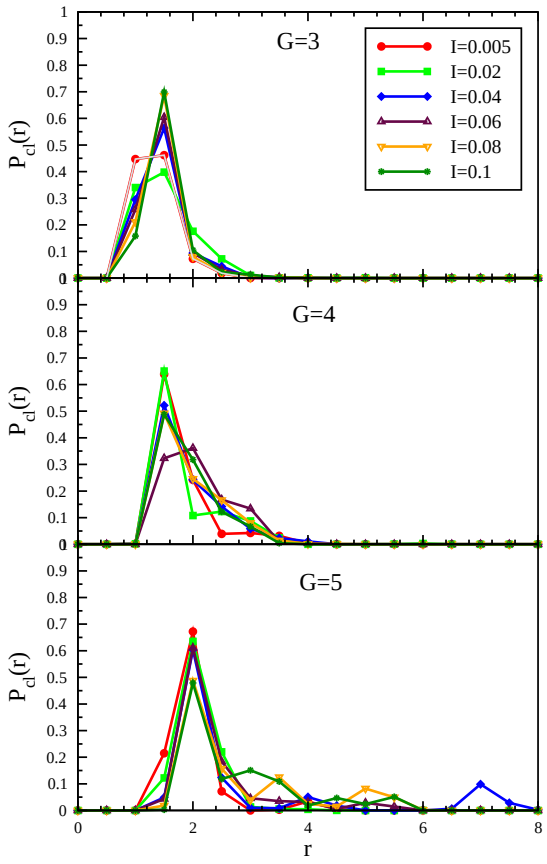

Figure 5.9: Probability distribution of cluster size, $P_{cl}(r)$, as a function of ionic strength for dendrimers of different generation. The lines are guide to the eye.

cluster, which may lead to assignment of some well-dispersed morphologies as being erroneously classified as large clusters.

Summarizing, the addition of salt has qualitatively similar effects for $G = 3, 4$ and 5 dendrimers. The peak in $g_{DEN-DEN}(r)$ is seen to decrease with increasing ionic strength suggesting decrease in binding between dendrimers. Smaller size/generation dendrimers are seen to exhibit stronger/enhanced effect of salt concentration which is attributed to small number of charged groups associated with smaller generation dendrimers. At low ionic strength, several small clusters are seen to form. While much of the preceding results are intuitive, an interesting outcome of our cluster analysis is the characterization of the size distributions as a function of the ionic strength which indicates the persistence of a preferred cluster size even for larger ionic strengths.

5.3.2.3 Effect of Dendrimer-LPE Charge Ratio

We now present results quantifying the influence of charge ratio between LPEs and dendrimers on the complexation behavior. For this purpose, we use a parameter β (referred as charge ratio in the text) defined as the ratio of total negative charge on LPE to the total positive charge on dendrimer:

$$\beta = \frac{n_{LPE} N_{LPE} z_{LPE}}{n_{DEN} N^{+}_{DEN} z_{DEN}}. \tag{5.17}$$

In the above, N^{+}_{DEN} denotes the number of positive charges on a dendrimer. We are motivated by previous experimental works which have suggested a significant influence of charge ratio on the properties of resulting clusters.[254]

Specifically, better binding between dendrimer and DNA has been observed when the total charge carried by the dendrimer is equal to or greater than the total charge on DNA. In this section, we quantify the effect of the charge ratio β on the properties and structure of clusters formed in dendrimer-LPE solution. We studied systems in which $\beta = 0.03, 0.5, 1.0, 1.5, 2.0$ and the simulations were carried out at a constant low ionic strength value of $0.005M$. Since the total charge on the dendrimers is not balanced by the total charge on LPEs, counterions have been included to ensure electrical neutrality.

In Figure 5.10 we display some simulation snapshots at conditions corresponding to excess dendrimer charge ($\beta = 0.5$), equal absolute charge ($\beta = 1.0$) and excess LPE charge ($\beta = 1.5$) for dendrimer-LPE solutions containing $G = 5$ dendrimers. For the system containing excess dendrimer charge ($\beta = 0.5$), we observe a state characterized by several dispersed clusters. With increase in β, enhanced bridging and consolidation of the clusters is evident. For the system containing excess LPE charge ($\beta = 1.5$), we see that the system again reverts to a state of dispersed clusters. For the case of $\beta = 1.5$ we see a number of LPEs which are attached to the dendrimer on one end but with a tail-like configuration which protrudes outside the complex. This can be understood to be a consequence of the excess LPE concentration due to which several LPEs partially compensates for the charge on a dendrimer. Hence, only a part of LPE chain complexes with the dendrimer and the other part remains outside the complex.

In Figure 5.11 we display the dendrimer-dendrimer radial distribution

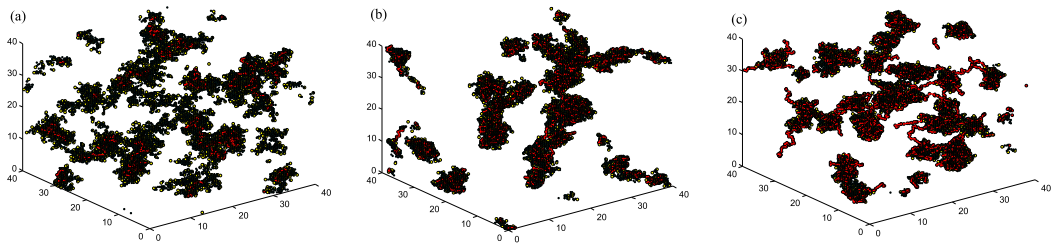

Figure 5.10: Snapshots from simulation for (a) $\beta = 0.5$, (b) $\alpha = 1.0$ and (c) $\beta = 1.5$ for $G = 5$ dendrimer. The uncharged dendrimer monomers are shown in blue whereas charged dendrimer monomers are shown in yellow. For clarity, uncharged dendrimer monomers are drawn smaller than charged dendrimer monomers. The LPE monomers are colored in red connected with thick red line.

functions, $g_{DEN-DEN}(r)$, for varying β. It can be observed that when β is close to zero i.e. when there are no (or very few) LPEs in the solution, the rdf gradually increases from zero to unity. Such a behavior is consistent with the behavior expected for a homogeneous solution of dendrimers characterized only by electrostatic and excluded volume interactions. Upon increasing β to $\beta = 1.0$, we observe that the magnitude of the peak in $g_{DEN-DEN}(r)$ grows and the peak location moves to smaller r. This indicates an increased propensity for aggregation between dendrimers and the formation of a more closely packed cluster of dendrimers (also seen in Figure 5.10b). Increasing β beyond $\beta = 1$ is seen to lead to a reduction in the magnitude of the peak and eventually at larger β we observe that the $g_{DEN-DEN}(r)$ reverts back to the form characteristic of a homogeneous solution of dendrimers.

The above results confirm that for all generation numbers the most

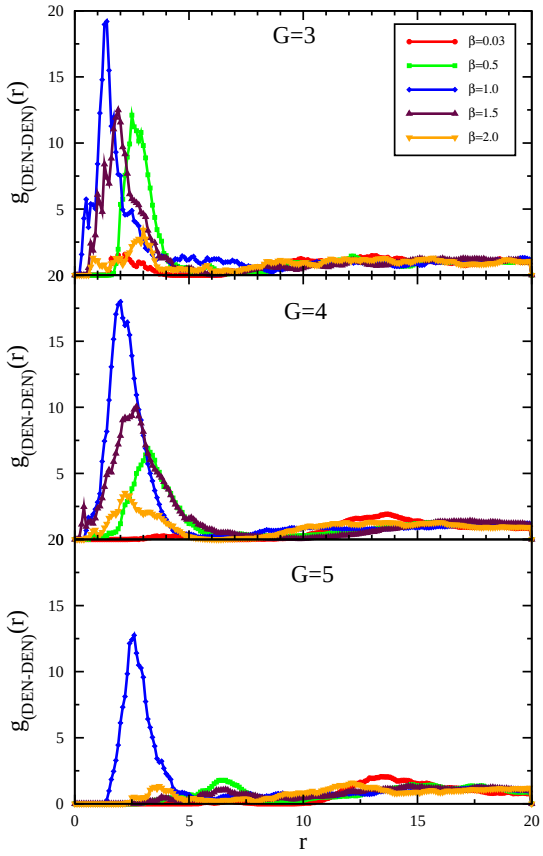

Figure 5.11: Dendrimer center to center radial distribution function, $g_{DEN-DEN}(r)$, for dendrimer generations $3, 4, 5$ as a function of charge ratio.

propensity for forming complexes occur for a situation in which the total charge carried by the dendrimers balance those on the LPEs. For the cases when $\beta \neq 1.0$ one may hypothesize that the unbalanced charges lead to some effective repulsions between the individual dendrimers complexed with LPEs. As a result there is expected to be reduced aggregation and less dense packing of the dendrimers in the clusters. The results presented in Figure 5.11 are consistent with such a hypothesis. Within this physical picture, one may expect that for a specified $\beta \neq 1$ the effective repulsions will be more pronounced and as a result the aggregation tendency will be reduced for higher generation dendrimers. The magnitudes of the peaks in Figure 5.11 at a specified β for the different generations are seen to be consistent with such a reasoning. Interestingly, for $G = 5$, clustering between dendrimers is observed only in systems with equal absolute charge ratio ($\beta = 1$). All other charge ratios are seen to exhibit a homogeneous mixture of dendrimers which is indicative of strong effective repulsions arising for the unbalanced charge situations ($\beta \neq 1.0$).

Figure 5.12 presents the average size of the clusters as a function of β. The average radius of gyration of the clusters is seen to exhibit a non-monotonic trend with β. The cluster size distributions shown in Figure 5.13 provides insights into the trends observed in average size of the cluster (we display the explicit cluster size distributions instead of the probability distributions). Explicitly, for small β we observe the presence of only a few clusters of finite and large sizes coexisting with very small complexes. Moreover, as seen in Figure 5.14, the bridging fraction of LPEs is close to unity in such regimes.

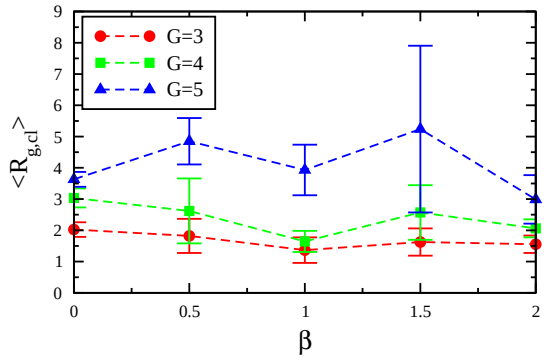

Figure 5.12: The average size of clusters as a function of α for different dendrimer generations. The lines are guide to the eye.

These results suggest that large clusters owe their existence to LPE bridging. With increasing β we observe that the bridging fractions (Figure 5.14) become reduced and correspondingly the size distribution moves towards smaller clusters. These trends are seen to be reflected in the reduction of the average R_g of the cluster displayed in Figure 5.12. Increasing β beyond $\beta = 1.0$ is seen to decrease the number of bridges between the clusters (Figure 5.14) which leads to an increase in the number of clusters with only little change in the most probable size of the clusters (Figure 5.13). This correspondingly leads to the increase in the average R_g of the cluster seen in Figure 5.12. The further decrease in average size of the clusters upon increasing β from 1.5 to 2.0 is a consequence of the occurrence of a large number of small clusters at $\beta = 2.0$ which contrasts with a broader distribution of cluster sizes at $\beta = 1.0$. The higher concentration of LPE molecules leads to complexation of a dendrimer with more than one LPE resulting in a net negative charge on the periphery of

the clusters (see cluster charge distribution discussed below). Such effect induces repulsion between clusters leading to decrease in average size of clusters observed at $\beta = 2.0$.

In Figure 5.15 we plot the average cluster charge, $< Q_{cl} >$ distribution for $\beta = 0.03 - 2.0$. The width of cluster charge distribution is seen to be correlated with the average size of the cluster displayed in Figure 5.12. Specifically, the cluster charge distributions are seen to be narrow and small in magnitude at $\beta = 1.0$ which suggests formation of several separated clusters when the absolute charge on dendrimer balanced by the opposite charge on LPE. In contrast, the cluster charge distribution shows an overall positive charge on the complex at the average cluster size for cases when the dendrimer concentration is equal or in excess as compared to the LPE concentration. Since the cell membrane is known to have a negative charge, the most suitable complexes for the purpose of gene delivery should possess a positive charge. In conjunction with the need to generate aggregates of dendrimers, this suggests that the systems with β close to but less than unity are likely to form the most suitable complexes for drug delivery.

5.4 Summary

We presented results for the complexes formed between dendrimers and linear polyelectrolyte molecules in a dilute solution under good solvent conditions with a focus on examining the effect of dendrimer generation/size on the complexation behavior. We examined the effect of LPE length, salt concen-

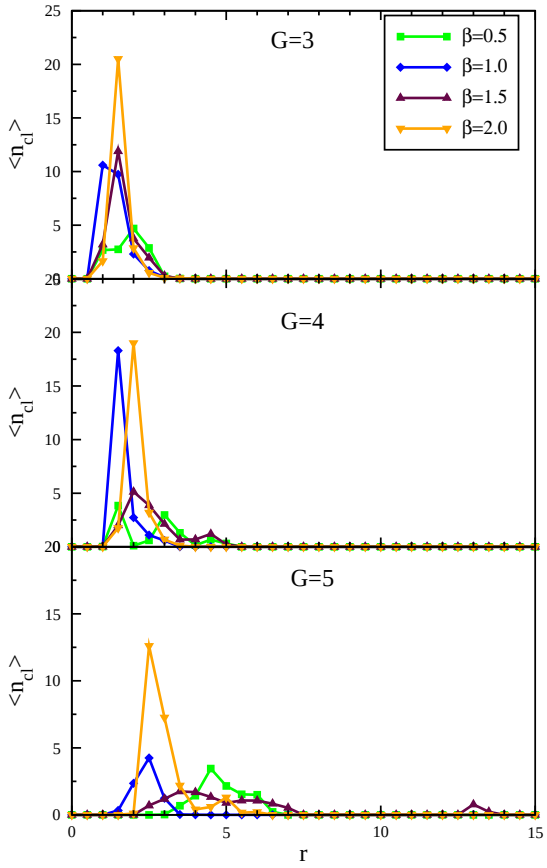

Figure 5.13: The cluster size distribution as a function of charge ratio for dendrimers of different generation. $< n_{cl} >$ represents the average number of clusters of size r in units of R_g. The lines are guide to the eye.

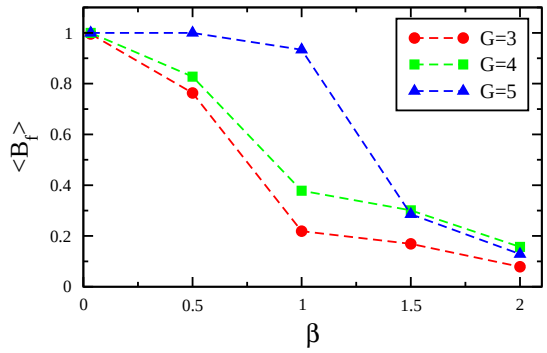

Figure 5.14: The bridging fraction B_f as a function of β for different dendrimer generations. The lines are guide to the eye.

tration and charge ratio on the static properties cluster/complexes formed.

The complexation behavior was seen to significantly depend upon dendrimer size in all cases. When the LPE lengths were increased, larger clusters were observed for all generations studied. The aggregation between dendrimers was seen to increase with increasing LPE length for smaller dendrimers ($G = 3, 4$). For larger dendrimers ($G = 5$), however, the aggregation between dendrimers was insensitive to LPE length although larger clusters were formed. This effect was attributed to bridging due to longer LPE chains which interconnects the clusters without increasing the aggregation between dendrimers. With addition of salt, the binding between dendrimer and LPE was seen to reduce. The effect of addition of salt was seen to be more pronounced for smaller generation dendrimers.

The charge ratio between dendrimers and LPEs had a substantial effect on the properties of clusters. Larger dendrimers ($G = 5$) were seen to be

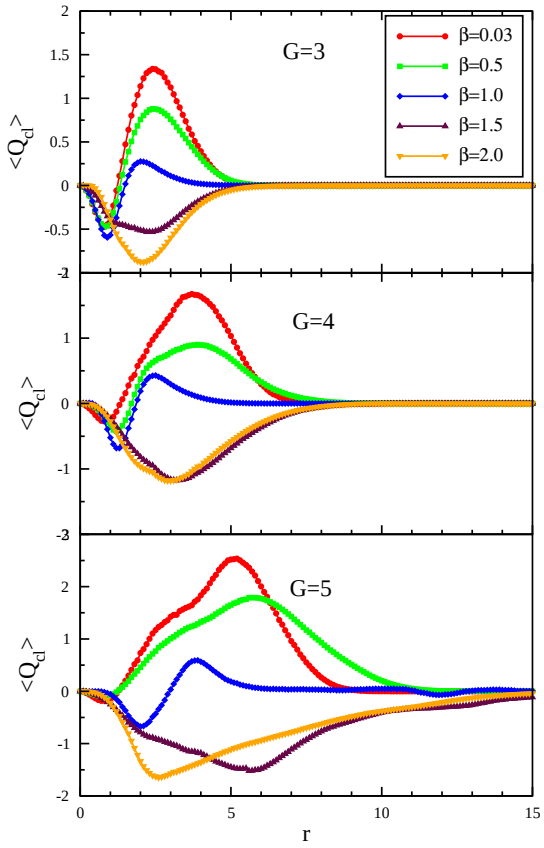

Figure 5.15: Average cluster charge distribution, $< Q_{cl} >$, as a function of dendrimer generation for varying β. The lines are guide to the eye.

most sensitive to charge ratio and formed aggregates only at balanced absolute charge case. Smaller dendrimers ($G = 3, 4$) displayed a non-monotonic behavior with increasing charge ratio eventually leading to redissolution at higher values of charge ratio.

The results presented in this chapter demonstrates that the SCMF approach can serve as a versatile framework to study and characterize the phenomena relevant to multi-body dendrimer-LPE interactions. In future studies we propose to consider physics relevant to systems comprising of stiff chains (which are more faithful models of DNA and RNA polymers) interacting with dendrimers.[104]

Chapter 6

Interactions, Clustering and Multibody Effects of Charged Nanoparticles in Uncharged Polymer Solutions

6.1 Introduction

Nanoclusters comprised of colloidal particles have attracted significant interest in the context of biomedical imaging, catalysis, electronics, sensors, electromagnetic imaging.[280–286] Adding polymers to suspensions of nanoparticles in order to induce clustering is emerging as a strategy to synthesize such equilibrium aggregates for a variety of applications. A number of experiments have demonstrated formation of equilibrium clusters in which the cluster size can be tuned by varying the nanoparticle and polymer concentrations, size and charge.[287–289] Such effects have been hypothesized to arise from the interplay between the short range depletion attraction induced by addition of polymers and the electrostatic repulsion between charged particles.[39, 290–292] Not surprisingly, there has arisen a significant interest in relating the cluster structure and sizes of the equilibrium aggregates to the physical parameters underlying the particle-polymer mixture.

Despite the significance of the above problem, theoretical advances in the context of mixtures of charged nanoparticle (CNP)-uncharged polymers

have been limited. Full-scale simulations in which the charged particles, polymers and ions are treated on an equal rigorous footing are computationally expensive.[262, 263] As a consequence, interparticle interactions are routinely approximated by the effective polymer-mediated two-body potentials deduced at the dilute limit of CNP concentrations, and are used in simulations involving just the particle system.[293–296] Such approaches typically invoke a short-range attraction to model the polymer depletion interaction, and a long-range repulsion to characterize the electrostatic interactions.[288, 292] It has been argued that the short range depletion attraction drives the aggregation of particles and promotes the growth of large clusters. However, the long-range electrostatic interactions dominates for larger clusters and thereby limits the cluster size and leads to an equilibrium size of aggregates.[287–289, 292]

Recently however, a number of studies have raised doubts about the above assumptions underlying the pair interaction potentials and their influence on the resulting clusters.[297, 298] Explicitly, a common assumption underlying many of the studies is that the effective interactions are identical for all pairs of CNPs and independent of the state of aggregation of the CNPs. Such an assumption ignores the change in the environment surrounding individual CNPs in an aggregate and the accompanying screening effects on depletion and electrostatic interactions.[297, 299–303] For instance, a recent work by Glotzer *et. al.* [298] employed such considerations (albeit, only in the context of the repulsive interactions) within a phenomenological approach to demonstrate that novel aggregation characteristics may result in CNP sys-

tems. Similarly, a number of studies in other contexts have shown that such "effective" interactions can be influenced by multibody effects, and can exert a significant influence on the structure of the particle phase.[299–303]

Motivated by the above issues, in this work we develop a simulation framework which enables multiparticle simulations of nanoparticle-polymer mixtures to study the structure of aggregates formed from the interplay of depletion and electrostatic effects. The approach presented avoids any assumptions about effective interparticle interactions or its dependence on the particle concentrations and aggregate characteristics. We specifically study the nanoparticle limit of CNP-polymer mixtures in which the particle sizes are comparable to the polymer sizes. In such regimes, multibody effects are expected to be relevant for both depletion and electrostatic interactions.[300–303] Using our computational approach, we address two broad questions:

1. What are the morphological characteristics of such systems when such multibody effects are accounted? Do equilibrium aggregates of finite sizes form in such a framework?

2. How signficant are multibody interactions in such systems and what is their influence upon the aggregate structures?

Towards the above objectives, we have adopted the single chain in mean field simulation (SCMF) framework[47–49, 53] to study suspensions of charged particles in uncharged polymer solutions. In prior studies, the SCMF-like methods has been successfully employed to study the phase behavior

of polymer blends,[47, 146] block copolymers,[48, 149] polymer nanoparticle mixtures,[150] semiflexible copolymers[151], BCP thin films[49, 304, 305] and dendrimer-polyelectrolyte solutions.[306] The SCMF methodology replaces the non-bonded pairwise interactions in the system by one-body interactions of the polymers with pseudo potential fields. Since such a methodology eliminates the need to track explicit pairwise interactions, such a framework allows significant parallelization and renders multiparticle simulations tractable (as we demonstrate in later sections). Another advantage of SCMF methodology is that the cluster characterization, including features such as polymer bridged clusters (which arise if the polymers are also charged) is straightforward.[306] Moreover, extensions to treat complexities such as inhomogeneities in dielectric permittivity and partial dissociation of charges are also possible within such a framework.

The rest of this chapter is arranged as follows: After an introduction to methodological details (Section 6.2), we present results validating the SCMF method for the system under consideration (Section 6.3). For this purpose, we compare the potential of mean force computed from SCMF methodology with the same computed from self consistent field theory (SCFT) framework[4] for just two particles in the polymer solution. Subsequently (Section 6.4), we use the SCMF method to study the structure of aggregates resulting in our system and quantify our findings through morphological "phase-diagrams" for varying particle charge, polymer concentration and particle volume fractions. Our results demonstrate the formation of equilibrium clusters even within the

multiparticle simulation framework, and exhibit characteristics consistent with the competition between depletion and electrostatic interactions. In the final section (Section 6.5), we quantify the origin and influence of the multibody interactions in our system.

6.2 Simulation Details

6.2.1 Model

In this work, we extend the single chain in mean field (SCMF) simulation methodology introduced by Muller and coworkers[47–49, 53] to study charged nanoparticles (CNPs) in uncharged polymer solution. In a previous study, we employed the SCMF methodology to study complexation between charged dendrimers and polyelectrolytes.[306] Our model and method used in the present study closely resembles our dendrimer-polyelectrolyte study, except in the approach used for modeling the charged particles.

Our system consists of N_p particles having radius, R_P, n polymer chains each having $N + 1$ segments, and counterions in volume, V. A schematic of this system is shown in Figure 6.1(a). The interactions which contribute to the energy of the system involves bonded and non-bonded interaction between polymer monomers, excluded volume interactions between polymer monomers, particle-polymer monomer, particle-counterions interactions, and electrostatic interactions between particles and counterions. The polymer chains are modeled as Gaussian chains consisting of $N + 1$ beads connected by harmonic

springs. The bonded energy, H_b, of this model is given by[4]

$$\frac{H_b[\boldsymbol{r}_i(s)]}{k_BT} = \frac{3}{2b^2}\sum_{i=1}^{n}\sum_{s=1}^{N}\Big[\boldsymbol{r}_i(s) - \boldsymbol{r}_i(s+1)\Big]^2 \tag{6.1}$$

where $\boldsymbol{r}_i(s)$ is the position of s^{th} monomer on the i^{th} chain and b is the bond length between two adjacent monomers.

The presence of particles and their interactions with polymer segments and counterions are modeled by incorporating a steeply repulsive potential to ensure the impenetrability of polymer segments and ions into the particle core. Explicitly, the potential is given as

$$W_{cp}(r) = 0.5\left[1 - \tanh\left(2\frac{r - \alpha R_p}{\beta}\right)\right] \times 10. \tag{6.2}$$

The coefficients α and β control the steepness and range over which the potential decays from 10 k_BT at the particle core to 0 k_BT outside the particle. Such a functional form provides an accurate representation of an impenetrable particle core and a soft penetrable outer shell. We used values $\alpha = 0.9$ and $\beta = 0.5$, and Figure 6.1(b) depicts the particle-monomer, particle-ion potential corresponding to this potential.

In SCMF methodology, the pairwise interactions are replaced by one-body interactions with fluctuating potential fields.[47–49, 53] The expressions for such potential fields are derived from saddle point approximation of the corresponding field theory. In our model, the excluded volume interaction between polymer monomers and electrostatic interactions are respectively accounted by using potential fields given as[4, 48]

$$w(\boldsymbol{r}) = u_0\rho(\boldsymbol{r}) \tag{6.3}$$

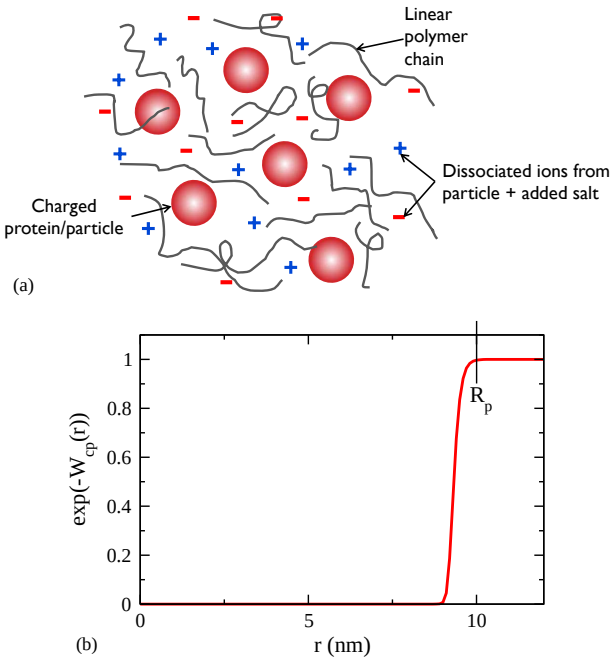

Figure 6.1: (a) Schematic of CNP and polymer system. (b) The particle-monomer, particle-ion interaction, W_{cp} as a function of distance between particle-monomer, ion (r) in nm. The parameters correspond to $R_p = 10$, $\alpha = 0.9$ and $\beta = 0.5$.

$$\nabla^2 \Phi(\boldsymbol{r}) = -4\pi l_B \rho_c(\boldsymbol{r}) \tag{6.4}$$

where u_0 represents the excluded volume parameter,[279, 307] the polymer monomer density, $\rho(\boldsymbol{r})$, and charge density, $\rho_c(\boldsymbol{r})$, are obtained via actual monomer, particle and counterion coordinates. Equation 6.4 above corresponds to the Poisson equation with constant dielectric value where l_B is the Bjerrum length. Using such a notation the potential fields acting on the particle ($U_p(\boldsymbol{r})$), polymer monomer ($U_{pol}(\boldsymbol{r})$) and the counterions ($U_{ion}(\boldsymbol{r})$) are

given as,

$$U_p(\boldsymbol{r}) = W_{cp}(r)(\rho(\boldsymbol{r}) + \rho_{ion}(\boldsymbol{r})) + z_p\Phi(\boldsymbol{r}) \tag{6.5}$$

$$U_{pol}(\boldsymbol{r}) = \beta H_b(\boldsymbol{r}) + w(\boldsymbol{r}) + W_{cp}(r) \tag{6.6}$$

$$U_{ion}(\boldsymbol{r}) = W_{cp}(r) \pm z_{ion}\Phi(\boldsymbol{r}) \tag{6.7}$$

where $\rho_{ion}(\boldsymbol{r})$ is the density of ions at position $\boldsymbol{r}$, and z_p, z_{ion} denote the charge on particle and ions respectively. We neglect all non-electrostatic interaction between ions. We assume a quenched charge model wherein all the charges on particles and ions are completely dissociated and the charge does not vary as a function of solution conditions.

6.2.2 SCMF Simulation Method and Parameters

The model described above was used in a Monte Carlo simulation approach wherein the configurational space was sampled using Metropolis algorithm.[168] The monomer, particle and ion positions were evolved in three dimensions using random displacement MC moves. In addition to the monomer displacement moves, slithering snake moves wherein the polymer chain is regrown by one segment in either direction were used. Each Monte Carlo step (MCS) consisted of 100 MC random displacement attempts per monomer and ion, one MC random displacement attempt per particle and one slithering snake move per chain. The fields $w(\boldsymbol{r}_i(s)), \pi(\boldsymbol{r}_i(s))$ are updated based on the inhomogeneous density of monomers, particles and ions after one MC step per monomer and one MC step per particle. After each particle displacement, we

attempt a large number of MC steps on polymer segments and ions to ensure sufficient relaxation and minimal overlap between particle and monomers, ions. Additional details of the algorithm are similar to those described elsewhere.[48] The system was equilibrated for 5×10^4 MCS after which the properties were averaged and clusters were analyzed.

In the results presented in following section, we worked in units in which $l_B = 0.7$ nm, the Bjerrum length of water at room temperature. We used a three dimensional simulation box of size 200 (nm^3) discretized with a uniform grid of $64 \times 64 \times 64$. We fixed particle size at $R_p = 10$ (nm) and polymer size at $R_g = 15$ (nm) where R_g is the unperturbed radius of gyration of polymer chain defined as $R_g^2 = Nb^2/6$. Admittedly, some of the multibody effects we propose to study are expected to be influenced by the relative ratio R_p/R_g. In this work we did not vary the particle or the polymer sizes and instead defer a more comprehensive study of such parameters to a future study.

We studied three cases for particle charge $Q_p = 5$, $Q_p = 10$ and 20. We model particles such that the charge is uniformly distributed within the particle. Thus, all grid points within the particle are assumed to carry a fractional charge z_p which is the ratio between total particle charge and number of grid points covering the particle. The ions in our simulation carry one elementary charge each i.e. $z_{ion} = \pm 1$. To model particle-monomer, particle-counterion interactions, we calculate the potential field created by every particle using $W_{cp}(r)$ (Eq. 6.2) where r is the distance between particle center and the grid point. We studied CNP-polymer mixture at particle volume fractions in the

range $2.5 - 20\%$ and polymer concentrations in the range $C/C^* = 0.25 - 1.0$, where C^* is the overlap concentration. The result presented in this chapter correspond to a fixed low salt concentration for which the Debye–Huckel screening length (given as $\lambda_D = [4\pi l_B \sum z_i^2 c_i]^{-1/2}$, where z_i and c_i are the charge and concentration of species i respectively) for the infinite dilution concentration of particles equals 10.9 nm. For a finite volume fraction of particles, the salt concentration is kept constant and counterions are included. Our simulations were initiated with particles placed in cubic lattice conformation and random configurations of polymer and ions. We carried out a pre-equilibration MC simulation on a system of just the polymer and ions to generate our initial configuration with minimal particle-polymer and particle-ion overlaps. To solve for $\Phi(\boldsymbol{r})$, the Poisson equation was solved using fast Fourier transform implementation. Necessarily, SCMF simulation approaches are influenced by discretization and finite size effects. In our previous article,[306] we presented results which demonstrated that for sufficiently small grid sizes, the results of SCMF match quantitatively with more refined field theories. In the present work, we opt for analyses and parametric studies which serve to provide qualitative insights, and hence, we do not embark on a detailed consideration of grid and box size effects.

6.2.3 Self Consistent Field Theory

In our previous study, we developed a theory and numerical framework based on a mean-field model to study the interactions between charged and

uncharged particles suspended in polymer solution.[308] In the present work, we use such a framework to compute the potential of mean force (PMF) between charged particles in the solution of uncharged polymers. Our goal is to validate the capability of SCMF framework to capture interactions between charged particles by comparing the PMF obtained from SCFT and SCMF simulations. We do note that the self consistent field theory framework neglects both fluctuation and charge correlation effects.[4] However, we expect the mean-field approximation to furnish semi-quantitatively accurate results for the interaction features of the charged/uncharged particle-polyelectrolyte systems, and hence, use SCFT to benchmark the proposed simulation methodology.

A detailed description of our SCFT formalism is provided in our previous article, and hence we avoid repeating the details here.[308] We utilize a model identical to that discussed in Section 6.2.1 to describe polymer chains and particle-monomer, particle-counterion interactions. By adopting a semi-grand canonical framework in which the activity coefficient of the polymer is fixed,[309–312] we compute the free energy of the system of two particles in the polymer solution as a function of the interparticle distance to deduce the polymer-mediated effective pair interactions between the charged particles.

6.2.4 Umbrella Sampling

For the comparisons with SCFT, we considered a system comprised of two particles in the polymer solution and used a classical umbrella sam-

pling[313] technique in conjunction with SCMF to compute the potential of mean force between the CNPs. We used a harmonic bias potential linking the particle positions r, $u = 1/2k(r - r_0)^2$ where r_0 is the equilibrium distance between the particles and k is the spring constant. Such biasing potential enforces a local constraint on r, enabling the system to overcome the energy barrier present in the original system. We perform N_w simulations each enforcing a different equilibrium separation, r_0, between CNPs. Each simulation window samples the distance between two particles with r_0 ranging from $20 - 100$ nm. For each simulation window, the distance between particles is binned to generate a probability distribution. Subsequently, the results from different simulation windows are combined using weighted histogram analysis method[314] to generate the PMF.

6.2.5 Structure Analysis

We carried out a systematic analysis of particle clusters formed as a result of depletion interactions induced by polymer molecules. The primary measure used to analyse the structure of CNP-polymer mixture is the particle-particle radial distribution function, $g(r)$, which quantifies the aggregation propensity of particles. Clusters are identified using a procedure proposed by Sevick et al.[253] in which the clusters are identified through a connectivity matrix based on physical contact between particles. The matrix is then further modified to account for indirect contact among particles. Particles are considered in physical contact with each other when the distance between particles

is less than one grid spacing i.e. the distance is less than $2R_p + \triangle x$. We expect this to be an appropriate measure since resolutions below $\triangle x$ are inherently coarse-grained in our simulation method.

For characterization of the clusters, we compute the radius of gyration of cluster defined as

$$R_{g,cl}(s) = \frac{1}{s}\sum_{i=1}^{n}(\boldsymbol{r}_i - \boldsymbol{r}_{com})^2 \tag{6.8}$$

where $\boldsymbol{r}_i, \boldsymbol{r}_{com}$ is the position of particle within the cluster and center of mass of cluster respectively. s denotes the number of particles in a cluster. The fractal dimension of clusters, d_f, is defined through

$$R_{g,cl} \propto s^{d_f} \tag{6.9}$$

is used to understand the morphology of the network. While computing d_f we exclude dimer clusters.

To identify the different kinds of clusters, we use an approach recently proposed by Godfrin *et. al.* [315] For this purpose, we compute $N(s)$, the average fraction of particles contained in a cluster of size s:

$$N(s) = (s/N_p)n(s), \tag{6.10}$$

(with N_p denoting total number of particles and $n(s)$ representing the average number of clusters of size s).[316] Subsequently, we classify the different clustered states as monomer dominated (M), clustered (CL) and percolated (P) states.[315, 317, 318] Monomer dominated states contain small clusters (comprising of less than 10 particles) in majority and do not exhibit a preferred

cluster size. A monotonically decaying $N(s)$ is classified as M.[315] States containing clusters which exhibit a preferred cluster size are classified as clustered (CL). In such states $N(s)$ develops a maximum at a size s^* larger than a monomer.[315] A percolated state is identified when a single cluster comprising of all the particles in the system emerges. If $N(s)$ exhibits a peak for $s \simeq N_p$, we classify such states as P.

6.3 Validation of Simulation Method

Prior to the present study, we are not aware of any other work which has used the methodology of SCMF to study charged particle and polymer mixtures. To validate the simulation framework we have employed, we compare the PMFs computed using SCMF methodology with the corresponding self consistent field theory results. To deduce the potential of mean force between the particles from SCMF simulations, we performed umbrella sampling simulations (discussed in Section 6.2.4).

In Figure 6.2 we display the PMFs obtained from SCFT (hollow markers) and SCMF (filled markers) method for polymer concentration of $C/C^* = 0.25, 0.5, 1.0$. The lines are a guide to the eye. In CNP-polymer systems, PMFs are expected to posses a combination of short-ranged attraction and long-ranged repulsion. The short-ranged attraction between CNPs arises from polymer-exclusion induced depletion interactions. Moreover, since the particles are charged, a repulsive force analogous to Yukawa like interactions is expected to manifest. The results displayed in Figure 6.2 is seen to exhibit trends

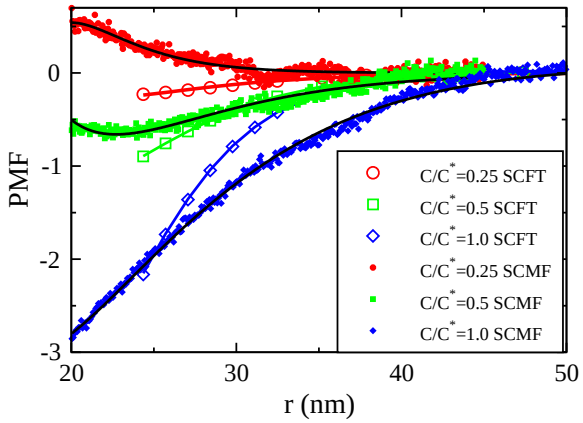

Figure 6.2: The potential of mean force calculated using umbrella sampling compared with the PMF obtained from SCFT simulations at $Q_p = 10$ for varying polymer concentration.

consistent with such expectations. In all cases, the magnitude of the strength of interaction is seen to increase with polymer concentration, consistent with increasing importance of depletion interactions. For the lowest polymer concentration, $C/C^* = 0.25$, PMF obtained from the SCMF method displays a weakly repulsive potential. In contrast, the SCFT predicts an interaction with a weak attractive potential well. However, the strength of potentials are weak in both cases and hence we are not able to calibrate the accuracy beyond statistical errors. For the cases of $C/C^* = 0.5, 1.0$, the PMF from SCMF is seen to be in good agreement with the one computed using SCFT. An interesting feature of the potentials for the parameters we have chosen is that the range of attractions are seen to be comparable to the range of repulsions. This differs from the models typically used in simulations, but is however consistent with the nanoparticle regime of particle-polymer sizes probed in this work.

Overall, for the set of interactions studied in this section, we observe that the SCMF methodology is able to capture the interplay between depletion and electrostatic interactions in the CNP-polymer system. We believe that the small discrepancies observed while comparing the PMFs obtained from SCFT and SCMF might be results of consequences of fluctuation effects (ignored in SCFT),[4] discretization effects inherent in SCMF simulations, and/or a dependence on the frequency with which we update the potential fields in SCMF. Despite these differences, we view the semiquantitative agreement between SCFT ad SCMF as support for validation of the SCMF methodology for the systems considered in this chapter.

6.4 Structure of Aggregates

In this section, we present results quantifying the structure of aggregates formed in CNP-polymer system. We study CNP volume fraction in the range, $\phi_p = 0.025 - 0.2$, and polymer concentration in the range, $C/C^* = 0.25 - 1.0$. Using the measures discussed in Section 6.2.5, we quantify the structure and size of the particle aggregates.

6.4.1 Radial Distribution Functions

We first present results for the particle-particle radial distribution functions ($g(r)$) of the CNP-polymer system for different polymer concentrations and CNP volume fractions. Figure 6.3(a) shows $g(r)$ for $Q_p = 10$ for polymer concentrations $C/C^* = 0.25 - 1.0$ and fixed CNP volume fraction, $\phi_p = 0.05$.

We observe that for the specified CNP volume fraction, the aggregation between CNPs increases with increasing polymer concentration. Such an effect is consistent with the higher strength of depletion interactions noted in Figure 6.2 with increasing polymer concentrations. At a fixed polymer concentration (Figure 6.3(b-c)), the aggregation between CNPs is seen to increase with CNP volume fraction. With increasing CNP volume fraction, the effective attraction between CNPs is expected to increase as a result of screening of electrostatic repulsion between CNPs. In addition, in our simulations, we fix the number of polymer chains in the system, and add more particles (i.e. maintain a canonical ensemble for polymers). In contrast, an equilibrium realization of CNP-polymer system would fix the chemical potential of the polymer (semi-grand canonical ensemble). Increasing particle volume fraction in such a framework would reduce the uptake of polymer chains as a result of the entropic costs arising from polymer exclusion from particle cores. In other words, maintaining a fixed concentration of polymers is equivalent to increasing the polymer's chemical potential with increasing particle volume fraction.[311] Therefore, the depletion interactions are expected to become stronger with increasing CNP volume fractions. As a consequence, we observe that the particle aggregation increases with both increasing polymer and particle concentration.

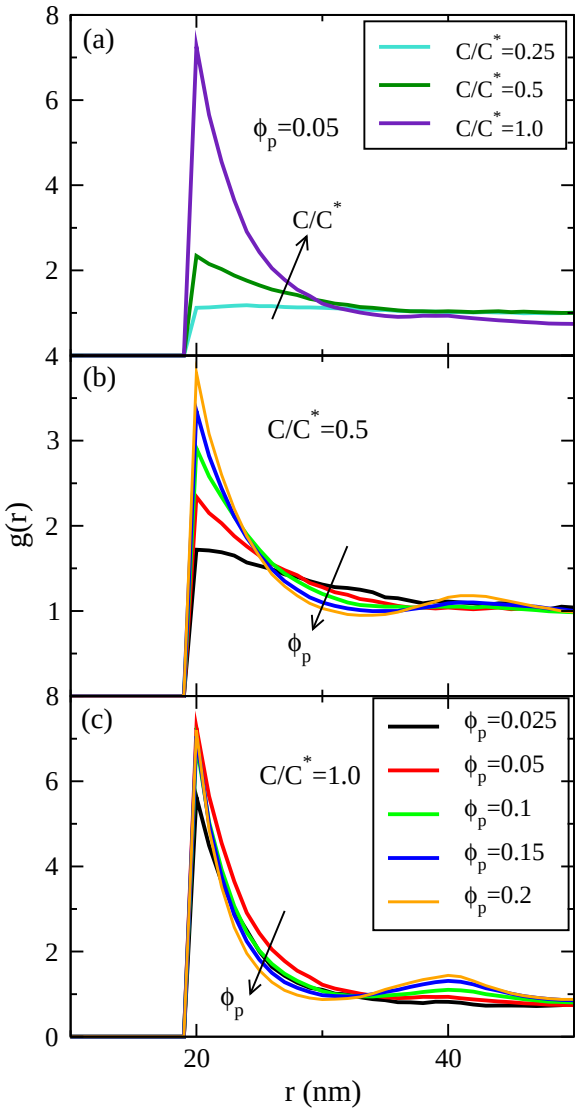

Figure 6.3: Particle-particle radial distribution functions, $g(r)$ (a) as a function of polymer concentration for $\phi_p = 0.05$ and as a function of particle volume fraction for polymer concentrations (legend indicated in (c) is common to (b) and (c)) (b) $C/C^* = 0.5$, (c) $C/C^* = 1.0$.

To characterize the effect of particle charge on the aggregation between

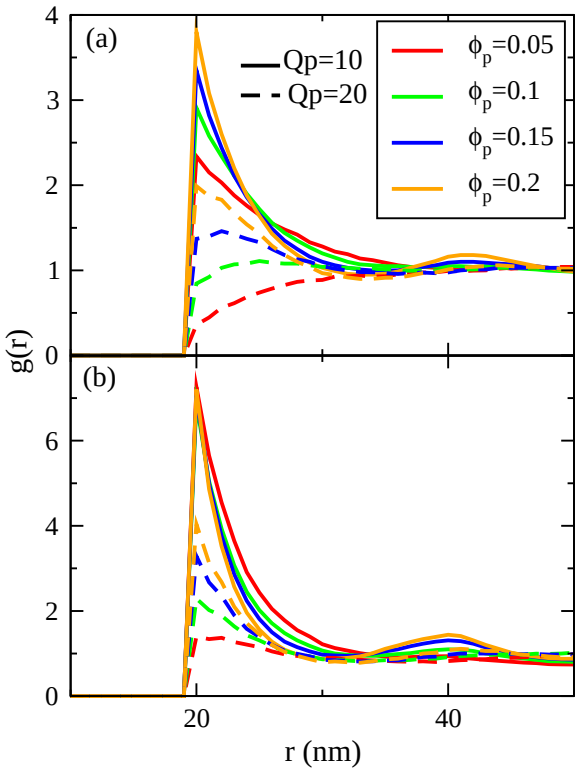

Figure 6.4: Effect of particle charge on the particle-particle radial distribution function for polymer concentrations (a) $C/C^* = 0.5$, (b) 1.0.

CNPs, in Figure 6.4 we display $g(r)$ for $Q_p = 10$ (solid line) and $Q_p = 20$ (dotted line) for polymer concentrations, $C/C^* = 0.5$ and $C/C^* = 1.0$. For lower CNP volume fraction and lower polymer concentration, the electrostatic repulsion dominates. Hence, the $g(r)$ gradually increases from zero at particle contact to unity at large r indicating a well dispersed solution of CNPs. With increasing Q_p, the peak in $g(r)$ is seen to reduce as a result of increasing electrostatic repulsion. However, even for $Q_p = 20$ we observe aggregation for CNP volume fractions larger than 15% for $C/C^* = 0.5$ and 5% for $C/C^* = 1.0$,

suggesting that high enough volume fraction of particles or concentration of polymer leads to aggregation of the CNPs.

6.4.2 Cluster Phase Diagram

In Figure 6.5 we display the cluster size distribution depicting the average fraction of particles, $N(s)$ contained in cluster of size s. Representative snapshots of the different cluster states corresponding to $C/C^* = 0.5$ are also displayed (in which each color represents an independent cluster and only clusters having two or more particles are shown). In the context of CNP-polymer system, the monomer dominated states (M) are seen to exist at low polymer concentrations and low CNP volume fractions where the electrostatic forces dominate depletion attractions. Clustered state (CL) are observed at intermediate particle volume fractions over the range of polymer concentrations examined. In such conditions, we may expect that the electrostatic repulsions is balanced by depletion attraction leading to a preferred cluster size. Percolated states (P) are seen to occur at high polymer concentrations and particle volume fractions when the depletion attraction is very strong such that all the particles are connected with each other.

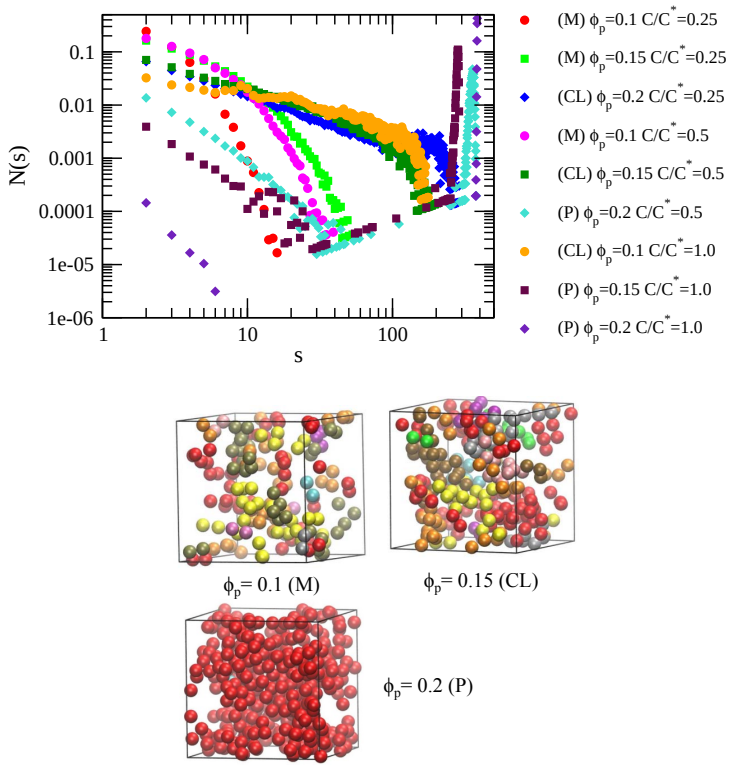

Figure 6.5: Cluster size distribution as a function of particle volume fraction and polymer concentration. M, CL and P denotes monomer dominated clusters, clustered and percolated particle aggregates. Representative cluster snapshots for monomer dominated (M), clustered (CL) and percolated (P) states are also displayed.

In Figure 6.6 we present "phase diagrams" summarizing the cluster states found in different simulations. In all cases, at low particle concentrations, we observe minimal clustering at low polymer concentrations due to weak depletion interactions. In contrast, screening of electrostatic interactions and stronger depletion interactions are seen to lead to percolated clusters at

high particle and polymer concentration. At a constant polymer concentration, the cluster states are seen to transform from monomer dominated to clustered to percolated (M→CL→P) with increasing particle volume fraction. We observe similar transitions while increasing the polymer concentrations at a fixed particle volume fraction. With increasing particle charge, overall clustering is seen to reduce as a consequence of increased electrostatic repulsion between particles. Also, the aggregate state boundaries are seen to shift towards higher particle volume fractions with increasing particle charge. Moreover, for the set of particle and polymer concentration studied in this chapter, we observe that clustered states (exhibiting preferred cluster size) for $Q_p = 10$ are seen to disappear for increased particle charge of $Q_p = 20$. The simulations carried out at a constant screening length were seen to exhibit the same aggregate states as observed in Figure 6.6 for which the salt concentration was kept fixed.

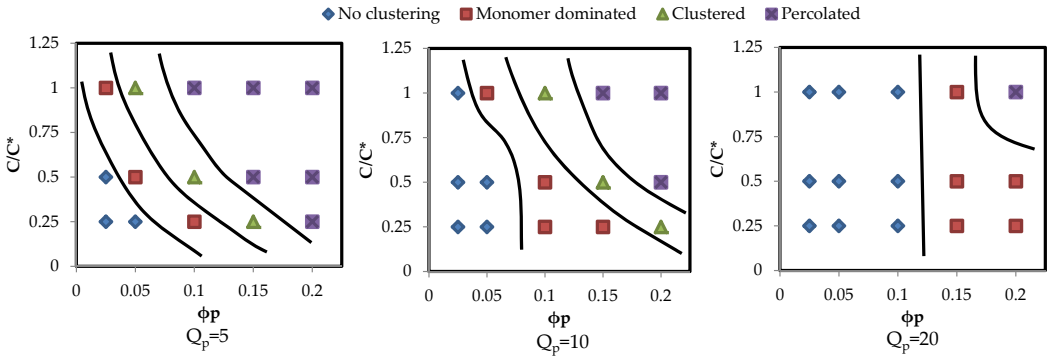

Figure 6.6: The state of aggregates formed as a function of particle volume fraction and polymer concentration for $Q_p = 5$, $Q_p = 10$, and $Q_p = 20$.

The results presented in Figure 6.6 serve to address the first of the ques-

tions raised in the introduction to this chapter. An interesting outcome of our result is the observation that "equilibrium" cluster states (CL) form at intermediate particle volume fractions and polymer concentrations. As discussed earlier, significant interest has arisen in such morphologies,[39, 287–292] and the formation of such states have been rationalized as arising from an interplay between depletion and electrostatic interactions.[287, 289, 319–321] Explicitly, the free energy contribution from depletion (electostatic) interactions decreases (increases) with an increase in the number of particles in the cluster.[319] In such a framework, equilibrium clusters are expected to form only for an intermediate range of particle charges and polymer concentrations such that there is a competition between the magnitudes of depletion and electrostatic interactions. Consistent with such considerations, in Figure 6.6 we observe the formation of clusters only for $Q_p = 5$ and $Q_p = 10$ for the range of polymer concentrations we examined. Moreover, the transition to the clustered phases are seen to move to higher ϕ_p with either decreasing C/C^* or increasing Q_p. The latter behavior accords with the lower energy gained by aggregating to clusters for such parametric conditions.

Together, the trends exhibited by the above results confirm that the clustering observed in our simulations is driven by the interplay between depletion attractions and electrostatic repulsions. However, a surprising aspect of our result is that in our system the depletion attraction and the electrostatic repulsions exhibit comparable range of interactions (see Figure 6.2). Such a feature contrasts with the present understanding that a long-range repulsion

is needed to stabilize such clusters.[287, 288, 292, 319] While we do not have a conclusive explanation for our results, in the next section we demonstrate the importance of multibody effects which indirectly suggests that considerations based on (effective) interparticle pair-interactions may not suffice to understand aggregation and clustering in such systems.

6.5 Multibody Effects

6.5.1 Demonstration of Multibody Interactions

In this section, we present results which address the second of the questions raised in the introduction, viz., "How signficant are multibody interactions in such systems and what is their influence upon the aggregate structures?" Towards the objective of quantifying multibody interactions, we first consider the commonly employed approximation in which the polymer degrees of freedom are integrated out, thereby reducing the CNP-polymer system to an one-component CNP system which interact via polymer-mediated effective potentials. While such an approximation is exact when interactions at all orders are accounted,[311, 322] the polymer-mediated potentials are typically further *approximated* as the potential of mean force computed at the *infinite dilution* limit (i. e. two particles in the polymer solution) of particle concentration. As a first step to demonstrate the influence of three and higher body interactions on the structure of aggregates, we compare the structural results from two cases: (i) Particle-only MC simulations, with however the particles interacting via polymer-mediated interactions obtained by PMF at infinite dilution con-

centration of the particles; and (ii) SCMF simulations on the complete model involving particles at finite concentrations, polymers and counterions. In the discussion below, we refer to the results from such simulations as cases (i) and (ii) respectively.

For the above comparisons, we ensure that the SCMF simulations are carried out at conditions corresponding to the same chemical potential of the polymer as the infinite dilution conditions. Such an approach is necessary since the reduction of the CNP-polymer mixture to an effective one-component system is valid only for semi-grand ensemble for polymers.[302, 322] Since employing a semi-grand canonical ensemble in SCMF-like approaches is relatively cumbersome, we opt to use an indirect approach to mimic such a framework within the SCMF methodology. In brief, we use the SCFT approach to deduce the polymer concentrations as a function of the volume fraction of particles for fixed chemical potential of polymers. We believe it is an approximate yet reasonable choice as the two methodologies (SCMF and SCFT) exhibit qualitatively similar PMF at infinite dilution concentration of particles (discussed in Section 6.3).

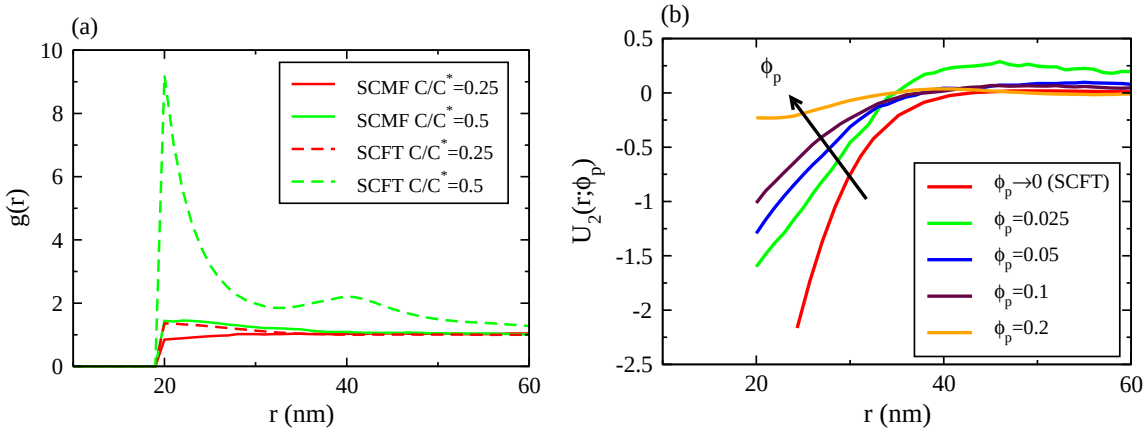

Figure 6.7: (a) The particle-particle radial distribution functions obtained from particle only MC simulations using PMF as the polymer mediated interparticle potential (case (i)) and the same obtained from SCMF simulations (case (ii)) for two polymer concentrations at $\phi_p = 0.05$. (b) $U_2(r;\phi_p)$ obtained using Inverse Boltzmann method for different particle volume fractions at a fixed $C/C^* = 1.0$.

In Figure 6.7(a) we display a comparison between the structure of CNPs obtained from cases (i) and (ii). We observe that the peaks of the $g(r)$ in case (i) are considerably higher than those observed in case (ii). Surprisingly, such differences are seen to manifest even for CNP volume fractions as low as 5%. As expected, the disparity between the results of cases (i) and (ii) grows with increasing volume fraction of particles (not shown). More interestingly, we observe that the results of cases (i) and (ii) exhibit more pronounced differences for larger C/C^*. Overall, these results suggest that, using $U_2(r)$ to represent the interparticle interactions (case (i)) greatly overestimates the aggregation propensity between particles.

In order to understand why multibody effects lead to reduced aggre-

gation, we compute a "ficticious interparticle potential," $U_2(r;\phi_p)$, which is capable of reproducing the structure formed in full scale SCMF simulations. To compute such an effective interparticle potential, we use Inverse Boltzmann methodology[323] in which we carry out MC simulations involving just particles, and iteratively refine $U_2(r;\phi_p)$ to reproduce the $g(r)$ obtained from the SCMF simulations. The initial guess for $U_2(r;\phi_p)$ is chosen as $-\ln g(r)$ and $U_2(r;\phi_p)$ is updated at the end of each iteration as

$$U_2(r,\phi_p)_{n+1} = U_2(r,\phi_p)_n + \lambda \ln\left(\frac{g(r)_n}{g(r)_t}\right) \tag{6.11}$$

where n is the iteration, λ is a prefactor between 0 and 1, and $g(r)_n$ is the radial distribution function obtained at n^{th} iteration and $g(r)_t$ is the target $g(r)$. Note that $U_2(r;\phi_p)$ deduced by such a process is expected to be dependent on the particle volume fraction, and is hence not a true interparticle potential. The computation of $U_2(r;\phi_p)$ was carried out for different particle volume fractions and polymer concentrations.

In Figure 6.7(b), we display the PMF corresponding to infinite dilute concentration for particles from SCFT (red line) along with $U_2(r;\phi_p)$ deduced from the structure resulting in SCMF simulations. We observe that the attractive component of the potential is maximum for the lowest particle concentration (i.e. $\phi_p \to 0$) and the strength of such component monotonically decreases with increasing particle concentration. Moreover, the range of the potential is also seen to decrease with increasing particle concentrations. These results suggest that the reduction in aggregation observed in Figure 6.7(a) can be

rationalized as a consequence of reduction of both strength and the range of the *effective* interparticle interactions with increasing particle concentration.

6.5.2 Origin of Multibody Effects

"What is the origin of the reduction in the strength and range of interaction between CNPs with the increase in CNP concentration?" To shed light on this issue, we probe the specific effects of multibody effects on the two main factors influencing interactions in our systems, viz., electrostatics and polymer depletion. To study the effects in the context of electrostatic interactions, we consider a system containing only charged particles in a counterion solution devoid of polymers. To study the corresponding effects in depletion interactions, we consider uncharged particles in a polymer solution. For each of these situations we perform corresponding SCMF simulations and use an approach similar to that described above to deduce the $U_2(r;\phi_p)$ which can reproduce the resulting $g(r)$.

In Figure 6.8(a) and (b) we display the effective pair potentials, $U_2(r;\phi_p)$, for different particle volume fractions for the situations described above. From Figure 6.8(a) we observe that both the strength and the range of the electrostatic repulsion between particles becomes reduced with increasing particle volume fraction. These results are consistent with the classical screening effects[324] expected for finite concentration of charged particles. Interestingly, at very large ϕ_p, we see that the interaction develops an attractive well. Such multibody correlations are known to arise due to non-linear counterion screen-

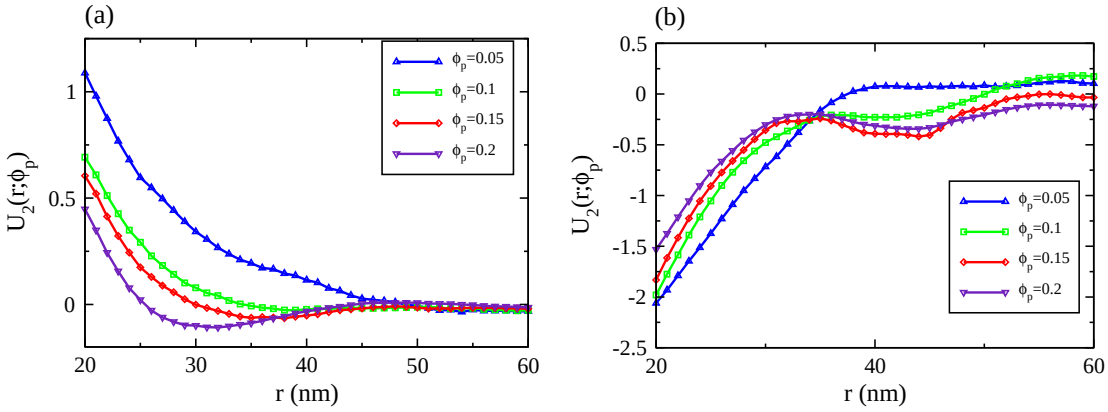

Figure 6.8: The effective two body potentials, $U_2(r;\phi_p)$, obtained using from SCMF simulations (a) for the case of only electrostatic interactions (just CNP system) at $Q_p = 10$ and (b) for only depletion interactions (uncharged particles) for $C/C^* = 1.0$

ing.[324]

In Figure 6.8(b) we observe that the strength of depletion interaction is strongest for the lowest particle volume fraction and that the strength and the range decreases with increasing particle volume fraction. A simple explanation of such effects is that a third particle experiences only a reduced polymer density (due to depletion) in the vicinity of other particle pairs.[312] Hence, the net three-particle interactions are expected to be lower than what may be expected based on the sum of the pair-interactions deduced at the infinite dilute limit. We note that similar effects have been noted and discussed in earlier studies.[300, 303]

Together the above results suggest that the multibody effects in our system arise as a consequence of the multibody effects in both electrostatic and

depletion interactions. Explicitly, such multibody effects are seen to reduce both the strength and the ranges of the repulsive electrostatic interactions and the attractive depletion interactions.

6.5.3 Influence of Multibody Interactions on the Cluster Morphology

In this final section, we illustrate the direct role of multibody interactions upon the aggregation and cluster morphologies. For this, we present the phase diagrams (Figure 6.9) obtained using the pair-interaction potentials deduced at infinite dilution particle concentrations. These phase diagrams constitute the analog of the corresponding results presented in Figure 6.6 for the multibody framework. In comparing Figure 6.6 and Figure 6.9, we observe significant differences in the regimes of occurrances of the M, CL and P states. Explicitly, for $Q_p = 10$ in Figure 6.9, we observe a narrower range of polymer concentrations (compared to Figure 6.6) where CL phases occur and a larger regime of percolated (P) states. Similarly, for $Q_p = 20$, we observe a stronger propensity to form monomer dominated (M) phases in Figure 6.9 for the regimes in Figure 6.6 which exhibited no aggregation. These results are consistent with the stronger propensity for aggregation noted in Figure 6.7 for such pair-interaction based approaches, and serve to reinforce the importance of accounting for the multibody interaction effects to study the aggregate morphologies in such systems.

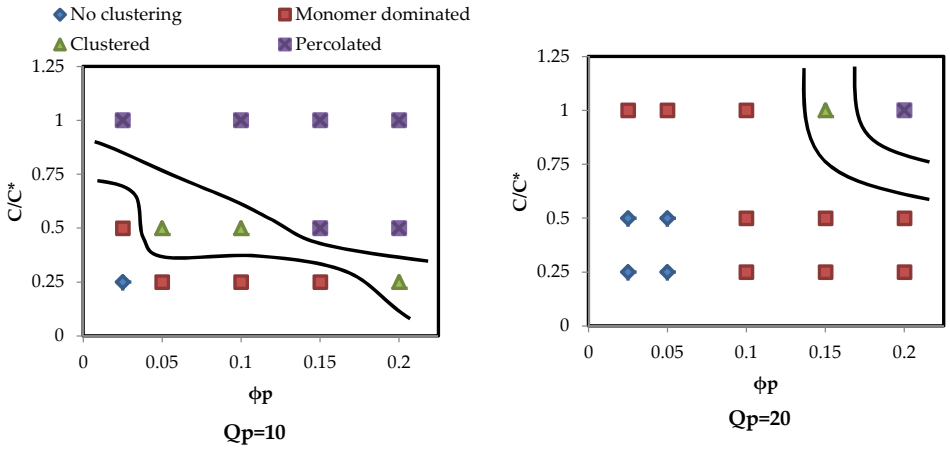

Figure 6.9: The state of aggregates obtained using the pair-interaction potentials deduced at infinite dilution concentration as a function of particle volume fraction and polymer concentration for $Q_p = 10$, and $Q_p = 20$. The legend is common to both plots.

6.6 Summary

In this chapter, we presented an extension of the single chain in mean field simulation framework to study charged nanoparticle-polymer systems. Such a framework treats particles, polymers and counterions on an equal footing enabling large scale simulations of nanoparticle-polymer systems at finite particle volume fractions. We validated the simulation method by comparing the potential of mean force computed from SCMF framework with the one obtained from self-consistent field theory method. The variation in cluster state and size was examined for varying particle charge, particle volume fraction and polymer concentration. Broadly, the clustering between particles was seen to increase with polymer concentration as a result of stronger depletion

interactions. Increasing particle charge was seen to reduce the propensity to form clusters as a consequence of increased repulsion between particles. By explicitly characterizing the cluster states, we demonstrated the formation of monomer dominated clusters at lower particle volume fractions and lower polymer concentrations, and percolated clusters at high particle volume fraction and high polymer concentration. At an intermediate range of particle and polymer concentrations, clustered states were observed in which the system exhibited a preferred cluster size.

We also elucidated the influence of multibody interactions on the structure of the charged particle-polymer system. The use of a two-body potential obtained at infinite dilution regime led to significant overestimation of clustering between particle even at particle volume fractions as low as 5%. The results were rationalized by demonstrating that, the pair-potentials fitted to reproduce structures formed in SCMF simulations exhibited weaker depletion attractions and electrostatic repulsions, and a much shorter-range for the potentials. Not suprisingly, the phase diagrams deduced based on the pair-interaction potentials approach exhibited markedly different characterstics when compared to those deduced from a full multibody simulation framework.

The results presented in this chapter demonstrate the ability of SCMF methodology to study the interactions and structures formed in nanoparticle-polymer systems. In future studies, we plan to extend this framework to study systems with more complex interactions arising from dielectric inhomogeneities and partial dissociation of charges in the system. Moreover, the multibody

effects discussed in the present chapter are expected to display a strong dependence on the particle sizes and its magnitude relative to the polymer sizes (or the correlation length of the polymer solution). In future work, we hope to explore a range of particle sizes to delineate the parametric conditions for which pair-interaction approaches can furnish accurate results.

Chapter 7

Summary and Future Work

7.1 Summary of Research

In this thesis, we examined various multicomponent polymeric systems using single chain in mean field simulations to study the effect of fluctuations in the context of uncharged polymer melts and solutions. This work provided important insights on the role of fluctuations in influencing the phase behavior of copolymer systems possessing different sequence architectures. We extended the SCMF framework to examine the structure, interactions in charged particle-polymer and charged dendrimer-polyelectrolyte solutions. We studied a range of dendrimer sizes, particle and polymer concentrations and examined the effects leading to various states of aggregation between dendrimers/particles.

An important contribution of this work is the development of the simulation framework utilized to study the interactions between nanoparticle and polymers which accounts for polymer induced depletion effects and electrostatic charges on any or both the components. The size and lengthscales involved in these systems render both the particle-based simulations as well as field theoretic approaches unsuitable. To address these challenges, we em-

ployed single chain in mean field methodology in which the conformations are sampled using Monte Carlo approach and the pairwise interactions are replaced with external potential fields. Such a methodology provides the advantage of directly quantifying the structure of the particle-polymer systems since the actual particle and polymer positions are retained. Incorporating fields instated of pairwise accounting of non bonded interactions makes the methodology computationally efficient. Our results indicate that such a framework is able to describe the essential physics of particle-polymer mixtures and hence, can be used to incorporate more complex phenomena which can lead to a more comprehensive understanding of the manner in which the interactions between nanoparticles influence the structure and phase behavior of the system.

7.2 Recommendations for Future Work

7.2.1 Incorporating Charge Dissociation and Dielectric Inhomogeneity

The simulation framework presented in Chapter 5 and 6 can be readily extended to incorporate more complex interactions such as charge dissociation and inhomogeneities in dielectric permittivity to closely mimic "real" conditions. These improvements will lead to a better charcterization of interparticle potentials, multibody effects and structure of the clusters.

7.2.2 Complexation and Phase behavior in Polyelectrolyte-Particle Mixtures

The SCMF framework used in this work can be utilized to study the interactions between charged nanoparticles suspended in polyelectrolyte solution. Such particle-polymer mixtures represent systems involving particles or proteins in presence of charged polymers such as polysaccharides, polyampholytes, etc., which are commonly encountered in a variety of industrial and biological applications. The theoretical work on such systems is limited as compared to their neutral counterparts. Such studies can specifically address the role of polyelectrolyte bridging interactions which have been speculated to play an important role in the phase behavior charged particle-polyelectrolyte mixture.

7.2.3 Grafted Nanoparticles

Dispersing nanoparticles in polymer matrices is a common strategy to improve the mechanical, electrical or optical properties of the polymer material. In order to enhance the dispersion of particles in the bulk polymer, nanoparticles grafted with polymer chemically identical to matrix polymer are utilized. Due to computational limitations, the theoretical studies in this context are limited to one or few nanoparticles dispersed in the polymer matrix. SCMF simulation framework employed in this work provides a straightforward approach to model grafted nanoparticles and thus, the effect of grafted nanoparticle properties such as grafting density, graft length, particle shape

and size on the level of dispersion of particles in the polymer matrix can be examined.

7.2.4 Anisotropic and Patchy Particles

The particle-polymer model studied in this work represents a generic model which can be developed to more closely mimic specific interactions such as anisotropic particles, protein structures from protein data bank, etc. To achieve this, the particle model can be modified to simulate proteins in globular state in which the uniform charge distribution within the particle employed in this study can be replaced by patches of hydrophobic and hydrophilic regions. Moreover, complex sequence architectures and stiffness of polyelectrolyte chains can also be incorporated. Such an approach will enable more reliable comparison of structural characteristics of complexes formed in the simulations with the experiments.

Bibliography

[1] K. M. Hong and J. Noolandi. Theory of inhomogeneous multicomponent polymer systems. *Macromolecules*, 14(3):727–736, 1981.

[2] M. W. Matsen and M. Schick. Self-assembly of block copolymers. *Current Opinion In Colloid & Interface Science*, 1(3):329–336, June 1996.

[3] G. H. Fredrickson, V. Ganesan, and F. Drolet. Field-theoretic computer simulation methods for polymers and complex fluids. *Macromolecules*, 35(1):16–39, January 2002.

[4] Glenn H. Fredrickson. *The equilibrium theory of inhomogeneous polymers*. Oxford University Press, 2006.

[5] Frank S. Bates and Glenn H. Fredrickson. Block copolymer thermodynamics: Theory and experiment. *Annual Review of Physical Chemistry*, 41(1):525–557, 1990.

[6] M W Matsen. The standard gaussian model for block copolymer melts. *Journal of Physics: Condensed Matter*, 14(2):R21, 2002.

[7] F. S. Bates, J. H. Rosedale, G. H. Fredrickson, and C. J. Glinka. Fluctuation-induced 1st-order transition of an isotropic system to a periodic state. *Physical Review Letters*, 61(19):2229–2232, November 1988.

[8] K. Almdal, F. S. Bates, and K. Mortensen. Order, disorder, and fluctuation effects in an asymmetric poly(ethylene-propylene)-poly(ethylethylene) diblock copolymer. *Journal Of Chemical Physics*, 96(12):9122–9132, June 1992.

[9] F. S. Bates, M. F. Schulz, A. K. Khandpur, S. Forster, J. H. Rosedale, K. Almdal, and K. Mortensen. Fluctuations, conformational asymmetry and block-copolymer phase-behavior. *Faraday Discussions*, 98:7–18, 1994.

[10] V. Ganesan and G. H. Fredrickson. Field-theoretic polymer simulations. *Europhysics Letters*, 55(6):814–820, September 2001.

[11] M. Muller and M. Schick. Bulk and interfacial thermodynamics of a symmetric, ternary homopolymer-copolymer mixture: A monte carlo study. *Journal Of Chemical Physics*, 105(19):8885–8901, November 1996.

[12] G. H. Fredrickson and F. S. Bates. Design of bicontinuous polymeric microemulsions. *Journal Of Polymer Science Part B-Polymer Physics*, 35(17):2775–2786, December 1997.

[13] F. S. Bates, W. W. Maurer, P. M. Lipic, M. A. Hillmyer, K. Almdal, K. Mortensen, G. H. Fredrickson, and T. P. Lodge. Polymeric bicontinuous microemulsions. *Physical Review Letters*, 79(5):849–852, August 1997.

[14] M. A. Hillmyer, W. W. Maurer, T. P. Lodge, F. S. Bates, and K. Almdal. Model bicontinuous microemulsions in ternary homopolymer block copolymer blends. *Journal Of Physical Chemistry B*, 103(23):4814–4824, June 1999.

[15] N. R. Washburn, T. P. Lodge, and F. S. Bates. Ternary polymer blends as model surfactant systems. *Journal Of Physical Chemistry B*, 104(30):6987–6997, August 2000.

[16] D. Duchs, V. Ganesan, G. H. Fredrickson, and F. Schmid. Fluctuation effects in ternary ab+a+b polymeric emulsions. *Macromolecules*, 36(24):9237–9248, December 2003.

[17] D. Duchs and F. Schmid. Formation and structure of the microemulsion phase in two-dimensional ternary ab+a+b polymeric emulsions. *Journal Of Chemical Physics*, 121(6):2798–2805, August 2004.

[18] M. P. Stoykovich, E. W. Edwards, H. H. Solak, and P. F. Nealey. Phase behavior of symmetric ternary block copolymer-homopolymer blends in thin films and on chemically patterned surfaces. *Physical Review Letters*, 97(14):147802, October 2006.

[19] S. Komura. Mesoscale structures in microemulsions. *Journal Of Physics-Condensed Matter*, 19(46):463101, November 2007.

[20] C. J. Ellison, A. J. Meuler, J. Qin, C. M. Evans, L. M. Wolf, and F. S. Bates. Bicontinuous polymeric microemulsions from polydisperse di-

block copolymers. *Journal Of Physical Chemistry B*, 113(12):3726–3737, March 2009.

[21] G. L. Liu, M. P. Stoykovich, S. X. Ji, K. O. Stuen, G. S. W. Craig, and P. F. Nealey. Phase behavior and dimensional scaling of symmetric block copolymer-homopolymer ternary blends in thin films. *Macromolecules*, 42(8):3063–3072, April 2009.

[22] S.L. Turgeon, C. Schmitt, and C. Sanchez. Protein-polysaccharide complexes and coacervates. *Current Opinion in Colloid & Interface Science*, 12(45):166 – 178, 2007.

[23] Eric Dickinson. Colloid science of mixed ingredients. *Soft Matter*, 2:642–652, 2006.

[24] V. Tolstoguzov. Phase behaviour of macromolecular components in biological and food systems. *Food / Nahrung*, 44(5):299–308, 2000.

[25] Vladimir Tolstoguzov. Some thermodynamic considerations in food formulation. *Food Hydrocolloids*, 17(1):1 – 23, 2003.

[26] Simona Sennato, Domenico Truzzolillo, and Federico Bordi. Aggregation and stability of polyelectrolyte-decorated liposome complexes in water-salt media. *Soft Matter*, 8:9384–9395, 2012.

[27] Rungsima Chollakup, John B. Beck, Klaus Dirnberger, Matthew Tirrell, and Claus D. Eisenbach. Polyelectrolyte molecular weight and

salt effects on the phase behavior and coacervation of aqueous solutions of poly(acrylic acid) sodium salt and poly(allylamine) hydrochloride. *Macromolecules*, 46(6):2376–2390, 2013.

[28] Y.A. Antonov and P. Moldenaers. Structure formation and phase-separation behaviour of aqueous caseinalginate emulsions in the presence of strong polyelectrolyte. *Food Hydrocolloids*, 25(3):350 – 360, 2011.

[29] M. Pelaez-Fernandez, A. Moncho-Jorda, and J. Callejas-Fernandez. Structure of charged colloid-polymer mixtures. *EPL (Europhysics Letters)*, 90(4):46005, 2010.

[30] Evan Spruijt, Adrie H. Westphal, Jan Willem Borst, Martien A. Cohen Stuart, and Jasper van der Gucht. Binodal compositions of polyelectrolyte complexes. *Macromolecules*, 43(15):6476–6484, 2010.

[31] F. Weinbreck, R. de Vries, P. Schrooyen, and C. G. de Kruif. Complex coacervation of whey proteins and gum arabic. *Biomacromolecules*, 4(2):293–303, 2003.

[32] K. W. Mattison, I. J. Brittain, and P. L. Dubin. Protein-polyelectrolyte phase boundaries. *Biotechnology Progress*, 11(6):632–637, November 1995.

[33] K. W. Mattison, Y. F. Wang, K. Grymonpre, and P. L. Dubin. Micro- and macro-phase behavior in protein-polyelectrolyte complexes. *Macromolecular Symposia*, 140:53–76, May 1999.

[34] J. L. Xia, H. W. Zhang, D. R. Rigsbee, P. L. Dubin, and T. Shaikh. Structural elucidation of soluble polyelectrolyte-micelle complexes - intrapolymer vs interpolymer association. *Macromolecules*, 26(11):2759–2766, May 1993.

[35] M Vikelouda and V Kiosseoglou. The use of carboxymethylcellulose to recover potato proteins and control their functional properties. *Food Hydrocolloids*, 18(1):21 – 27, 2004.

[36] Antonia Montilla, Enriqueta Casal, F. Javier Moreno, Josefina Belloque, Agustn Olano, and Nieves Corzo. Isolation of bovine -lactoglobulin from complexes with chitosan. *International Dairy Journal*, 17(5):459 – 464, 2007.

[37] K. Damianou and V. Kiosseoglou. Stability of emulsions containing a whey protein concentrate obtained from milk serum through carboxymethylcellulose complexation. *Food Hydrocolloids*, 20(6):793 – 799, 2006.

[38] D G A L Aarts, R Tuinier, and H N W Lekkerkerker. Phase behaviour of mixtures of colloidal spheres and excluded-volume polymer chains. *Journal of Physics: Condensed Matter*, 14(33):7551, 2002.

[39] O Spalla. Nanoparticle interactions with polymers and polyelectrolytes. *Current Opinion in Colloid & Interface Science*, 7(34):179 – 185, 2002.

[40] P. Kolhe, E. Misra, R. M. Kannan, S. Kannan, and M. Lieh-Lai. Drug complexation, in vitro release and cellular entry of dendrimers and hy-

perbranched polymers. *International Journal of Pharmaceutics*, 259(1-2):143–160, June 2003.

[41] P. Kolhe, J. Khandare, O. Pillai, S. Kannan, M. Lieh-Lal, and R. M. Kannan. Preparation, cellular transport, and activity of polyamidoamine-based dendritic nanodevices with a high drug payload. *Biomaterials*, 27(4):660–669, February 2006.

[42] M. F. Neerman. The efficiency of a pamam dendrimer toward the encapsulation of the antileukernic drug 6-mercaptopurine. *Anti-cancer Drugs*, 18(7):839–842, August 2007.

[43] Y. Y. Cheng, Z. H. Xu, M. L. Ma, and T. W. Xu. Dendrimers as drug carriers: Applications in different routes of drug administration. *Journal of Pharmaceutical Sciences*, 97(1):123–143, January 2008.

[44] Y. Y. Cheng, Y. W. Li, Q. L. Wu, H. H. Zhang, and T. W. Xu. Generation-dependent encapsulation/electrostatic attachment of phenobarbital molecules by poly(amidoamine) dendrimers: Evidence from 2d-noesy investigations. *European Journal of Medicinal Chemistry*, 44(5):2219–2223, May 2009.

[45] S. Svenson. Dendrimers as versatile platform in drug delivery applications. *European Journal of Pharmaceutics and Biopharmaceutics*, 71(3):445–462, March 2009.

[46] M. A. Mintzer and M. W. Grinstaff. Biomedical applications of dendrimers: a tutorial. *Chemical Society Reviews*, 40(1):173–190, 2011.

[47] M. Muller and G. D. Smith. Phase separation in binary mixtures containing polymers: A quantitative comparison of single-chain-in-mean-field simulations and computer simulations of the corresponding multichain systems. *Journal Of Polymer Science Part B-Polymer Physics*, 43(8):934–958, April 2005.

[48] K. C. Daoulas and M. Muller. Single chain in mean field simulations: Quasi-instantaneous field approximation and quantitative comparison with monte carlo simulations. *Journal Of Chemical Physics*, 125(18):184904, November 2006.

[49] K. C. Daoulas, M. Muller, M. P. Stoykovich, H. Kang, J. J. de Pablo, and P. F. Nealey. Directed copolymer assembly on chemical substrate patterns: A phenomenological and single-chain-in-mean-field simulations study of the influence of roughness in the substrate pattern. *Langmuir*, 24(4):1284–1295, February 2008.

[50] R. Wang, W. H. Li, Y. W. Luo, B. G. Li, A. C. Shi, and S. P. Zhu. Phase behavior of ternary homopolymer/gradient copolymer blends. *Macromolecules*, 42(6):2275–2285, March 2009.

[51] L. Wang and L. J. Broadbelt. Explicit sequence of styrene/methyl methacrylate gradient copolymers synthesized by forced gradient copoly-

merization with nitroxide-mediated controlled radical polymerization. *Macromolecules*, 42(20):7961–7968, October 2009.

[52] J. F. Wang and M. Muller. Memory effects of diblock copolymer brushes and mixed brushes. *Langmuir*, 26(2):1291–1303, January 2010.

[53] B. Steinmuller, M. Muller, K. R. Hambrecht, G. D. Smith, and D. Bedrov. Properties of random block copolymer morphologies: Molecular dynamics and single-chain-in-mean-field simulations. *Macromolecules*, 45(2):1107–1117, January 2012.

[54] F. S. Bates and G. H. Fredrickson. Block copolymer thermodynamics - theory and experiment. *Annual Review Of Physical Chemistry*, 41:525–557, 1990.

[55] M. T. Krejchi, E. D. T. Atkins, A. J. Waddon, M. J. Fournier, T. L. Mason, and D. A. Tirrell. Chemical sequence control of beta-sheet assembly in macromolecular crystals of periodic polypeptides. *Science*, 265(5177):1427–1432, September 1994.

[56] S. J. M. Yu, V. P. Conticello, G. H. Zhang, C. Kayser, M. J. Fournier, T. L. Mason, and D. A. Tirrell. Smectic ordering in solutions and films of a rod-like polymer owing to monodispersity of chain length. *Nature*, 389(6647):167–170, September 1997.

[57] M. J. Fasolka and A. M. Mayes. Block copolymer thin films: Physics and applications. *Annual Review Of Materials Research*, 31:323–355,

2001.

[58] C. J. Hawker, A. W. Bosman, and E. Harth. New polymer synthesis by nitroxide mediated living radical polymerizations. *Chemical Reviews*, 101(12):3661–3688, December 2001.

[59] S. Aoshima, S. Sugihara, M. Shibayama, and S. Kanaoka. Synthesis and self-association of stimuli-responsive diblock copolymers by living cationic polymerization. *Macromolecular Symposia*, 215:151–163, August 2004.

[60] G. Moad, E. Rizzardo, and S. H. Thang. Radical addition-fragmentation chemistry in polymer synthesis. *Polymer*, 49(5):1079–1131, March 2008.

[61] K. Matyjaszewski and N. V. Tsarevsky. Nanostructured functional materials prepared by atom transfer radical polymerization. *Nature Chemistry*, 1(4):276–288, July 2009.

[62] M. Dadmun. Effect of copolymer architecture on the interfacial structure and miscibility of a ternary polymer blend containing a copolymer and two homopolymers. *Macromolecules*, 29(11):3868–3874, May 1996.

[63] T. E. Patten and K. Matyjaszewski. Atom transfer radical polymerization and the synthesis of polymeric materials. *Advanced Materials*, 10(12):901–915, August 1998.

[64] J. Kim, M. K. Gray, H. Y. Zhou, S. T. Nguyen, and J. M. Torkelson. Polymer blend compatibilization by gradient copolymer addition during

melt processing: Stabilization of dispersed phase to static coarsening. *Macromolecules*, 38(4):1037–1040, February 2005.

[65] C. L. H. Wong, J. Kim, C. B. Roth, and J. M. Torkelson. Comparison of critical micelle concentrations of gradient copolymer and block copolymer in homopolymer: Novel characterization by intrinsic fluorescence. *Macromolecules*, 40(16):5631–5633, August 2007.

[66] J. Kim, R. W. Sandoval, C. M. Dettmer, S. T. Nguyen, and J. M. Torkelson. Compatibilized polymer blends with nanoscale or sub-micron dispersed phases achieved by hydrogen-bonding effects: Block copolymer vs blocky gradient copolymer addition. *Polymer*, 49(11):2686–2697, May 2008.

[67] R. Malik, C. K. Hall, and J. Genzer. Effect of copolymer compatibilizer sequence on the dynamics of phase separation of immiscible binary homopolymer blends. *Soft Matter*, 7(22):10620–10630, 2011.

[68] M. Kryszewski. Gradient polymers and copolymers. *Polymers For Advanced Technologies*, 9(4):244–259, April 1998.

[69] U. Beginn. Gradient copolymers. *Colloid And Polymer Science*, 286(13):1465–1474, November 2008.

[70] Y. Sha, C. Y. Hui, E. J. Kramer, S. F. Hahn, and C. A. Berglund. Fracture toughness and failure mechanisms of epoxy/rubber-modified

polystyrene (hips) interfaces reinforced by grafted chains. *Macromolecules*, 29(13):4728–4736, June 1996.

[71] J. Kim, M. M. Mok, R. W. Sandoval, D. J. Woo, and J. M. Torkelson. Uniquely broad glass transition temperatures of gradient copolymers relative to random and block copolymers containing repulsive comonomers. *Macromolecules*, 39(18):6152–6160, September 2006.

[72] S. Jouenne, J. A. Gonzalez-Leon, A. V. Ruzette, P. Lodefier, S. Tence-Girault, and L. Leibler. Styrene/butadiene gradient block copolymers: Molecular and mesoscopic structures. *Macromolecules*, 40(7):2432–2442, April 2007.

[73] P. Hodrokoukes, G. Floudas, S. Pispas, and N. Hadjichristidis. Microphase separation in normal and inverse tapered block copolymers of polystyrene and polyisoprene. 1. phase state. *Macromolecules*, 34(3):650–657, January 2001.

[74] S. Asakura and F. Oosawa. Interaction between particles suspended in solutions of macromolecules. *Journal of Polymer Science*, 33(126):183–192, 1958.

[75] A. Vrij. Polymers at interfaces and interactions in colloidal dispersions. *Pure and Applied Chemistry*, 48(4):471–483, 1976.

[76] W. Poon. Colloids as big atoms. *Science*, 304(5672):830–831, May 2004.

[77] A. M. Chen, L. M. Santhakumaran, S. K. Nair, P. S. Amenta, T. Thomas, H. X. He, and T. J. Thomas. Oligodeoxynucleotide nanostructure formation in the presence of polypropyleneimine dendrimers and their uptake in breast cancer cells. *Nanotechnology*, 17(21):5449–5460, November 2006.

[78] G.R. Newkome, C.N. Moorefield, and F. Vögtle. *Dendrimers and dendrons: concepts, syntheses, applications*. Wiley-VCH, 2001.

[79] D. A. Tomalia, A. M. Naylor, and W. A. Goddard. Starburst dendrimers - molecular-level control of size, shape, surface-chemistry, topology, and flexibility from atoms to macroscopic matter. *Angewandte Chemie-international Edition In English*, 29(2):138–175, February 1990.

[80] Mingjun Liu and Jean M.J. Frechet. Designing dendrimers for drug delivery. *Pharmaceutical Science & Technology Today*, 2(10):393 – 401, 1999.

[81] Mary X. Tang, Carl T. Redemann, and Francis C. Szoka. In vitro gene delivery by degraded polyamidoamine dendrimers. *Bioconjugate Chemistry*, 7(6):703–714, 1996.

[82] Youngseon Choi, Thommey Thomas, Alina Kotlyar, Mohammad T. Islam, and James R. Baker Jr. Synthesis and functional evaluation of dna-assembled polyamidoamine dendrimer clusters for cancer cell-specific targeting. *Chemistry & Biology*, 12(1):35 – 43, 2005.

[83] N Malik, R Wiwattanapatapee, R Klopsch, K Lorenz, H Frey, J.W Weener, E.W Meijer, W Paulus, and R Duncan. Dendrimers:: Relationship between structure and biocompatibility in vitro, and preliminary studies on the biodistribution of 125i-labelled polyamidoamine dendrimers in vivo. *Journal of Controlled Release*, 65(12):133 – 148, 2000.

[84] Hui-Li Fu, Si-Xue Cheng, Xian-Zheng Zhang, and Ren-Xi Zhuo. Dendrimer/dna complexes encapsulated functional biodegradable polymer for substrate-mediated gene delivery. *The Journal of Gene Medicine*, 10(12):1334–1342, 2008.

[85] Christine Dufes, Ijeoma Uchegbu, and Andreas Schatzlein. Dendrimers in gene delivery. *Advanced drug delivery reviews*, 57(15):2177–2202, 2005.

[86] Jonathan D. Eichman, Anna U. Bielinska, Jolanta F. Kukowska-Latallo, and James R. Baker Jr. The use of pamam dendrimers in the efficient transfer of genetic material into cells. *Pharmaceutical Science & Technology Today*, 3(7):232 – 245, 2000.

[87] Xiaoxuan Liu, Cheng Liu, Erik Laurini, Paola Posocco, Sabrina Pricl, Fanqi Qu, Palma Rocchi, and Ling Peng. Efficient delivery of sticky sirna and potent gene silencing in a prostate cancer model using a generation 5 triethanolamine-core pamam dendrimer. *Molecular Pharmaceutics*, 9(3):470–481, 2012.

[88] Narendra K Jain and Umesh Gupta. Application of dendrimer drug complexation in the enhancement of drug solubility and bioavailability. *Expert Opinion on Drug Metabolism & Toxicology*, 4(8):1035–1052, 2008.

[89] Jayant Khandare, Marcelo Calderon, Nilesh M. Dagia, and Rainer Haag. Multifunctional dendritic polymers in nanomedicine: opportunities and challenges. *Chem. Soc. Rev.*, 41:2824–2848, 2012.

[90] Prabal Maiti and Biman Bagchi. Structure and dynamics of DNA-dendrimer complexation: role of counterions, water, and base pair sequence. *Nano letters*, 6(11):2478–2485, 2006.

[91] V. Vasumathi and Prabal K. Maiti. Complexation of siRNA with dendrimer: A molecular modeling approach. *Macromolecules*, 43, 2010.

[92] D. Ouyang, H. Zhang, H. S. Parekh, and S. C. Smith. The effect of ph on pamam dendrimer-sirna complexation - endosomal considerations as determined by molecular dynamics simulation. *Biophysical Chemistry*, 158(2-3):126–133, October 2011.

[93] Linda Jensen, Giovanni Pavan, Marina Kasimova, Sandra Rutherford, Andrea Danani, Hanne Nielsen, and Camilla Foged. Elucidating the molecular mechanism of PAMAM-siRNA dendriplex self-assembly: effect of dendrimer charge density. *International journal of pharmaceutics*, 416(2):410–418, 2011.

[94] Bidisha Nandy and Prabal Maiti. Dna compaction by a dendrimer. *The journal of physical chemistry. B*, 115(2):217–230, 2011.

[95] Kostas Karatasos, Paola Posocco, Erik Laurini, and Sabrina Pricl. Poly(amidoamine)-based dendrimer/siRNA complexation studied by computer simulations: effects of pH and generation on dendrimer structure and siRNA binding. *Macromolecular bioscience*, 12(2):225–240, 2012.

[96] P. Welch and M. Muthukumar. Dendrimer-polyelectrolyte complexation: A model guest-host system. *Macromolecules*, 33(16):6159–6167, August 2000.

[97] S. V. Lyulin, A. A. Darinskii, and A. V. Lyulin. Computer simulation of complexes of dendrimers with linear polyelectrolytes. *Macromolecules*, 38(9):3990–3998, May 2005.

[98] S. V. Lyulin, A. A. Darinskii, and A. V. Lyulin. Energetic and conformational aspects of dendrimer overcharging by linear polyelectrolytes. *Physical Review E*, 78(4):041801, October 2008.

[99] S. V. Larin, S. V. Lyulin, A. V. Lyulin, and A. A. Darinskii. Charge inversion of dendrimers in complexes with linear polyelectrolytes in the solutions with low ph. *Polymer Science Series A*, 51(4):459–468, April 2009.

[100] S. V. Larin, A. A. Darinskii, A. V. Lyulin, and S. V. Lyulin. Linker formation in an overcharged complex of two dendrimers and linear poly-

electrolyte. *Journal of Physical Chemistry B*, 114(8):2910–2919, March 2010.

[101] W. D. Tian and Y. Q. Ma. Complexation of a linear polyelectrolyte with a charged dendrimer: Polyelectrolyte stiffness effects. *Macromolecules*, 43(3):1575–1582, February 2010.

[102] J. S. Klos and J. U. Sommer. Monte carlo simulations of charged dendrimer-linear polyelectrolyte complexes and explicit counterions. *Journal of Chemical Physics*, 134(20):204902, May 2011.

[103] J. S. Klos and J. U. Sommer. Simulation of complexes between a charged dendrimer and a linear polyelectrolyte with finite rigidity. *Macromolecular Theory and Simulations*, 21(7):448–460, August 2012.

[104] Thomas Lewis, Gunja Pandav, Ahmad Omar, and Venkat Ganesan. Complexation between weakly basic dendrimers and linear polyelectrolytes: effects of grafts, chain stiffness, and pOH. *Soft Matter*, 9, 2013.

[105] S. A. Brazovskii. *Sov. Phys. JETP*, 41:85, 1975.

[106] G. H. Fredrickson and E. Helfand. Fluctuation effects in the theory of microphase separation in block copolymers. *Journal Of Chemical Physics*, 87(1):697–705, July 1987.

[107] O. N. Vassiliev and M. W. Matsen. Fluctuation effects in block copolymer melts. *Journal Of Chemical Physics*, 118(16):7700–7713, April 2003.

[108] A. L. Schmitt and M. K. Mahanthappa. Polydispersity-driven shift in the lamellar mesophase composition window of peo-pb-peo triblock copolymers. *Soft Matter*, 8(7):2294–2303, 2012.

[109] J. M. Widin, A. K. Schmitt, A. L. Schmitt, K. Im, and M. K. Mahanthappa. Unexpected consequences of block polydispersity on the self-assembly of aba triblock copolymers. *Journal Of The American Chemical Society*, 134(8):3834–3844, February 2012.

[110] A. V. Dobrynin. Microphase separation transition of random copolymers in a random media. *Physical Review E*, 56(1):750–757, July 1997.

[111] Z. G. Wang. Concentration fluctuation in binary polymer blends: chi parameter, spinodal and ginzburg criterion. *Journal Of Chemical Physics*, 117(1):481–500, July 2002.

[112] Z. G. Wang. Fluctuation in electrolyte solutions: The self energy. *Physical Review E*, 81(2):021501, February 2010.

[113] P. Grzywacz, J. Qin, and D. C. Morse. Renormalization of the one-loop theory of fluctuations in polymer blends and diblock copolymer melts. *Physical Review E*, 76(6):061802, December 2007.

[114] D. C. Morse and J. A. Qin. Relationships among coarse-grained field theories of fluctuations in polymer liquids. *Journal Of Chemical Physics*, 134(8):084902, February 2011.

[115] J. Qin, P. Grzywacz, and D. C. Morse. Renormalized one-loop theory of correlations in disordered diblock copolymers. *Journal Of Chemical Physics*, 135(8):084902, August 2011.

[116] J. Qin and D. C. Morse. Fluctuations in symmetric diblock copolymers: Testing theories old and new. *Physical Review Letters*, 108(23):238301, June 2012.

[117] J. Glaser, J. Qin, P. Medapuram, M. Muller, and D. C. Morse. Test of a scaling hypothesis for the structure factor of disordered diblock copolymer melts. *Soft Matter*, 8(44):11310–11317, 2012.

[118] P. F. Zhang, X. H. Zhang, B. H. Li, and Q. Wang. Quantitative study of fluctuation effects by fast lattice monte carlo simulations. i. compressible homopolymer melts. *Soft Matter*, 7(9):4461–4471, 2011.

[119] P. F. Zhang, B. H. Li, and Q. Wang. Quantitative study of fluctuation effects by fast lattice monte carlo simulations. 2. homopolymer brushes in an implicit, good solvent. *Macromolecules*, 44(19):7837–7852, October 2011.

[120] P. Zhang, Y. Wang, Y. Yang, J. Zhang, X. Cao, W. Chen, and K. Li. One factor influencing the oil-displacement ability of polymer flooding: Apparent viscosity or effective viscosity in porous media? *Petroleum Science and Technology*, 30(14):1424–1432, 2012.

[121] K. Matyjaszewski and J. H. Xia. Atom transfer radical polymerization. *Chemical Reviews*, 101(9):2921–2990, September 2001.

[122] M. Ouchi, T. Terashima, and M. Sawamoto. Transition metal-catalyzed living radical polymerization: Toward perfection in catalysis and precision polymer synthesis. *Chemical Reviews*, 109(11):4963–5050, November 2009.

[123] N. A. Lynd and M. A. Hillmyer. Influence of polydispersity on the self-assembly of diblock copolymers. *Macromolecules*, 38(21):8803–8810, October 2005.

[124] N. A. Lynd and M. A. Hillmyer. Effects of polydispersity on the order-disorder transition in block copolymer melts. *Macromolecules*, 40(22):8050–8055, October 2007.

[125] N. A. Lynd, B. D. Hamilton, and M. A. Hillmyer. The role of polydispersity in the lamellar mesophase of model diblock copolymers. *Journal Of Polymer Science Part B-Polymer Physics*, 45(24):3386–3393, December 2007.

[126] N. A. Lynd, A. J. Meuler, and M. A. Hillmyer. Polydispersity and block copolymer self-assembly. *Progress In Polymer Science*, 33(9):875–893, September 2008.

[127] N. A. Lynd, M. A. Hillmyer, and M. W. Matsen. Theory of polydisperse

block copolymer melts: Beyond the schulz-zimm distribution. *Macromolecules*, 41(12):4531–4533, June 2008.

[128] T. M. Beardsley and M. W. Matsen. Effects of polydispersity on the order-disorder transition of diblock copolymer melts. *European Physical Journal E*, 27(3):323–333, November 2008.

[129] T. M. Beardsley and M. W. Matsen. Monte carlo phase diagram for a polydisperse diblock copolymer melt. *Macromolecules*, 44(15):6209–6219, August 2011.

[130] Yue Li, Hu-Jun Qian, and Zhong-Yuan Lu. The influence of one block polydispersity on phase separation of diblock copolymers: The molecular mechanism for domain spacing expansion. *Polymer*, 54(14):37163722, 2013.

[131] S. W. Sides and G. H. Fredrickson. Continuous polydispersity in a self-consistent field theory for diblock copolymers. *Journal Of Chemical Physics*, 121(10):4974–4986, September 2004.

[132] D. M. Cooke and A. C. Shi. Effects of polydispersity on phase behavior of diblock copolymers. *Macromolecules*, 39(19):6661–6671, September 2006.

[133] M. W. Matsen. Polydispersity-induced macrophase separation in diblock copolymer melts. *Physical Review Letters*, 99(14):148304, October 2007.

[134] C. D. Sfatos and E. I. Shakhnovich. Statistical mechanics of random heteropolymers. *Physics Reports-Review Section Of Physics Letters*, 288(1-6):77–108, September 1997.

[135] P. Debnath and B. J. Cherayil. Semiflexible random a-b block copolymers under tension. *Journal Of Chemical Physics*, 118(4):1970–1978, January 2003.

[136] C. E. Soteros and S. G. Whittington. The statistical mechanics of random copolymers. *Journal Of Physics A-Mathematical And General*, 37(41):R279–R325, October 2004.

[137] K. Chrissopoulou, V. A. Pryamitsyn, S. H. Anastasiadis, G. Fytas, A. N. Semenov, M. Xenidou, and N. Hadjichristidis. Dynamics of the most probable composition fluctuations of "real" diblock copolymers near the ordering transition. *Macromolecules*, 34(7):2156–2171, March 2001.

[138] J. F. Wang and M. Muller. Microphase separation of mixed polymer brushes: Dependence of the morphology on grafting density, composition, chain-length asymmetry, solvent quality, and selectivity. *Journal Of Physical Chemistry B*, 113(33):11384–11402, August 2009.

[139] L. Wang and L. J. Broadbelt. Factors affecting the formation of the monomer sequence along styrene/methyl methacrylate gradient copolymer chains. *Macromolecules*, 42(21):8118–8128, November 2009.

[140] A. S. Cho and L. J. Broadbelt. Stochastic modelling of gradient copolymer chemical composition distribution and sequence length distribution. *Molecular Simulation*, 36(15):1219–1236, 2010.

[141] L. Wang and L. J. Broadbelt. Model-based design for preparing styrene/methyl methacrylate structural gradient copolymers. *Macromolecular Theory And Simulations*, 20(3):191–204, March 2011.

[142] K. C. Gallow, Y. K. Jhon, W. Tang, J. Genzer, and Y-L Loo. Cloud point suppression in dilute solutions of model gradient copolymers with prespecified composition profiles. *Journal Of Polymer Science Part B-Polymer Physics*, 49(9):629–637, May 2011.

[143] D. M. Trombly, V. Pryamitsyn, and V. Ganesan. Self-assembly of diblock copolymer on substrates modified by random copolymer brushes. *Macromolecules*, 44(24):9867–9881, December 2011.

[144] K. C. Gallow, Y. K. Jhon, J. Genzer, and Y-L Loo. Influence of gradient strength and composition profile on the onset of the cloud point transition in hydroxyethyl methacrylate/dimethylaminoethyl methacrylate gradient copolymers. *Polymer*, 53:1131–1137, 2012.

[145] Marcus Muller and Kostas Ch Daoulas. Calculating the free energy of self-assembled structures by thermodynamic integration. *The Journal of Chemical Physics*, 2008.

[146] B. Narayanan, V. A. Pryamitsyn, and V. Ganesan. Interfacial phenomena in polymer blends: A self-consistent brownian dynamics study. *Macromolecules*, 37(26):10180–10194, December 2004.

[147] B. Narayanan and V. Ganesan. Flow deformation of polymer blend droplets and the role of block copolymer compatibilizers. *Physics Of Fluids*, 18(4):042109, April 2006.

[148] F. A. Detcheverry, H. M. Kang, K. C. Daoulas, M. Muller, P. F. Nealey, and J. J. de Pablo. Monte carlo simulations of a coarse grain model for block copolymers and nanocomposites. *Macromolecules*, 41(13):4989–5001, July 2008.

[149] F. A. Detcheverry, D. Q. Pike, U. Nagpal, P. F. Nealey, and J. J. de Pablo. Theoretically informed coarse grain simulations of block copolymer melts: method and applications. *Soft Matter*, 5(24):4858–4865, 2009.

[150] S. W. Sides, B. J. Kim, E. J. Kramer, and G. H. Fredrickson. Hybrid particle-field simulations of polymer nanocomposites. *Physical Review Letters*, 96(25):250601, June 2006.

[151] N. A. Kumar and V. Ganesan. Communication: Self-assembly of semiflexible-flexible block copolymers. *Journal Of Chemical Physics*, 136(10):101101, March 2012.

[152] G. V. Schulz. The kinetics of chain polymerisation v. the influence of various types of reactions on the poly-molecularity. *Zeitschrift Fur Physikalische Chemie-Abteilung B-Chemie Der Elementarprozesse Aufbau Der Materie*, 43(1):25–46, May 1939.

[153] B. H. Zimm. Apparatus and methods for measurement and interpretation of the angular variation of light scattering - preliminary results on polystyrene solutions. *Journal Of Chemical Physics*, 16(12):1099–1116, 1948.

[154] Milton Abramowitz and Irene A. Stegun. *Handbook of Mathematical Functions: with Formulas, Graphs, and Mathematical Tables*. Dover books on mathematics. Dover, New York, June 1972.

[155] R. E. Cunningham and M. R. Treiber. Preparation and stressstrain properties of aba-type block polymers of styrene and isoprene or butadiene. *J. Appl. Polym. Sci.*, 12:2334, 1968.

[156] Y. Tsukahara, N. Nakamura, T. Hashimoto, H. Kawai, T. Nagaya, Y. Sugimura, and S. Tsuge. Structure and properties of tapered block polymers of styrene and isoprene. *Polym. J.*, 12:455466, 1980.

[157] T. Hashimoto, Y. Tsukahara, K. Tachi, and H. Kawai. *Macromolecules*, 16:64–57, 1983.

[158] M. Y. Zaremski, D. I. Kalugin, and V. B. Golubev. Gradient copolymers: Synthesis, structure, and properties. *Polymer Science Series A*,

51(1):103–122, January 2009.

[159] I. Kuntz. The copolymerization of 1,3-butadiene with styrene by butyllithium initiation. *J. Polym. Sci.*, 54:569–586, 1961.

[160] M. Lobert, R. Hoogenboom, C. A. Fustin, J. F. Gohy, and U. S. Schubert. Amphiphilic gradient copolymers containing fluorinated 2-phenyl-2-oxazolines: Microwave-assisted one-pot synthesis and self-assembly in water. *Journal Of Polymer Science Part A-Polymer Chemistry*, 46(17):5859–5868, September 2008.

[161] N. Singh, M. S. Tureau, and T. H. Epps. Manipulating ordering transitions in interfacially modified block copolymers. *Soft Matter*, 5(23):4757–4762, 2009.

[162] R. Roy, J. K. Park, W. S. Young, S. E. Mastroianni, M. S. Tureau, and T. H. Epps. Double-gyroid network morphology in tapered diblock copolymers. *Macromolecules*, 44(10):3910–3915, May 2011.

[163] W. F. Kuan, R. Roy, L. X. Rong, B. S. Hsiao, and T. H. Epps. Design and synthesis of network-forming triblock copolymers using tapered block interfaces. *Acs Macro Letters*, 1(4):519–523, April 2012.

[164] D. M. Trombly and V. Ganesan. Curvature effects upon interactions of polymer-grafted nanoparticles in chemically identical polymer matrices. *Journal of Chemical Physics*, 133(15):154904–1–7, October 2010.

[165] D. M. Trombly, V. Pryamitsyn, and V. Ganesan. Surface energies and self-assembly of block copolymers on grafted surfaces. *Physical Review Letters*, 107(14):148304–1–5, September 2011.

[166] D. M. Trombly, V. Pryamitsyn, and V. Ganesan. Interfacial properties of statistical copolymer brushes in contact with homopolymer melts. *Journal of Chemical Physics*, 134(15):154903–1–12, April 2011.

[167] G. Pandav, V. Pryamitsyn, K. C. Gallow, Y. L. Loo, J. Genzer, and V. Ganesan. Phase behavior of gradient copolymer solutions: a monte carlo simulation study. *Soft Matter*, 8(24):6471–6482, 2012.

[168] N. Metropolis, A. Rosenbluth, M. Rosenbluth, A. Teller, and E. Teller. Equation of state calculations by fast computing machines. *Journal of Chemical Physics*, 21:1087–1092, 1953.

[169] A. Alexander-Katz, A. G. Moreira, and G. H. Fredrickson. Simulations of polymer solutions: A field-theoretic approach. *Mesoscale Phenomena In Fluid Systems*, 861:279–289, 2003.

[170] Z. G. Wang. Effects of ion solvation on the miscibility of binary polymer blends. *Journal of Physical Chemistry B*, 112(50):16205–16213, December 2008.

[171] A. Alexander-Katz and G. H. Fredrickson. Diblock copolymer thin films: A field-theoretic simulation study. *Macromolecules*, 40(11):4075–4087, May 2007.

[172] A. Alexander-Katz, A. G. Moreira, and G. H. Fredrickson. Field-theoretic simulations of confined polymer solutions. *Journal Of Chemical Physics*, 118(19):9030–9036, May 2003.

[173] A. Alexander-Katz, A. G. Moreira, S. W. Sides, and G. H. Fredrickson. Field-theoretic simulations of polymer solutions: Finite-size and discretization effects. *Journal Of Chemical Physics*, 122(1):014904, January 2005.

[174] Y. O. Popov, J. H. Lee, and G. H. Fredrickson. Field-theoretic simulations of polyelectrolyte complexation. *Journal Of Polymer Science Part B-Polymer Physics*, 45(24):3223–3230, December 2007.

[175] S. F. Edwards. Statistical mechanics of polymers with excluded volume. *Proceedings Of The Physical Society of London*, 85(546P):613, 1965.

[176] E. Helfand and Y. Tagami. Theory of interface between immiscible polymers. *Journal Of Polymer Science Part B-Polymer Letters*, 9(10):741, 1971.

[177] E. Helfand and Y. Tagami. Theory of interface between immiscible polymers .2. *Journal Of Chemical Physics*, 56(7):3592, 1972.

[178] E. Helfand. Theory of inhomogeneous polymers - fundamentals of gaussian random-walk model. *Journal Of Chemical Physics*, 62(3):999–1005, 1975.

[179] J. Noolandi and K. M. Hong. Interfacial properties of immiscible homopolymer blends in the presence of block copolymers. *Macromolecules*, 15(2):482–492, 1982.

[180] M. W. Matsen. Phase-behavior of block-copolymer homopolymer blends. *Macromolecules*, 28(17):5765–5773, August 1995.

[181] M. W. Matsen. Stabilizing new morphologies by blending homopolymer with block-copolymer. *Physical Review Letters*, 74(21):4225–4228, May 1995.

[182] F. Schmid. Self-consistent-field theories for complex fluids. *Journal Of Physics-Condensed Matter*, 10(37):8105–8138, September 1998.

[183] J. R. Naughton and M. W. Matsen. Nonperiodic lamellar phase in ternary diblock copolymer/homopolymer blends. *Macromolecules*, 35(24):8926–8928, November 2002.

[184] R Lipowsky and S Leibler. Unbinding transitions of interacting membranes. *Physical Review Letters*, 56:2541–2544, 1986.

[185] B. H. Jones and T. P. Lodge. Nanocasting nanoporous inorganic and organic materials from polymeric bicontinuous microemulsion templates (vol 44, pg 131, 2012). *Polymer Journal*, 44(4):370–370, April 2012.

[186] N. Zhou, F. S. Bates, and T. P. Lodge. Mesoporous membrane templated by a polymeric bicontinuous microemulsion. *Nano Letters*, 6(10):2354–2357, October 2006.

[187] B. H. Jones and T. P. Lodge. High-temperature nanoporous ceramic monolith prepared from a polymeric bicontinuous microemulsion template. *Journal Of The American Chemical Society*, 131(5):1676, February 2009.

[188] B. H. Jones and T. P. Lodge. Nanoporous materials derived from polymeric bicontinuous microemulsions. *Chemistry Of Materials*, 22(4):1279–1281, February 2010.

[189] J. Y. Ying. Nanostructural tailoring: Opportunities for molecular engineering in catalysis. *Aiche Journal*, 46(10):1902–1906, October 2000.

[190] R. E. Morris and P. S. Wheatley. Gas storage in nanoporous materials. *Angewandte Chemie-International Edition*, 47(27):4966–4981, 2008.

[191] N. Haberkorn, M. C. Lechmann, B. H. Sohn, K. Char, J. S. Gutmann, and P. Theato. Templated organic and hybrid materials for optoelectronic applications. *Macromolecular Rapid Communications*, 30(14):1146–1166, July 2009.

[192] E. A. Jackson and M. A. Hillmyer. Nanoporous membranes derived from block copolymers: From drug delivery to water filtration. *Acs Nano*, 4(7):3548–3553, July 2010.

[193] F. S. Bates, W. Maurer, T. P. Lodge, M. F. Schulz, M. W. Matsen, K. Almdal, and K. Mortensen. Isotropic lifshitz behavior in block

copolymer-homopolymer blends. *Physical Review Letters*, 75(24):4429–4432, December 1995.

[194] P. K. Janert and M. Schick. Phase behavior of ternary homopolymer/diblock blends: Microphase unbinding in the symmetric system. *Macromolecules*, 30(13):3916–3920, June 1997.

[195] P. K. Janert and M. Schick. Phase behavior of ternary homopolymer/diblock blends: Influence of relative chain lengths. *Macromolecules*, 30(1):137–144, January 1997.

[196] H. S. Jeon, J. H. Lee, and N. P. Balsara. Intramolecular and intermolecular signatures of incipient ordering in a multicomponent polymer blend. *Physical Review Letters*, 79(17):3274–3277, October 1997.

[197] H. S. Jeon, J. H. Lee, and N. P. Balsara. Predictions of the thermodynamic properties of multicomponent polyolefin blends from measurements on two-component systems. *Macromolecules*, 31(10):3328–3339, May 1998.

[198] H. S. Jeon, J. H. Lee, N. P. Balsara, and M. C. Newstein. An experimental study of the thermodynamic properties of multicomponent polyolefin blends with ordered and disordered phases. *Macromolecules*, 31(10):3340–3352, May 1998.

[199] M. W. Matsen. Elastic properties of a diblock copolymer monolayer and their relevance to bicontinuous microemulsion. *Journal Of Chemical*

Physics, 110(9):4658–4667, March 1999.

[200] R. B. Thompson and M. W. Matsen. Effective interaction between monolayers of block copolymer compatiblizer in a polymer blend. *Journal Of Chemical Physics*, 112(15):6863–6872, April 2000.

[201] R. B. Thompson and M. W. Matsen. Improving polymeric microemulsions with block copolymer polydispersity. *Physical Review Letters*, 85(3):670–673, July 2000.

[202] D. C. Sun and H. X. Guo. Influence of compositional gradient on the phase behavior of ternary symmetric homopolymer-copolymer blends: A monte carlo study. *Polymer*, 52(25):5922–5932, November 2011.

[203] D. C. Sun and H. X. Guo. Monte carlo studies on the interfacial properties and interfacial structures of ternary symmetric blends with gradient copolymers. *Journal Of Physical Chemistry B*, 116(31):9512–9522, August 2012.

[204] Y. Lyatskaya, D. Gersappe, N. A. Gross, and A. C. Balazs. Designing compatibilizers to reduce interfacial tension in polymer blends. *Journal Of Physical Chemistry*, 100(5):1449–1458, February 1996.

[205] V. Ganesan, N. A. Kumar, and V. Pryamitsyn. Blockiness and sequence polydispersity effects on the phase behavior and interfacial properties of gradient copolymers. *Macromolecules*, 45(15):6281–6297, August 2012.

[206] P. G. Degennes and C. Taupin. Micro-emulsions and the flexibility of oil-water interfaces. *Journal Of Physical Chemistry*, 86(13):2294–2304, 1982.

[207] M. Muller and G. Gompper. Elastic properties of polymer interfaces: Aggregation of pure diblock, mixed diblock, and triblock copolymers. *Physical Review E*, 66(4):041805, October 2002.

[208] R. A. Riggleman, R. Kumar, and G. H. Fredrickson. Investigation of the interfacial tension of complex coacervates using field-theoretic simulations. *Journal Of Chemical Physics*, 136(2):024903, January 2012.

[209] V. Ganesan and V. Pryamitsyn. Dynamical mean-field theory for inhomogeneous polymeric systems. *Journal Of Chemical Physics*, 118(10):4345–4348, March 2003.

[210] G. Pandav and V. Ganesan. Fluctuation effects on the order-disorder transition of polydisperse copolymer melts. *The Journal of Chemical Physics*, 139:214905, 2013.

[211] Dominik Dchs. *Field theories for copolymer blends : self-consistent approaches and Monte Carlo simulations*. PhD thesis, Bielefeld University, 2003.

[212] Alexander-Katz Alfredo, Moreira Andre G., and Fredrickson Glenn H. *Simulations of Polymer Solutions: A Field-Theoretic Approach*, chapter 18, pages 279–289.

[213] M. Teubner and R. Strey. Origin of the scattering peak in microemulsions. *Journal Of Chemical Physics*, 87(5):3195–3200, September 1987.

[214] K. V. Schubert and R. Strey. Small-angle neutron-scattering from microemulsions near the disorder line in water formamide octane-ciej systems. *Journal Of Chemical Physics*, 95(11):8532–8545, December 1991.

[215] K. V. Schubert, R. Strey, S. R. Kline, and E. W. Kaler. Small-angle neutron-scattering near lifshitz lines - transition from weakly structured mixtures to microemulsions. *Journal Of Chemical Physics*, 101(6):5343–5355, September 1994.

[216] R. D. Koehler, K. V. Schubert, R. Strey, and E. W. Kaler. The lifshitz line in binary-systems - structures in water c(4)e(1) mixtures. *Journal Of Chemical Physics*, 101(12):10843–10849, December 1994.

[217] S. Okabe, K. Seno, S. Kanaoka, S. Aoshima, and M. Shibayama. Small-angle neutron scattering study on block and gradient copolymer aqueous solutions. *Polymer*, 47(21):7572–7579, October 2006.

[218] S. Okabe, K. Seno, S. Kanaoka, S. Aoshima, and M. Shibayama. Micellization study on block and gradient copolymer aqueous solutions by dls and sans. *Macromolecules*, 39(4):1592–1597, February 2006.

[219] R. Hoogenboom, H. M. L. Lambermont-Thijs, M. J. H. C. Jochems, S. Hoeppener, C. Guerlain, C. A. Fustin, J. F. Gohy, and U. S. Schubert. A schizophrenic gradient copolymer: switching and reversing

poly(2-oxazoline) micelles based on ucst and subtle solvent changes. *Soft Matter*, 5(19):3590–3592, 2009.

[220] N. Merlet-Lacroix, E. Di Cola, and M. Cloitre. Swelling and rheology of thermoresponsive gradient copolymer micelles. *Soft Matter*, 6(5):984–993, 2010.

[221] A. Aksimentiev and R. Holyst. Single-chain statistics in polymer systems. *Progress In Polymer Science*, 24(7):1045–1093, September 1999.

[222] M. D. Lefebvre, M. O. de la Cruz, and K. R. Shull. Phase segregation in gradient copolymer melts. *Macromolecules*, 37(3):1118–1123, February 2004.

[223] R. Jiang, Q. H. Jin, B. H. Li, D. T. Ding, R. A. Wickham, and A. C. Shi. Phase behavior of gradient copolymers. *Macromolecules*, 41(14):5457–5465, July 2008.

[224] N. B. Tito, S. T. Milner, and J. E. G. Lipson. Self-assembly of lamellar microphases in linear gradient copolymer melts. *Macromolecules*, 43(24):10612–10620, December 2010.

[225] T. Pakula and K. Matyjaszewski. Copolymers with controlled distribution of comonomers along the chain .1. structure, thermodynamics and dynamic properties of gradient copolymers. computer simulation. *Macromolecular Theory And Simulations*, 5(5):987–1006, September 1996.

[226] K. R. Shull. Interfacial activity of gradient copolymers. *Macromolecules*, 35(22):8631–8639, October 2002.

[227] G. T. Pickett. Linear gradient copolymer melt brushes. *Journal Of Chemical Physics*, 118(8):3898–3903, February 2003.

[228] Y. A. Kuznetsov, E. G. Timoshenko, and K. A. Dawson. Kinetics at the collapse transition of homopolymers and random copolymers. *Journal Of Chemical Physics*, 103(11):4807–4818, September 1995.

[229] J. M. P. van den Oever, F. A. M. Leermakers, G. J. Fleer, V. A. Ivanov, N. P. Shusharina, A. R. Khokhlov, and P. G. Khalatur. Coil-globule transition for regular, random, and specially designed copolymers: Monte carlo simulation and self-consistent field theory. *Physical Review E*, 65(4):041708–1–13, April 2002.

[230] A. R. Khokhlov and P. G. Khalatur. Protein-like copolymers: Computer simulation. *Physica A*, 249(1-4):253–261, February 1998.

[231] A. R. Khokhlov and P. G. Khalatur. Conformation-dependent sequence design (engineering) of ab copolymers. *Physical Review Letters*, 82(17):3456–3459, April 1999.

[232] T. M. Beardsley and M. W. Matsen. Monte carlo phase diagram for diblock copolymer melts. *European Physical Journal E*, 32(3):255–264, July 2010.

[233] K. Lewandowski and M. Banaszak. Intraglobular structures in multiblock copolymer chains from a monte carlo simulation. *Physical Review E*, 84(1):011806–1–9, July 2011.

[234] J. Houdayer and M. Muller. Phase diagram of random copolymer melts: A computer simulation study. *Macromolecules*, 37(11):4283–4295, June 2004.

[235] A. Cavallo, M. Muller, and K. Binder. Formation of micelles in homopolymer-copolymer mixtures: Quantitative comparison between simulations of long chains and self-consistent field calculations. *Macromolecules*, 39(26):9539–9550, December 2006.

[236] K. Binder and W. Paul. Recent developments in monte carlo simulations of lattice models for polymer systems. *Macromolecules*, 41(13):4537–4550, July 2008.

[237] B. M. Baysal and F. E. Karasz. Coil-globule collapse in flexible macromolecules. *Macromolecular Theory And Simulations*, 12(9):627–646, December 2003.

[238] T. Pakula, K. Karatasos, S. H. Anastasiadis, and G. Fytas. Computer simulation of static and dynamic behavior of diblock copolymer melts. *Macromolecules*, 30(26):8463–8472, December 1997.

[239] H. P. Deutsch and K. Binder. Interdiffusion and self-diffusion in polymer mixtures - a monte-carlo study. *Journal Of Chemical Physics*,

94(3):2294–2304, February 1991.

[240] W. Jilge, Carmesin I, K. Kremer, and K. Binder. A monte-carlo simulation of polymer-polymer interdiffusion. *Macromolecules*, 23(23):5001–5013, November 1990.

[241] M. Muller, K. Binder, and W. Oed. Structural and thermodynamic properties of interfaces between coexisting phases in polymer blends - a monte-carlo simulation. *Journal Of The Chemical Society-Faraday Transactions*, 91(16):2369–2379, August 1995.

[242] A. Hoffmann, J. U. Sommer, and A. Blumen. Statics and dynamics of dense copolymer melts: A monte carlo simulation study. *Journal Of Chemical Physics*, 106(16):6709–6721, April 1997.

[243] H. Weber and W. Paul. Penetrant diffusion in frozen polymer matrices: A finite-size scaling study of free volume percolation. *Physical Review E*, 54(4):3999–4007, October 1996.

[244] V. Pryamitsyn, B. Hanson, and V. Ganesan. Coarse-grained simulations of penetrant transport in polymer nanocomposites. *Macromolecules*, 44(24):9839–9851, December 2011.

[245] J. P. Wittmer, A. Cavallo, T. Kreer, J. Baschnagel, and A. Johner. A finite excluded volume bond-fluctuation model: Static properties of dense polymer melts revisited. *Journal of Chemical Physics*, 131(6):064901, August 2009.

[246] K. Hukushima and K. Nemoto. Exchange monte carlo method and application to spin glass simulations. *Journal Of The Physical Society Of Japan*, 65(6):1604–1608, June 1996.

[247] Daan Frenkel and B. Smit. *Understanding Molecular Simulation, Second Edition: From Algorithms to Applications (Computational Science)*. Academic Press, 2 edition, November 2001.

[248] Y. H. Li, M. Mascagni, and A. Gorin. A decentralized parallel implementation for parallel tempering algorithm. *Parallel Computing*, 35(5):269–283, May 2009.

[249] M. Mascagni and A. Srinivasan. Algorithm 806. sprng: A scalable library for pseudorandom number generation (vol 26, pg 436, 2000). *Acm Transactions On Mathematical Software*, 26(4):618–619, December 2000.

[250] M. Surve, V. Pryamitsyn, and V. Ganesan. Universality in structure and elasticity of polymer-nanoparticle gels. *Physical Review Letters*, 96(17):177805–1–4, May 2006.

[251] M. Surve, V. Pryamitsyn, and V. Ganesan. Nanoparticles in solutions of adsorbing polymers: Pair interactions, percolation, and phase behavior. *Langmuir*, 22(3):969–981, January 2006.

[252] C. V. Mahajan and V. Ganesan. Atomistic simulations of structure of solvated sulfonated poly(ether ether ketone) membranes and their com-

parisons to nafion: I. nanophase segregation and hydrophilic domains. *Journal of Physical Chemistry B*, 114(25):8357–8366, July 2010.

[253] E. M. Sevick, P. A. Monson, and J. M. Ottino. Monte-carlo calculations of cluster statistics in continuum models of composite morphology. *Journal Of Chemical Physics*, 88(2):1198–1206, January 1988.

[254] V. A. Kabanov, V. G. Sergeyev, O. A. Pyshkina, A. A. Zinchenko, A. B. Zezin, J. G. H. Joosten, J. Brackman, and K. Yoshikawa. Interpolyelectrolyte complexes formed by dna and astramol poly(propylene imine) dendrimers. *Macromolecules*, 33, 2000.

[255] I. Tanis, K. Karatasos, P. Posocco, E. Laurini, and S. Pricl. Complexes between poly(amido amine) dendrimers and poly(methacrlyic acid): Insight from molecular dynamics simulations. *Macromolecular Symposia*, 331-332, 2013.

[256] Simon Jones Anna Barnard Paola Posocco, Sabrina Pricl and David K. Smith. Less is more multiscale modelling of self-assembling multivalency and its impact on DNA binding and gene delivery. *Chemical Science*, 1, 2010.

[257] E Eleftheriou and K Karatasos. Modeling the formation of ordered nano-assemblies comprised by dendrimers and linear polyelectrolytes: the role of coulombic interactions. *The Journal of chemical physics*, 137(14), 2012.

[258] A. V. Dobrynin. Theory and simulations of charged polymers: From solution properties to polymeric nanomaterials. *Current Opinion In Colloid & Interface Science*, 13(6):376–388, December 2008.

[259] Jonghoon Lee, Yuri Popov, and Glenn Fredrickson. Complex coacervation: a field theoretic simulation study of polyelectrolyte complexation. *The Journal of chemical physics*, 128(22), 2008.

[260] Marie Jonsson and Per Linse. Polyelectrolyte-macroion complexation ii. effect of chain flexibility. *The Journal of Chemical Physics*, 115(23):10975, 2001.

[261] Marie Jonsson and Per Linse. Polyelectrolytemacroion complexation. i. effect of linear charge density, chain length, and macroion charge. *The Journal of Chemical Physics*, 115(7):3406, 2001.

[262] Marie Skepo and Per Linse. Dissolution of a polyelectrolyte-macroion complex by addition of salt. *Physical Review E*, 66:051807, 2002.

[263] Fredrik Carlsson, Per Linse, and Martin Malmsten. Monte carlo simulations of PolyelectrolyteProtein complexation. *The Journal of Physical Chemistry B*, 105(38):90409049, 2001.

[264] Anna Akinchina and Per Linse. Monte carlo simulations of polyion-macroion complexes. 1. equal absolute polyion and macroion charges. *Macromolecules*, 35, 2002.

[265] Anna Akinchina and Per Linse. Monte carlo simulations of polyion-macroion complexes. 2. polyion length and charge density dependence. *The Journal of Physical Chemistry B*, 107, 2003.

[266] Fredrik Carlsson, Martin Malmsten, and Per Linse. Protein-polyelectrolyte cluster formation and redissolution: a monte carlo study. *Journal of the American Chemical Society*, 125(10):3140–3149, 2003.

[267] M. Surve, V. Pryamitsyn, and V. Ganesan. Polymer-bridged gels of nanoparticles in solutions of adsorbing polymers. *Journal of Chemical Physics*, 125(6):064903, August 2006.

[268] D. W. Yin, M. O. de la Cruz, and J. J. de Pablo. Swelling and collapse of polyelectrolyte gels in equilibrium with monovalent and divalent electrolyte solutions. *Journal of Chemical Physics*, 131(19):194907, November 2009.

[269] W. D. Tian and Y. Q. Ma. Molecular dynamics simulations of a charged dendrimer in multivalent salt solution. *Journal of Physical Chemistry B*, 113(40):13161–13170, October 2009.

[270] J. S. Klos and J.-U. Sommer. Simulations of neutral and charged dendrimers in solvents of varying quality. *Macromolecules*, 46, 2013.

[271] Q. Wang, T. Taniguchi, and G. H. Fredrickson. Self-consistent field theory of polyelectrolyte systems. *Journal of Physical Chemistry B*, 108(21):6733–6744, May 2004.

[272] A. C. Shi and J. Noolandi. Theory of inhomogeneous weakly charged polyelectrolytes. *Macromolecular Theory and Simulations*, 8(3):214–229, May 1999.

[273] Thomas Lewis, Victor Pryamitsyn, and Venkat Ganesan. Mean field theory of charged dendrimer molecules. *The Journal of chemical physics*, 135(20), 2011.

[274] Thomas Lewis and Venkat Ganesan. Conjugation of polybasic dendrimers with neutral grafts: effect on conformation and encapsulation of acidic drugs. *Soft Matter*, 8:11817–11830, September 2012.

[275] Thomas Lewis and Venkat Ganesan. Mean-field modeling of the encapsulation of weakly acidic molecules in polyelectrolyte dendrimers. *The Journal of Physical Chemistry B*, 116(28):8269–8281, 2012.

[276] Thomas Lewis and Venkat Ganesan. Interactions between grafted cationic dendrimers and anionic bilayer membranes. *Journal of Physical Chemistry B*, 117(33):9806–9820, August 2013.

[277] Prateek K. Jha, Jos W. Zwanikken, François A. Detcheverry, Juan J. de Pablo, and Monica Olvera de la Cruz. Study of volume phase transitions in polymeric nanogels by theoretically informed coarse-grained simulations. *Soft Matter*, 7, 2011.

[278] Prateek K. Jha, Jos W. Zwanikken, François A. Detcheverry, Juan J. de Pablo, and Monica Olvera de la Cruz. Study of volume phase tran-

sitions in polymeric nanogels by theoretically informed coarse-grained simulations. *Soft Matter*, 7, 2011.

[279] M. Doi and S. Edwards. *The theory of polymer dynamics*. Clarendon Press: New York, 1986.

[280] R. Shenhar, T. B. Norsten, and V. M. Rotello. Polymer-mediated nanoparticle assembly: Structural control and applications. *Advanced Materials*, 17(6):657–669, March 2005.

[281] A. K. Boal, F. Ilhan, J. E. DeRouchey, T. Thurn-Albrecht, T. P. Russell, and V. M. Rotello. Self-assembly of nanoparticles into structured spherical and network aggregates. *Nature*, 404(6779):746–748, April 2000.

[282] T. Trindade, P. O'Brien, and N. L. Pickett. Nanocrystalline semiconductors: Synthesis, properties, and perspectives. *Chemistry of Materials*, 13(11):3843–3858, November 2001.

[283] A. N. Shipway, E. Katz, and I. Willner. Nanoparticle arrays on surfaces for electronic, optical, and sensor applications. *Chemphyschem*, 1(1):18–52, August 2000.

[284] M. C. Daniel and D. Astruc. Gold nanoparticles: Assembly, supramolecular chemistry, quantum-size-related properties, and applications toward biology, catalysis, and nanotechnology. *Chemical Reviews*, 104(1):293–346, January 2004.

[285] Jasmine M. Tam, Justina O. Tam, Avinash Murthy, Davis R. Ingram, Li Leo Ma, Kort Travis, Keith P. Johnston, and Konstantin V. Sokolov. Controlled assembly of biodegradable plasmonic nanoclusters for near-infrared imaging and therapeutic applications. *Acs Nano*, 4(4):2178–2184, April 2010.

[286] Yunsheng Xia, Trung Dac Nguyen, Ming Yang, Byeongdu Lee, Aaron Santos, Paul Podsiadlo, Zhiyong Tang, Sharon C. Glotzer, and Nicholas A. Kotov. Self-assembly of self-limiting monodisperse supraparticles from polydisperse nanoparticles. *Nature Nanotechnology*, 6(9):580–587, September 2011.

[287] Anna Stradner, Helen Sedgwick, Frédéric Cardinaux, Wilson C Poon, Stefan U Egelhaaf, and Peter Schurtenberger. Equilibrium cluster formation in concentrated protein solutions and colloids. *Nature*, 432(7016):492–495, 2004.

[288] Keith P Johnston, Jennifer A Maynard, Thomas M Truskett, Ameya U Borwankar, Maria A Miller, Brian K Wilson, Aileen K Dinin, Tarik A Khan, and Kevin J Kaczorowski. Concentrated dispersions of equilibrium protein nanoclusters that reversibly dissociate into active monomers. *ACS nano*, 6(2):1357–1369, 2012.

[289] Avinash K Murthy, Robert J Stover, Ameya U Borwankar, Golay D Nie, Sai Gourisankar, Thomas M Truskett, Konstantin V Sokolov, and

Keith P Johnston. Equilibrium gold nanoclusters quenched with biodegradable polymers. *ACS Nano*, 7(1), 2013.

[290] Christos N. Likos. Effective interactions in soft condensed matter physics. *Physics Reports*, 348(45):267 – 439, 2001.

[291] R Tuinier, J Rieger, and C.G de Kruif. Depletion-induced phase separation in colloid-polymer mixtures. *Advances in Colloid and Interface Science*, 103(1):1 – 31, 2003.

[292] Francesco Sciortino, Stefano Mossa, Emanuela Zaccarelli, and Piero Tartaglia. Equilibrium cluster phases and low-density arrested disordered states: The role of short-range attraction and long-range repulsion. *Phys. Rev. Lett.*, 93:055701, Jul 2004.

[293] P G Bolhuis and A A Louis. How to derive and parameterize effective potentials in colloid-polymer mixtures. *Macromolecules*, 35(5):1860–1869, 2002.

[294] William Kung, Pedro Gonzalez-Mozuelos, and Monica Olvera de la Cruz. A minimal model of nanoparticle crystallization in polar solvents via steric effects. *Journal of Chemical Physics*, 133(7):074704, August 2010.

[295] Dongsheng Zhang, Pedro Gonzalez-Mozuelos, and Monica Olvera de la Cruz. Cluster formation by charged nanoparticles on a surface in aqueous solution. *Journal of Physical Chemistry C*, 114(9):3754–3762, March 2010.

[296] Nicoletta Gnan, Emanuela Zaccarelli, and Francesco Sciortino. Tuning effective interactions close to the critical point in colloidal suspensions. *Journal of Chemical Physics*, 137(8):084903, August 2012.

[297] Kipton Barros and Erik Luijten. Dielectric effects in the self-assembly of binary colloidal aggregates. *Physical Review Letters*, 113(1):017801, July 2014.

[298] Trung Dac Nguyen, Benjamin A. Schultz, Nicholas A. Kotov, and Sharon C. Glotzer. Generic, phenomenological, on-the-fly renormalized repulsion model for self-limited organization of terminal supraparticle assemblies. *Proceedings of the National Academy of Sciences of the United States of America*, 112(25):E3161–E3168, June 2015.

[299] Jean-Pierre Hansen and Hartmut Lowen. Effective interactions between electric double layers. *Annual Review of Physical Chemistry*, 51(1):209–242, 2000. PMID: 11031281.

[300] Evert Jan Meijer and Daan Frenkel. Computer simulation of polymer-induced clustering of colloids. *Phys. Rev. Lett.*, 67:1110–1113, Aug 1991.

[301] PG Bolhuis, AA Louis, and JP Hansen. Accurate effective pair potentials for polymer solutions. *Journal Of Chemical Physics*, 114:4296, 2001.

[302] AA Louis. Beware of density dependent pair potentials. 2002.

[303] Rajarshi Chakrabarti and Kenneth S. Schweizer. Polymer-mediated spatial organization of nanoparticles in dense melts: Transferability and an effective one-component approach. *The Journal of Chemical Physics*, 133(14):–, 2010.

[304] Mark P. Stoykovich, Huiman Kang, Kostas Ch. Daoulas, Guoliang Liu, Chi-Chun Liu, Juan J. de Pablo, Marcus Mller, and Paul F. Nealey. Directed self-assembly of block copolymers for nanolithography: Fabrication of isolated features and essential integrated circuit geometries. *ACS Nano*, 1(3):168–175, 2007.

[305] Marcus Muller and Kostas Daoulas. Ordering of diblock copolymer materials on patterned substrates: a single chain in mean field simulation study. *Macromolecular Symposia*, 252(1):68–75, 2007.

[306] G Pandav and V Ganesan. Computer simulations of DendrimerPolyelectrolyte complexes. 2014.

[307] B. H. Zimm, W. H. Stockmayer, and M. Fixman. Excluded volume in polymer chains. *Journal of Chemical Physics*, 21(10):1716–1723, 1953.

[308] Victor Pryamitsyn and Venkat Ganesan. Interplay between depletion and electrostatic interactions in PolyelectrolyteNanoparticle systems. *Macromolecules*, 47(17), 2014.

[309] W. G. McMillan and J. E. Mayer. The statistical thermodynamics of multicomponent systems. *Journal of Chemical Physics*, 13(7):276–305,

1945.

[310] M. Dijkstra, R. van Roij, and R. Evans. Phase behavior and structure of binary hard-sphere mixtures. *Physical Review Letters*, 81(11):2268–2271, September 1998.

[311] Megha Surve, Victor Pryamitsyn, and Venkat Ganesan. Depletion and pair interactions of proteins in polymer solutions. *The Journal of Chemical Physics*, 122(15):154901, 2005.

[312] Victor Pryamitsyn and Venkat Ganesan. Effect of confinement on polymer-induced depletion interactions between nanoparticles. *The Journal of Chemical Physics*, 138(23):234905, 2013.

[313] GM Torrie and JP Valleau. Non-physical sampling distributions in monte-carlo free-energy estimation - umbrella sampling. *Journal of Computational Physics*, 23(2):187–199, 1977.

[314] Alan Grossfield. Wham: the weighted histogram analysis method, version 2.0.9.

[315] P. Douglas Godfrin, Ramon Castaneda-Priego, Yun Liu, and Norman J. Wagner. Intermediate range order and structure in colloidal dispersions with competing interactions. *Journal of Chemical Physics*, 139(15):154904, October 2013.

[316] D. Stauffer. Scaling theory of percolation clusters. *Physics Reports-review Section of Physics Letters*, 54(1):1–74, 1979.

[317] S H Chen, J Rouch, F Sciortino, and P Tartaglia. Static and dynamic properties of water-in-oil microemulsions near the critical and percolation points. *Journal of Physics: Condensed Matter*, 1994.

[318] Ryan B Jadrich, Jonathan A Bollinger, Keith P Johnston, and Thomas M Truskett. Origin and detection of microstructural clustering in fluids with spatial-range competitive interactions. *Physical Review E*, 91(4), 2015.

[319] Jan Groenewold and Willem K Kegel. Anomalously large equilibrium clusters of colloids. *The Journal of Physical Chemistry B*, 2001.

[320] H Sedgwick, S U Egelhaaf, and W C K Poon. Clusters and gels in systems of sticky particles. *Journal of Physics: Condensed Matter*, 2004.

[321] Emanuela Zaccarelli. Colloidal gels: equilibrium and non-equilibrium routes. *Journal of Physics: Condensed Matter*, 2007.

[322] M. Dijkstra, R. van Roij, and R. Evans. Phase diagram of highly asymmetric binary hard-sphere mixtures. *Physical Review E*, 59(5):5744–5771, May 1999.

[323] Dirk Reith, Mathias Ptz, and Florian Mller-Plathe. Deriving effective mesoscale potentials from atomistic simulations. *Journal of Computational Chemistry*, 24(13):1624–1636, 2003.

[324] H Lowen and E Allahyarov. The role of effective triplet interactions in charged colloidal suspensions. *Journal of Physics: Condensed Matter*, 10(19), 1998.

Vita

Gunja Rajesh Pandav was born in Aallapalli, India on 7 July 1985. She received the Bachelor of Engineering degree in Chemical Engineering from the Nagpur University, India in 2007 and the Master of Technology from the Indian Institute of Technology Bombay, India in 2010. She started her graduate studies at the University of Texas at Austin in August, 2010.

Permanent address: 312C West 34th St.
Austin, Texas 78705

This dissertation was typeset with LaTeX[†] by the author.

[†]LaTeX is a document preparation system developed by Leslie Lamport as a special version of Donald Knuth's TeX Program.